

AD-A158 489

A PRELIMINARY FIELD STUDY OF TURBULENT FLOW OVER AND
INSIDE A FOREST EDGE(U) CONNECTICUT UNIV STORRS
J D LIN ET AL 01 JUL 85 ARO-21156 1-GS

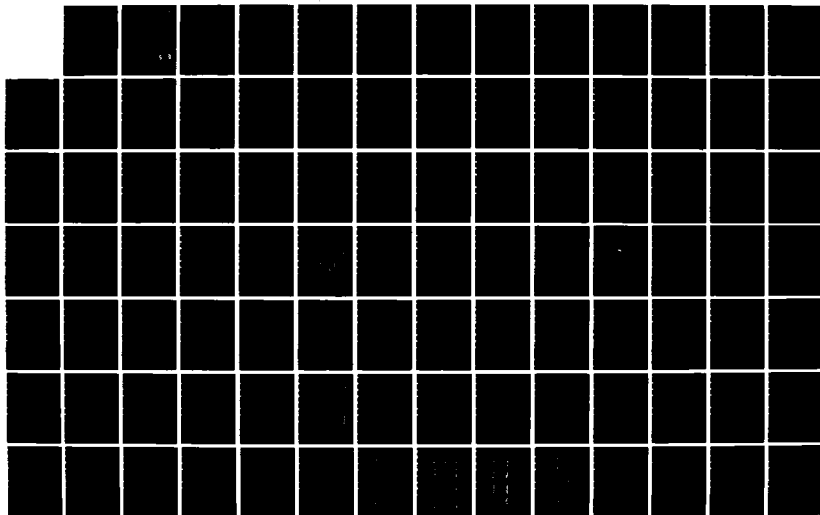
1/2

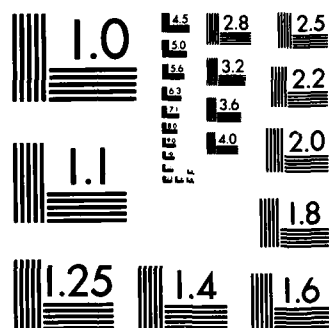
UNCLASSIFIED

DAAG29-84-K-0017

F/G 4/2

NL





MICROCOPY RESOLUTION TEST CHART
NATIONAL BUREAU OF STANDARDS-1963-A

(2)

AD-A158 409

*A preliminary field study of
turbulent flow over and inside
A forest edge*

Interim Technical Report

J.D. LIN AND D.R. MILLER

U.S. Army Research Office

Grant Number DRAAG-29-84-K-0017

Departments of Renewable Natural Resources and Civil Engineering
The University of Connecticut
Storrs, Connecticut 06268

Approved for Public Release - Distribution Unlimited

DTIC
ELECTE
AUG 29 1985
S D E

July 1, 1985

Research in Microclimate at the Forest-Urban Interface - Progress Report #11

85 8 23 172

DTIC FILE COPY

A PRELIMINARY FIELD STUDY OF TURBULENT FLOW
OVER AND INSIDE A FOREST EDGE



Interim Technical Report

J.D. LIN AND D.R. MILLER

Accession For	
NTIS GRA&I	<input checked="checked" type="checkbox"/>
DTIC TAB	<input type="checkbox"/>
Unannounced	<input type="checkbox"/>
Justification	
By	
Distribution/	
Availability Codes	
Dist	Avail and/or Special
A-1	

U.S. Army Research Office

Grant Number DDAG-29-84-K-0017

Departments of Renewable Natural Resources and Civil Engineering
The University of Connecticut
Storrs, Connecticut 06268

Approved for Public Release - Distribution Unlimited

July 1, 1985

Research in Microclimate at the Forest-Urban Interface - Progress Report #11

REPORT DOCUMENTATION PAGE		READ INSTRUCTIONS BEFORE COMPLETING FORM
1. REPORT NUMBER ARO 21156.1-65	2. GOVT ACCESSION NO. AD-A158 409	3. RECIPIENT'S CATALOG NUMBER
4. TITLE (and Subtitle) A Preliminary Field Study of Turbulent Flow Over and Inside a Forest Edge		5. TYPE OF REPORT & PERIOD COVERED Interim Technical Rpt.
		6. PERFORMING ORG. REPORT NUMBER
7. AUTHOR(s) J. D. Lin and D. R. Miller		8. CONTRACT OR GRANT NUMBER(s) DAAG 29 84 K 0017
9. PERFORMING ORGANIZATION NAME AND ADDRESS Depts. of Renewable Natural Resources and Civil Engineering. University of Connecticut, Storrs, Connecticut 06268		10. PROGRAM ELEMENT, PROJECT, TASK AREA & WORK UNIT NUMBERS
11. CONTROLLING OFFICE NAME AND ADDRESS U.S. Army Forest Research Office Post Office Box 12211 Research Triangle Park, NC 27709		12. REPORT DATE July 1, 1985
		13. NUMBER OF PAGES 106
14. MONITORING AGENCY NAME & ADDRESS (if different from Controlling Office)		15. SECURITY CLASS. (of this report)
		15a. DECLASSIFICATION/DOWNGRADING SCHEDULE
16. DISTRIBUTION STATEMENT (of this Report) Approved for public release; distribution unlimited.		
17. DISTRIBUTION STATEMENT (of the abstract entered in Block 20, if different from Report)		
18. SUPPLEMENTARY NOTES THE VIEW, OPINIONS, AND/OR FINDINGS CONTAINED IN THIS REPORT ARE THOSE OF THE AUTHOR(S) AND SHOULD NOT BE CONSTRUED AS AN OFFICIAL DEPARTMENT OF THE ARMY POSITION, POLICY, OR DECISION, UNLESS SO DESIGNATED BY OTHER DOCUMENTATION.		
19. KEY WORDS (Continue on reverse side if necessary and identify by block number) Forest Edge, Turbulent flow, Turbulence sensors, 3-D wind sensors, micrometeorology, Forest Canopy, Hot-films.		
20. ABSTRACT (Continue on reverse side if necessary and identify by block number) A basic research project on turbulent flow over and inside a forest edge was initiated at the University of Connecticut at the beginning of 1984. The study is focused on field measurements to determine the spatial variability of the turbulence characteristics under various atmospheric and forest canopy conditions. A high speed multi-channel data acquisition system has been configured and tested. Two wind velocity sensors are being tested and evaluated in the laboratory for their capability to measure the three-dimensional flow regime in a forest canopy. A number of field measurements were made over and inside the forest. These are documented in the report.		

Study Summary

/ ABSTRACT

A basic research project on turbulent flow over and inside a forest edge was initiated at the University of Connecticut at the beginning of 1984. The study is focused on field measurements to determine the spatial variability of the turbulence characteristics under various atmospheric and forest canopy conditions. A high-speed multi-channel data acquisition system has been configured and tested. Fixed and movable observation towers have been set up in the University experimental forest in Coventry, Connecticut for this study. Two wind velocity sensors, are being tested and evaluated in the laboratory for their capability to measure the three-dimensional flow with high turbulence intensity that generally characterizes the flow regime in a forest canopy. These are a dual triple-split hot-film probe and a tri-diagonal hot-film probe with a wind octant electronic sensor (WOES). The calibration of the triple-split hot-films has been completed and the probe is ready for field applications. The response of WOES tested in the low-speed wind nozzle appears to be promising and its compatibility with the tri-diagonal hot-film probe is being evaluated. A number of field measurements has been conducted over and inside the forest canopy, using a vertical array of velocity sensors which includes a propeller anemometer, and x-hot wire and hot film anemometers. This report documents the results of these preliminary studies of turbulent flow over and inside the forest canopy and the instrumentation development and site measurements during the first contractual year.

TABLE OF CONTENTS

	Page
Abstract	i
List of Tables	iii
List of Figures	iv
I. Introduction	1
II. Quantitative Specification of the Experimental Forest Canopy	2
Point Drop Method and Procedures	2
Error Analysis of the Point Drop Measurement	3
Results of Measurement	5
Canopy Architecture Analysis	6
III. Description of the Field Data Acquisition System	8
IV. Sensor Development	9
The Use of an x-hot film Probe in 3-D Atmospheric Flows	10
Calibration of a Dual-Triple Split Hot Film 3-D sensor	14
Calibration of a Miniature Octant Wind Direction Sensor	20
Correction of the Gill Anemometer Cosine Response Error	22
V. Preliminary Study of the Turbulent Flow at a Forest Edge	23
Data Collected	23
The Above-Canopy Flow Regime with a Forest Fetch	28
Some Flow Characteristics With the Wind through the Forest Edge	29
Kolmogorov Subrange and Canopy Filtering of Turbulent Eddies	30
Conditional Analysis of the Momentum Flux Over and Inside the Forest Canopy	32
VI. Conclusions and Future Plans	33
Literature Cited	36

LIST OF TABLES

Table 2.1	The number of point drop sample points necessary at different levels of significance with $V = 0.72$
Table 4.1a	Bridge settings and calibration coefficients for x-hot film probe (DISA Ser. 9055 R0611)
Table 4.1b	Coefficients for Eqs. (4.1 and 4.2)
Table 4.2	Coefficients for Eq. (4.9)
Table 4.3	Step voltage code for octant indication by WOES
Table 5.1	Data run summary, 1984

LIST OF FIGURES

- Figure 2.1 (a) Average maple leaf and (b) idealized maple leaf
- Figure 2.2 LAI distribution in the experimental plot
- Figure 2.3 LAI variation from the stand edge to inside the stand
- Figure 2.4 Leaf inclination angle distribution for Red Maple
- Figure 2.5 Leaf azimuth angle distribution for Red Maple
- Figure 2.6 Three-dimensional plot of the canopy surface
- Figure 2.7 The two-dimensional power spectrum for the canopy surface
- Figure 2.8 The smoothed canopy surface reconstructed from the significant harmonics
- Figure 2.9 The two-dimensional power spectrum for the LAI distribution
- Figure 2.10 The two-dimensional power spectra for LAI distributions in four different layers in the canopy
- Figure 3.1 Flow diagram outlining the recording and data reduction steps for the pressure and linear tree displacement sensors
- Figure 3.2 As Figure 3.1 for the temperature sensors
- Figure 3.3 As Figure 3.1 for the cup anemometers
- Figure 3.4 As Figure 3.1 for the thermal anemometers
- Figure 3.5 As Figure 3.1 for the wind direction vanes and propeller anemometers
- Figure 4.1 Triple-split hot film anemometer
- Figure 4.2 Sum of the squared sensor voltages as a function of wind speed for Probe a
- Figure 4.3 Roll angle response of the three elements on Probe a
- Figure 4.4 Polynomial coefficients B_{ij0} , B_{ij1} , B_{ij2} , B_{ij3} as functions of wind speed
- Figure 4.5 Yaw angle response of Probe a
- Figure 4.6 Dual triple-split hot films orthogonally mounted on a single holder

- Figure 4.7 Coordinate system for dual triple-split hot film probe
- Figure 4.8 The wind octant electronic sensor (WOES)
- Figure 5.1 Tower and sensor arrangement in the experimental plot
- Figure 5.2 Raw voltage signals for a 120 sec run with the sensors in position 1
- Figure 5.3 Spectra of the wind components, uw cospectra, uw quadrature spectra, and uw amplitude spectra at two levels above the canopy with the wind from a forest fetch
- Figure 5.4 Time series of the wind components from the propeller anemometer at 20m and from the x-hot films at four different levels in the canopy
- Figure 5.5 Spectra of u, v , and w at different levels in the canopy computed from the data in Figure 5.4
- Figure 5.6 Profiles of uw cospectra computed from the data in Figure 5.4 at four levels: (a) above the canopy at 20m; (b) at the average canopy height; (c) at the maximum foliage level; and (d) below the canopy
- Figure 5.7 Conditional analysis of u and w with a forest fetch. Calculated from the same data as Figure 5.3.
- Figure 5.8 Conditional analysis of u and w with the wind from the edge. Data is from Figure 5.4. Quadrant numbers are shown.

I. INTRODUCTION

A basic research project entitled "Field Study of Wind Through and Over Forest Edges" was initiated at the University of Connecticut at the beginning of 1984 to study the three-dimensional wind field over and inside forest edges. The initial phase of this study has been focused on field measurements to determine the spatial variability of the turbulence characteristics inside and near a forest canopy, which involves arraying fast-response three-dimensional wind sensors horizontally and vertically through a forest edge stand and taking simultaneous measurement of the flow at a number of locations. To design a complete sampling scheme for the fundamental study of the variability of turbulence and the mean flow across a forest edge, the time and space characteristics of the experimental site must be established. Preliminary turbulent flow measurements have been completed at the experimental site in preparation for the coming field measurement season in 1985. Vertical profiles of the wind components have been measured above and within the canopy. Sensors were arrayed in several configurations and the data were analyzed to establish appropriate sampling rates, sensor locations, and experimental procedures.

A high speed multi-channel data logging system has been configured and tested. Measurements have been conducted in the laboratory to test the response and the compatibility of three-dimensional fast response velocity sensors.

Additional work in 1984 was conducted to quantify the experimental forest. The experimental site is located in a Red Maple (*Acer rubrum* L.) tree stand, which is located on the University of Connecticut experimental farm in Coventry, CT (Lat 41 47'30" N, Long. 72 22'29"W). The site is a level wetland in a bowl shaped valley bottom adjacent to a 10 hectare corn field.

The purpose of this report is to document these preliminary studies.

II. QUANTITATIVE SPECIFICATION OF THE EXPERIMENTAL FOREST CANOPY

The experimental plot is a Red Maple stand two tree heights (h) square (28 m x 28 m) beginning at the forest edge. The forest overstory is almost entirely Red Maple with a single White Pine (*Pinus strobus* L.) and a clump of Trembling Aspen (*Populus trembloides* L.) at the edge. The average canopy height is 14 m with the tallest tree about 17 m.

Measurements of the three-dimensional spatial distributions of leaf area in the experimental stand were made by a "point drop" method which is a variation of the point quadrant sampling method. Miller and Lin (1985) reported on the basic techniques that were used and the canopy structure. Wang (1985) studied the errors involved in the technique and further analyzed the data so that the canopy architecture can be described in terms compatible with the current turbulent flow study. This chapter summarizes this work.

Point Drop Method and Procedures

The experimental plot was surveyed and divided into two meter grids. The point drop sample points were at the nodes of each grid. At each sampling point, a plumb-weighted line was dropped through the

top of the canopy to the ground. Each leaf touched by the line was considered as a sample leaf. Its height above the ground, inclination angle (α), and the azimuth angle (θ) of the normal to its upper surface were measured with a hand compass and an angle gage. The leaf area index (LAI) at each drop point was calculated by summing the number of leaves touched by the drop line in the vertical segment. Before summing, each leaf touched was weighted by its angle from the horizontal (i.e. $1/\cos \alpha$, $\alpha \neq 90^\circ$).

Error Analysis of the Point Drop Measurement

There are two types of errors in the point drop measurement. One is the measurement error resulting from the thickness of the drop line. The second is the sample error caused by an inadequate sample size.

In the point drop method the basic assumption is made that a sample point, like a geometrical point, has no thickness. But the true "point" has the thickness of the drop line. The error arises because the sample point may pass just outside the edge of a leaf but a thick line would actually touch the leaf. Therefore, the leaf area may be overestimated by an area equal in size to $1/2$ the line diameter times the perimeter of the leaf.

To examine this source of error a "normal" leaf size and shape (Figure 2.1a) were specified by averaging 50 sample leaves. For ease of calculation the geometrical shape of the red maple leaf was idealized in Figure 2.1b. When a line with diameter of .5 mm is used, it may touch the border of a leaf as shown in Figure 2.1. The error introduced is that encompassed by the dashed line. The error increases with line diameter, and the relative error becomes larger as leaf size decreases. It is also affected by leaf shape since a

deeper lobed leaf has a larger perimeter to area ratio. The maximum error calculated for the Red Maple leaf in Figure 2.1 for a 0.5 mm line diameter was 3.14%.

Considering the drop points as non-repeated samples, the probability of the actual mean, \bar{x} , falling in the interval,

$$\bar{x} \pm U_a S / \sqrt{n-1} ,$$

$$P \left(\bar{x} - \frac{U_a S}{\sqrt{n-1}} \leq \bar{x} \leq \bar{x} + \frac{U_a S}{\sqrt{n-1}} \right) = 1 - a \quad (2.1)$$

where U_a is the significant parameter, \bar{x} is the sample average, S is the sample standard deviation and n is the sample number. Thus the necessary sample number for a given confidence P ($P=1-a$) is defined by

$$n = (U_a V_x / a)^2 \quad (2.2)$$

where a is the risk of error estimation, and V_x is the coefficient of variation.

The value of V_x was calculated to be .72 from the measurements in the stand and checked in two smaller plots. Then Eq. (2.2) was used to calculate the necessary sample numbers shown in Table 2.1 at different levels of significance.

as depicted in Figure 4.6. One probe can be used to determine the components in the x,z plane and the second in the y,z plane as shown in Figure 4.7. The geometric relations provide the velocity components:

$$u = U \sin \alpha_b = U \cos \alpha_a \cos \theta_a \quad (4.12)$$

$$v = U \cos \alpha_b \sin \theta_b = U \sin \alpha_b \tan \theta_a$$

$$w = U \sin \alpha_a = U \cos \alpha_b \cos \theta_b$$

$$\text{and } |\vec{U}| = U = (u^2 + v^2 + w^2)^{1/2}$$

Thus, a three-dimensional flow can be represented either by the velocity components (u,v,w) or by (U, θ_e, α_e) for $e = a$ or b .

The procedure for calculation of (u,v,w) from a set of measured E_i ($i=1,2,3$) for Probes a and b is summarized as follows:

1. Calculate FE_i for Probes a and b .
2. Use Eq. (4.7) to calculate the effective velocities U_a and U_b .
3. Compare U_a and U_b . If $U_a > U_b$, let $U \approx U_a$; otherwise $U \approx U_b$.
4. Assuming $U:U_a > U_b$, then θ_a can be calculated from Eq. (4.8).
If $U:U_b > U_a$, a and b should be interchanged for the following procedure.
5. From Eq. (4.10), for Probe b

$$U_b = \frac{2D_{0b} + D_{1b} + \sqrt{D_{1b}^2 - 4D_{2b}(D_{0b} - U_b/U)}}{2D_{2b}} \quad (4.13)$$

where D_{ib} are determined by equations similar to Eqs. (4.11) and (4.12).

The yaw angle responses of both triple-split hot film sensors are required to sort out the wind magnitude and two angles, which define the wind vector in polar coordinates. Figure 4.5 shows that Probe a has essentially no yaw angle effect when the wind vector is within $\pm 20^\circ$ from the normal to the probe axis. Then, the signal decreases from $\pm 20^\circ$ to $\pm 90^\circ$ in terms of the effective velocity, U calculated from Eq. (4.7). These are different from the ranges of 0 to -45° and 45° to 90° indicated by Jorgensen (1982). The ranges shown by Jorgensen would allow the establishment of mutually exclusive conditions by two orthogonal probes as discussed by Lin et al. (1985). But this approach cannot be used with the yaw angle response shown in Figure 4.5. The yaw angle response shown for Probe a can be represented by the following:

$$U_a/U = 1.0 \text{ for } 0 \leq \alpha \leq 20^\circ$$

and

$$U_a/U = D_0 + D_1 (\alpha - 20) + D_2 (\alpha - 20)^2 \text{ for } \alpha > 20^\circ \quad (4.10)$$

where for $20^\circ < \alpha < 45^\circ$, $D_0 = 1$, $D_1 = -0.373 - 0.045U$

$D_2 = -0.9E-4$; for $\alpha > 45^\circ$, $D_2 = 0$

when $U < 1.7$ m/s, $D_0 = 0.84$, $D_1 = -0.009$

$1.7 < U < 5$ m/s, $D_0 = 0.865 - 0.015U$, $D_1 = -0.0085 - 0.0003U$

$U > 5$ m/s, $D_0 = 0.79$, $D_1 = -0.010 \quad (4.11)$

Now, we have the complete set of calibration coefficients for Probe a. A similar set has also been obtained for Probe b.

To measure all three velocity components with the probe fixed and the wind direction variable we have mounted two triple-split hot film probes on a single holder. The probes are oriented orthogonally

Table 4.2
Coefficients for Eqs. (4.9)

i	j	C_{ij0}	C_{ij1}	C_{ij2}	C_{ij3}	C_{ij4}
1	0	0.62629E0	0.25189E0	-0.13844E-1	0.86900E-4	0.18730E-4
	1	0.55318E-1	-0.21735E-1	0.22293E-2	-0.36799E-3	0.20872E-4
	2	-0.71016E-2	0.57812E-2	-0.39144E-2	-0.32200E-3	0.35934E-4
	3	-0.13523E0	0.71316E-1	-0.13922E-1	0.11956E-2	-0.39043E-4
2	0	-0.36711E0	0.36440E0	-0.22351E-1	0.49981E-3	0.79869E-5
	1	-0.86108E0	0.22011E0	0.25287E-2	-0.23650E-2	0.11179E-3
	2	-0.64736E0	0.15791E0	-0.31027E-2	-0.12271E-2	0.68309E-4
	3	-0.13523E0	0.71316E-1	-0.71316E-1	0.11956E-2	-0.39043E-4
3	0	0.42434E0	0.21089E0	-0.14702E-1	0.12470E-2	-0.52845E-4
	1	0.78068E0	-0.36248E0	0.58648E-1	-0.45592E-2	0.13406E-3
	2	-0.26390E0	0.54262E-1	0.11157E-1	-0.18650E-2	0.73315E-4
	3	-0.13523E0	0.71316E-1	-0.13922E-1	0.11956E-2	-0.39043E-4

The roll angle responses of the three different sensors, shown in figure 4.3 for Probe a, are used to determine the vector direction in the normal plane. The sensor responses are not completely symmetrical; therefore, it is necessary to express the voltage output of each sensor as a function of roll angle, θ , and velocity, U , (or $\sum E_i^2$) in the Fourier series,

$$E_i(U, \theta) = B_{i0} + B_{i1} \cos \theta + B_{i2} \sin \theta + B_{i3} \cos 2\theta + B_{i4} \sin 2\theta + B_{i5} \cos 3\theta + B_{i6} \sin 3\theta + B_{i7} \cos 4\theta + B_{i8} \sin 4\theta \quad (4.8)$$

The Fourier coefficients B_{ij} are calculated from calibration data and are functions of wind speed, U , or squared voltage sum, $\sum E_i^2$ which are represented by power series similar to Eq. (4.7) in terms of a set of coefficients, C_{ijk} , i.e.

$$B_{ij} = C_{ij0} + C_{ij1} \sum E_i^2 + C_{ij2} (\sum E_i^2)^2 + C_{ij3} (\sum E_i^2)^3 + C_{ij4} (\sum E_i^2)^4 \quad (4.9)$$

Thus, a set of 140 coefficients, which have been obtained in the absence of the yaw angle effect, is needed for each probe. Figure 4.3 shows the Fourier series representation by Eq. (4.8). The coefficients, B_{ij} , can be calculated by multiplying Eq. (4.2) by $\cos n\theta$ or $\sin n\theta$ and integrated over a range of 2π . It was found that only the first four coefficients are necessary for a good approximation as shown in the Figure 4a-d.

The coefficients, B_{ij} , of Eq. (4.8) shown in Figure 4.4 are considered as a function of $\sum E_i^2$. The coefficients C_{ijk} of Eq. (4.9) are given in Table 4.2.

Table 4.1b
Coefficients for Eqs. (4.1) and (4.2)

$A_0 = 0.80763 \times 10$	$B_0 = 0.11962 \times 10$
$A_1 = 0.14645 \times 10$	$B_1 = 0.25119 \times 10$
$A_2 = -0.40882 \times 10$	$B_2 = -0.14057 \times 10$
$A_3 = -0.62714 \times 10$	$B_3 = -0.26605 \times 10$
$A_4 = 0.39092 \times 10$	$B_4 = 0.36965 \times 10$
$h_1 = 0.23$	$h_2 = 0.17$

Calibration of a Dual Triple-Split Hot Film Probe

Consider a single probe oriented perpendicularly to the mean flow and used to determine the wind vector in the plane normal to the long axis of the probe. The sum of the squared signals, $\sum E_i^2$, from the three films is an increasing function of wind velocity, U . Figure 4.2 shows the monotonic increase of $\sum E_i^2$ as a function of U from calibration of Probe a. The curve in Figure 4.2 can be approximated by a fourth-order polynomial (Jorgensen, 1982),

$$U = A_0 + A_1 (\sum E_i^2) + A_2 (\sum E_i^2)^2 + A_3 (\sum E_i^2)^3 + A_4 (\sum E_i^2)^4 \quad (4.7)$$

in which the coefficients are given by $A_0 = -0.10677 \text{ E}+2$, $A_1 = 0.13870 \text{ E}+1$, $A_2 = 0.44066 \text{ E}+0$, $A_3 = -0.79152 \text{ E}-1$, and $A_4 = 0.3646 \text{ E}-2$.

origin of the coordinates on the junction of the films. The bridge setting and calibration coefficients for the film probe used in the summer of 1984 are given in Tables 4.1a and b.

Table 4.1a
Bridge Settings and Calibration Coefficients
for x-Hot Film Probe
(DISA Ser. 9055 R0611)

Sensor resistance	Film #1	Film #2
R_{20}	7.11	7.77
R_0	0.6	0.6
α_{20}	0.39	0.38
Bridge Settings		
Overheat	0101	0101
Hot resistance	0011	0011
Cable length	1000	1000
Gain	0000	0000
Filter	11	11
Shape	10	10

$$U_{effi} = U(\sin^2\theta_i + h_i^2 \cos^2\theta_i) \quad (4.2)$$

where h_i is a parameter depending on the characteristic of the film and must be calibrated in the measured values of U, E_i and θ_i . Then, given measured values of E_i , Eqs. (4.1) and (4.2) can be used to solve for the wind speed, U_i , and θ_i using the condition,

$$\theta_1 + \theta_2 = 90^\circ \quad (4.3)$$

Eqs. (4.1) and (4.2) can now be modified and combined with the horizontal angle (ϕ) in the x, y plane measured by another sensor, to determine the velocity components (u, v, w). For a non-zero value of ϕ , the true yaw angle α_i and U can be solved from

$$(\cos\alpha_1 + \cos\alpha_2)^2 - (\cos\alpha_1 - \cos\alpha_2)^2 = 2\cos^2\phi \quad (4.4)$$

and

$$U_{effi} = U (\sin^2\alpha_i + h_i^2 \cos^2\alpha_i) \quad (4.5)$$

Also, note that $\alpha_1 + \alpha_2 \neq 90^\circ$.

Now, consider the x -films are on the x, z plane and the x -axis makes a 45° angle with both films, then the velocity components can be calculated from

$$\begin{aligned} u &= -\sqrt{2}/2 U(\cos\alpha_1 + \cos\alpha_2) \\ v &= -\sqrt{2}/2 U \tan\phi (\cos\alpha_1 + \cos\alpha_2) \\ w &= -\sqrt{2}/2 U(\cos\alpha_1 - \cos\alpha_2) \end{aligned} \quad (4.6)$$

where U is the magnitude of the velocity vector directing toward the

the time and length scales of the flow are too small to reliably use wind vanes. The two-dimensional x-films have some very desirable characteristics for use in forests in a multi-sensor array. They are very small, highly sensitive sensors, and relatively simple and cheap. Therefore, we have devised a calibration procedure for using them on a stationary mount in conjunction with a nearby sensor which can measure the horizontal angle in the x,y plane. For use inside a canopy a nearby three-dimensional sensor is necessary, while in the open atmosphere a nearby wind vane is needed.

x-Hot Film Calibration

The 90-degree x-film probe was mounted on a positioning device in front of a contracting air nozzle of 3 inches in diameter in the laboratory. Output voltages were measured over a range of wind speeds from 0 to 15 m/s with the wind vector positioned in the plane of the films at various yaw angles (15-degree intervals) from perpendicular ($\theta=90^\circ$), to parallel ($\theta=0^\circ$), to the cylindrical film. The entire procedure was carried out for both sensors, film 1 and film 2.

First, a fourth-order polynomial is used to define the relationship between the effective wind speeds U_{ei} and output voltages E_i , i.e. with the wind perpendicular to one of the films.

$$U_{eff1} = A_0 + A_1 E_1 + A_2 E_1^2 + A_3 E_1^3 + A_4 E_1^4$$

and

(4.1)

$$U_{eff2} = B_0 + B_1 E_2 + B_2 E_2^2 + B_3 E_2^3 + B_4 E_2^4$$

With the wind perpendicular to one of the films, one set of the coefficients in Eq. (4.1) can be determined. The other set can be similarly determined. Next, the relationship for the variation of yaw angles with the velocity is approximated by

distinguish the eddies shedding off canopy elements and not interfere with the flow, and are capable of measuring three-dimensional flow. One prototype probe which may fulfill these requirements uses two perpendicular triple-split hot films. The two sensors on this probe are triple-split hot films manufactured by Dantec Electronics (DISA 55R93). Each probe employs three thin film sensors, used as constant temperature anemometers, spaced evenly around a cylindrical quartz-fiber core, 4.0 in diameter, as diagrammed in Figure 4.1. The probes were calibrated by means of a 3-inch free jet from a contracting nozzle and a probe positioning device which allows the probe to be oriented for both roll and yaw angle calibration.

In order to initiate the preliminary field study an x-hot film was used to measure the velocity components over the forest canopy in conjunction with a wind vane.

Another three-dimensional flow sensor under development and testing is a combination of a tri-diagonal hot film sensor with a wind octant direction sensor.

Use of an x-Hot Film Probe in Three Dimensional Atmospheric Flows.

Flow measurement with a x-hot film probe is generally restricted to situations where the flow vector lies inside a quarter plane (the x,z plane) defined by the two slanting wires of the probe. Previous efforts to overcome this limitation in the atmosphere where the wind velocity fluctuations are almost always off the mean plane have been to mount the probe on fast response wind vanes (Larsen and Busch, 1974). This arrangement allows the horizontal wind direction in the x,y plane to be measured with the vanes while maintaining the x-film probe oriented into the mean wind direction. For measurements over and inside a forest canopy stationary sensors are necessary because

inch tape drive.

The data collection is performed through two 32 channel, differential input, Data Translation analog-digital boards. These A/D are 12-bit, -10 to +10 volt range, with 50KHz per board throughput capacity. Resident on the hard disk are data collection programs through which the operator controls sampling frequency, sampling period, channel selection, etc. Also resident are calibration files and software which allow quick conversion from voltages to the units of the monitored quantity.

Extensive graphics and statistical softwares are kept in the system to allow quick, preliminary evaluation of data. The statistical programs range widely from means and variances to autocorrelations and frequency spectra. Graphs of the data can either be displayed on the VT101 terminal or drawn by the Decwriter IV printer. Due to the size of the data sets, more extensive statistical analyses and graphics are performed on the IBM 3081 at the University of Connecticut. Data is first reformatted into a convenient form and then put on magnetic tapes which can be mounted on the IBM. Figures 3.1 - 3.5 are block diagrams for each sensor type showing the flow of information from the sensor through the signal conditioning/controlling electronics and the data collection/analysis system.

IV. SENSOR DEVELOPMENT

Turbulent flow measurements in plant canopies require sensors that are fixed, have a high frequency response, are small enough to

The double Fourier analysis of canopy height data from the Red Maple stand shown in Figure 2.6 yields the power spectrum shown in Figure 2.7. Three major peaks are apparent on the diagram at (1,1), (2,2), and (3,2). They represent the three significant harmonics. The contribution of these three significant harmonics to the total variance is 89%. Thus, construction of a canopy from the Fourier series can be done, without losing much of the original canopy form, by using only the three significant harmonics. The recalculated canopy height, H , results in a smoothed surface shown in Figure 2.8. The characteristic wave length from this analysis was approximately 6m which is also the approximate spacing between the tallest emergent tree crowns.

The double Fourier analysis was also performed on the spatial distribution of LAI. The power spectrum (Figure 2.9) indicates that the leaf distribution is more variable than the canopy surface. The spectra for four layers of the canopy, each of which are 5m thick, are shown in Figure 2.10.

$$S_{nm}^2 = \alpha_{nm}^2 + \beta_{nm}^2 + \gamma_{nm}^2 + \delta_{nm}^2 \quad (2.5)$$

III. DESCRIPTION OF THE FIELD DATA ACQUISITION SYSTEM

The heart of the data acquisition system is a LSI 11/23 computer with a 9x4 Q-Bus. The computer is matched with a Scientific Micro-Systems 35.6 megabyte Winchester hard disk. Also, in the system are 256K bytes of board memory and a dual sided floppy disk drive. For transferring or storing large data sets and for system back-up, the computer is interfaced with a Digi-Data model 1740 1/2

The purpose of the analysis is to find all the Fourier coefficients from H_{ij} , x_1 and x_2 . For this study, H_{ij} are measured on the regular grid points with a 2m distance between adjacent points. In this case of observations, which have been made on a rectangular grid, all of the cross product terms of sine and cosine in Eq. (2.3) become zero. The inverse equations for finding the Fourier coefficients of any harmonic are

$$\begin{aligned}
 \alpha_{nm} &= \frac{k}{NM} \sum_{n=1}^N \sum_{m=1}^M H_{ij} \cos \frac{2\pi n x_{1i}}{N} \cos \frac{2\pi n x_{2j}}{M} \\
 \beta_{nm} &= \frac{k}{NM} \sum_{n=1}^N \sum_{m=1}^M H_{ij} \cos \frac{2\pi n x_{1i}}{N} \sin \frac{2\pi n x_{2j}}{M} \\
 \gamma_{nm} &= \frac{k}{NM} \sum_{n=1}^N \sum_{m=1}^M H_{ij} \sin \frac{2\pi n x_{1i}}{N} \cos \frac{2\pi n x_{2j}}{M} \\
 \delta_{nm} &= \frac{k}{NM} \sum_{n=1}^N \sum_{m=1}^M H_{ij} \sin \frac{2\pi n x_{1i}}{N} \sin \frac{2\pi n x_{2j}}{M}
 \end{aligned} \tag{2.4}$$

where $k=1$ if $n=0$ and $m=0$

$k=2$ if $n=0$ or $m=0$ but not both

$k=4$ if $n>0$ and $m>0$

n =harmonic number in direction x_1

m =harmonic number in direction x_2

N =number of grid points in direction x_1

M =number of grid points in direction x_2

Once the Fourier coefficients have been calculated the two-dimensional power spectrum can be calculated

canopy. The azimuth angle distribution is close to random for all four layers.

Canopy Architecture Analysis

The canopy height surface is shown in Figure 2.6. This was measured by taking the canopy surface height at every grid point during the point drop measurements.

To analyze the repeating pattern of the canopy surface, a double Fourier analysis was applied after Watson (1971). A complex undulating forest canopy surface can be considered to be the sum of two-dimensional sinusoidal wave forms, each containing many harmonics of differing amplitudes and wave lengths. The distribution of the height H_{ij} over the canopy surface can be represented by a double Fourier series of the form

$$\begin{aligned}
 H_{ij} = & \sum_{n=1}^N \sum_{m=1}^M \alpha_{nm} \cos \frac{2\pi n x_{1i}}{\lambda_1} \cos \frac{2\pi m x_{2j}}{\lambda_2} + \\
 & \beta_{nm} \cos \frac{2\pi n x_{1i}}{\lambda_1} \sin \frac{2\pi m x_{2j}}{\lambda_2} + \\
 & \gamma_{nm} \sin \frac{2\pi n x_{1i}}{\lambda_1} \cos \frac{2\pi m x_{2j}}{\lambda_2} + \\
 & \delta_{nm} \sin \frac{2\pi n x_{1i}}{\lambda_1} \sin \frac{2\pi m x_{2j}}{\lambda_2}
 \end{aligned} \tag{2.3}$$

where λ_1 and λ_2 refer to the fundamental wavelengths along the two orthogonal coordinates x_1 and x_2 , and n and m refer to the harmonics in the x_1 and x_2 directions respectively. α_{nm} , β_{nm} , γ_{nm} and δ_{nm} are Fourier coefficients for the different harmonics.

Table 2.1
The Number of Point Drop Sample Numbers Necessary
at Different Levels of Significance with $V_x=0.72$

Significant	U_a	Minimum number of sample point
0.01	2.58	34507
0.05	1.96	797
0.10	1.64	139
0.15	1.44	48
0.20	1.28	21

Results of Measurement

LAI measured at each point are shown in figure 2.2. In the figure the LAI in the first and second rows shows many zeros because the forest edge is uneven. Once inside the forest, the LAI values become large due to the "edge effects" (Figure 2.3). About 14 m from the forest edge, the LAI becomes smaller and more homogeneous. The largest values of LAI in Figure 2.2 are at the locations of dominant trees. The probability densities of the leaf inclination and azimuth angles were also calculated and are shown in Figures 2.4 and 2.5 (Miller and Lin, 1985). The Red Maple leaves tend to be more upright in their inclination angle distribution in the sunlit upper part of the canopy and essentially horizontal in the shaded lower part of the

The range of α_b can be determined by

$$\begin{aligned} 0^\circ \leq \alpha_b \leq 90^\circ & \text{ if } -90^\circ < \theta_a \leq 90^\circ \\ \text{or} & \\ -90^\circ \leq \alpha_b < 0 & \text{ if } 90^\circ \leq \theta_a < 270^\circ \end{aligned} \quad (4.14)$$

6. From Eq. (4.12), α_a can be calculated from

$$|\alpha_a| = \arcsin (\sin \alpha_b / \cos \theta_a) \quad (4.15)$$

7. If $|\alpha_a| < 20^\circ$, we have the solution in terms of $(U, \theta_a, |\alpha_a|)$. However, the sign of α_a has yet to be determined. If $|\alpha_a| > 20^\circ$, it can be shown that $\alpha_a < 45^\circ < \alpha_b$ if $U_a > U_b$. As shown in Figure 4.5, $U_a/U < 1$ and an iterative approach is now required. A better approximation for U can be calculated from Eq. (4.10) for the above values of U_a and $|\alpha_a|$; Steps 5 and 6 have to be repeated until $(U, |\alpha_a|)$ converge to approximately constant values.
8. The sign of α_a must be determined by solving Eq. (4.8) for θ_b for Probe b. However, in order to use Eq. (4.8) for a non-zero yaw angle, the values of E_i are obtained approximately as follows. By definition of Eq. (4.7),

$$\begin{aligned} U_b/U = (\Lambda_0 + A_1 \Sigma E_{id}^2 + \dots) / \\ (\Lambda_0 + A_1 \Sigma E_i^2 + \dots) \end{aligned} \quad (4.16)$$

This equation may be used to solve for ΣE_i^2 , then

$$E_i = E_{id} (\sum E_{i\alpha}^2 / \sum E_i^2)^{-1/2} \quad (4.17)$$

where the subscript α indicates non-zero yaw angle.

The computer programs that are required for calibration and for calculation of the components of turbulent flow velocity have been prepared for the dual triple-split hot film probe.

Calibration of a Miniature Wind Octant Electronic Sensor (WOES)

The use of an auxiliary WOES wind direction sensor with a tri-diagonal hot film probe at a point was first developed and tested by Fox et al. (1980). The WOES unit we are testing is a 1 cm plastic cube with platinum resistance temperature sensors on each face. The sensors on opposite faces are wired differentially and the three pairs are recorded separately. The gages are heated and balanced under no flow conditions. When exposed to the wind, the upwind sensor of each pair is cooled more than the downwind one.

Simultaneous recording of the unbalance voltage of the three pairs on the cube allows the resolution of the flow into eight directions (octant) relative to the cube. When the cube is mounted close to a tri-diagonal hot film probe with the cube normals aligned with the sensor axes then the direction and magnitude of the flow can be obtained.

The sensor is diagrammed in Figure 4.9 and the stepped voltage code for octant indication is presented in Table 4.3 (after Fox, personal communication, 1983).

Table 4.3
Step-Voltage Code for Octant Indication
by Wind Octant Electronic Sensor

Octant	Sign of stated component of total velocity directed toward coordinate origin in given octant			Step-voltage value for stated component in given octant, zero for negative component (volts)			Summed step-voltage code for given octant (volts)
	U_x	U_y	U_z	E_x	E_y	E_z	
1	-	-	-	0	0	0	0
2	+	-	-	2	0	0	2
3	+	+	-	2	4	0	6
4	-	+	-	0	4	0	4
5	-	-	+	0	0	1	1
6	+	-	+	2	0	1	3
7	+	+	+	2	4	1	7
8	-	+	+	0	4	1	5

Correction of the Gill Propeller Anemometer for its Noncosine

Response Error

When the angles between the wind vector and the Gill axis are small the error due to a non-cosine response increases. Using a correction factor C_i measured by Horst (1973), the data was corrected by the parabolic interpolation method. Angles between the wind vector and the Gill axis ($\theta_u, \theta_v, \theta_w$) were calculated from the three propeller signals:

$$\begin{aligned}\theta_u &= \cos^{-1} [U/(u^2 + v^2 + w^2)^{1/2}] \\ \theta_v &= \cos^{-1} [V/(u^2 + v^2 + w^2)^{1/2}] \\ \theta_w &= \cos^{-1} [W/(u^2 + v^2 + w^2)^{1/2}]\end{aligned}\quad (4.18)$$

For a θ located within three points (θ_{i-1}, C_{i-1}), (θ_i, C_i), and (θ_{i+1}, C_{i+1}) the correction factor is

$$\begin{aligned}C &= \frac{(\theta - \theta_i)(\theta - \theta_{i+1})}{(\theta_{i-1} - \theta_i)(\theta_{i-1} - \theta_{i+1})} C_{i-1} + \frac{(\theta - \theta_{i+1})(\theta - \theta_{i-1})}{(\theta_i - \theta_{i+1})(\theta_i - \theta_{i-1})} C_i \\ &+ \frac{(\theta - \theta_{i-1})(\theta - \theta_i)}{(\theta_{i+1} - \theta_{i-1})(\theta_{i+1} - \theta_i)} C_{i+1}\end{aligned}\quad (4.19)$$

The wind (horizontal) direction, α , is calculated from the corrected Gill data by

$$\alpha = \arctan |v/u| \quad (4.20)$$

V. PRELIMINARY STUDY OF TURBULENT FLOW AT A FOREST EDGE

Data Collected

The flow measurements at the site of the experimental forest canopy were made with cross hot wire (x-wire) and cross hot-film (x-film) sensors oriented and calibrated to measure the u and w components of the wind. These 2-D sensors and a Gill u,v,w propeller anemometer were the primary wind sensors used in the preliminary study.

The instruments were arrayed vertically on the fixed tower at a location 2H inside the forest edge for all the runs. Figure 5.1 shows the tower and approximate sensor arrangements. Data runs were made with the wind direction from the forest (forest fetch) and from the edge (corn field fetch). The sensors were primarily arrayed above the canopy in order to characterize the above canopy flow regime. One series of runs were also made with the x-film sensor located at different heights inside the forest canopy with the wind blowing from the edge. The parameters generally measured and instruments used were:

<u>Measurement</u>	<u>Instrument</u>	<u># of levels</u>
wind direction	climatronics	1
u,v,w	Gill Anemom.	1
u,w	x-wire	1
u,w	x-film	1
temperature	fine wire TC	4
pressure	microphone	ground
tree movement	linear displacemnt	1

The data runs made are listed in Table 5.1. Overall there were 26 short runs at 10 Hz, 5 short runs at 100 Hz, and 2 long runs of 35 minutes at 10 Hz.

Table 5.1

Data Run Summary, 1984

Date	Sensors	Height (m)	Run Length (min)	Rate (Hz)	File Name	Fetch
8/28		Position 1				Forest
	Dir	22.7	2	10	G28401.CPD	
	Gill,uvw	19.85	2	10	G28402.CPD	
	TC1	21.3	2	10	G28409.CPD	
	TC2	18.8	2	10	G28410.CPD	
	TC3	15.2				
	x-film	14.73				
	x-wire	12.34				
8/28	Dir		35	10	LR208A.A01	
	Gill,uvw					
	TC2,TC3					
	x-film	19.85				
8/28		Position 2				
	All the same as position 1 except:					
	x-film	14.73	3	10	G28404.CPD	
	x-wire	17.80	3	10	G28407.CPD	

8/28

Position 3

All the same as position 1 except:

x-film	16.68	3	10	G28405.CPD
x-wire	18.16	3	10	G28406.CPD

8/30

Position 1

Forest

3	10	G30401.CPD
3	10	G30402.CPD

8/31

Position 1

Corn

Field

x-film

(330)	2	10	G31401.CPD
	2	10	G31402.CPD

x-wire

(330)	2	10	G31403.CPD
	2	10	G31409.CPD

8/31 Dir

Gill,uvw	5	100	BIG08A.A01
----------	---	-----	------------

x-wire	5	100	BIG08A.A02
--------	---	-----	------------

8/31

Position

2		
2	10	G31404.CPD
2	10	G31405.CPD
2	10	G31408.CPD

8/31	Position	3		
		2	10	G31406.CPD
		2	10	G31407.CPD

9/5 Same as 8/31

Corn

Field

except:

TC3	14.00	5	100	FW4:505404.CPD
x-film	14.00	2	10	FW5:505404.CPD
		2	10	FW5:505408.CPD

9/5 Same except:

x-film	11.00	5	100	FW4:505403.CPD
		2	10	FW5:505403.CPD
		2	10	FW5:505407.CPD

9/5 Same except:

x-film	7.67	5	100	FW4:505402.CPD
		2	10	FW5:505402.CPD
		2	10	FW5:505407.CPD

9/5 Same except:

x-film	4.34	5	100	FW4:505401.CPD
		2	10	FW5:505401.CPD
		2	10	FW5:505405.CPD

The preliminary nature of the data needs to be stressed. We were looking at a number of different things simultaneously during this stage of the study in order to design appropriate sampling schemes for the coming season.

Figure 5.2 shows the raw voltage data from a 120 sec time segment of a sample run with the instruments in Position 1 (from Table 5.1) above the canopy with the wind coming from the forest fetch. The wind direction is from the wind vane. The u,v,w components are from the Gill propellers with the u propeller axis pointing west at 270 degrees and the v propeller pointing south at 180 degrees. Films #1 and #2 are the x-films of the stationary probe oriented vertically in the direction of the prevailing wind. Film #3 was a single film mounted near the Gill. The temperature trace is from a thermocouple at the level of the Gill anemometer. The pressure is from a microphone at the ground level below the canopy. The displacement is from a linear displacement sensor mounted on a tree limb to record its movement.

Comparison of the hot-film data to the Gill data in Figure 5.2 demonstrates the higher sensitivity of the films. To check if this difference in sensitivity would make comparison of data from the two instruments invalid, we mounted a single hot film near the Gill for a number of runs. No consistent differences could be detected between the spectra derived from the Gill data and that from the hot film data. Therefore, we concluded that at the level above the canopy where the Gill was mounted, no significant information would be lost due to its slower response. If the Gill is to be used closer to the canopy its response would have to be checked again at that level.

The displacement gage only showed one sway of the tree limb during this run because the tree on which it was mounted was sheltered from the SW wind by a taller crown on the adjacent tree. The single movement was 10 to 12 seconds after an abrupt wind direction shift to the NW which slowly drifted back to the SW. This mounting of the displacement gage gave us little information about the tree crown movement during these short runs in a very light wind speed. In future measurements, care must be taken to mount the instrument on a branch on the tree crown which is exposed in all directions. Mounting two sensors, one on a tall tree and one on an adjacent shorter crown, may give us some insight into the drag effect of the tree crowns touching each other and dampening their movement.

The Above Canopy Flow Regime with a Forest Fetch

Velocity component spectra computed from measurements at two levels above the canopy during a period of flow from the forest fetch are shown in figure 5.3. These are typical of all the measurements above the canopy. The spectra at these levels from short (three minutes) runs with a forest fetch consistently show three or four peaks at .5-.8 hz, .9-1.5 hz, 2-3 hz, and often at about 5 hz. The lowest of these is the strongest peak in the w-component spectrum, which probably indicates thermal turbulence at these frequencies. The horizontal components had their strongest peaks between .9 and 1.5 hz in essentially all the runs at all locations. Apparently 1 hz is a characteristic frequency for this site, possibly set by the surrounding topography or wake effects from groups of trees. Characteristic peaks in the spectrum at frequencies higher than 3 hz were only present in the horizontal components, not in the w component. These, if real, are probably the wake effects from nearby

elements or single tree crowns.

Comparison of the spectra at 20 m to those at lower levels, 15 and 16.8 m, seems to show a slight shift of peaks to higher frequencies at the lower levels, but this is not certain.

Some Flow Characteristics with the Wind from the Corn Field Fetch Through the Forest Edge

Figure 5.4 shows velocity components computed from the Gill propeller at 20 m above the canopy and the hot-film anemometers at different levels inside the canopy. The wind direction angle computed from the Gill at 20 m was used in Eq. (4.6) to calculate the three velocity components from hot-film data.

The run shown is the corn field fetch with the wind approximately normal to the edge. Figure 5.5 shows spectra from the data in Figure 5.4. These spectra show considerably less regularity than those with the wind from the forest fetch. Even at the 20 m level it shows the effect of the wind blowing over the edge with fewer, less regular peaks at higher frequencies above .13 Hz. Inside the canopy, all the data had the characteristic low frequency peak at 6 .1 - .13 Hz.

In these runs, the x-film probe was moved to 4 different levels within the canopy. In Figure 5.4a, it was at 14 m just below the top of the canopy. In Figure 5.4b, 3 minutes later it was at 11 m, at the densest level of the canopy. Three minutes later it was at 7.67 m (Figure 5.4c) at the bottom of the tree canopy. And three minutes after that it was at 4.34 m in the trunk space (Figure 5.4d). The fact that the measurements at all levels were not simultaneous suggests that care must be taken when comparing their unscaled signals. The Gill at 20 m was simultaneously recorded with each of

the hot film runs. Comparisons of the spectra from the different Gill runs show little difference between them, indicating similar flow conditions above the canopy for all the data in Figure 5.4.

Near the top of the canopy all three components continue to show peaks at about 1 Hz with only a suggestion of peaks at higher frequencies. Whereas, three meters lower inside the canopy an apparent weak peak at about 3 Hz is present. At the lowest two levels below the crown the vertical component has practically disappeared with little contribution to the variance at any frequency. In addition to the peak at 1 Hz, the horizontal components appear to have a weak peak at about 4 Hz. The apparent shift of peaks to slightly higher frequencies indicates that the canopy may act to increase the rate of energy transfer from large to small size eddies.

Kolmogorov Subrange and Canopy Filtering Action

The turbulent energy spectra generally had similar shapes from all locations above the canopy. The spectra generally show the Kolmogorov inertial subrange (Lumley and Panofsky, 1964) between .5 and 5 Hz. With the wind from a forest fetch the $-5/3$ slope starts at about .8 to 1 Hz at the highest level (the Gill data). Near the canopy top, no detectable inertial subrange is present in the vertical component. When the wind was from the corn field fetch through the edge, the starting frequencies at the highest level above the canopy are about 1-2 Hz, which is higher than that with a forest fetch. Inside the canopy with the wind blowing through the edge the $-5/3$ slope starts at much higher frequencies (i.e. 3-5 Hz). Thus, it appears that the size of the eddies in the region of the inertial subrange becomes smaller near the canopy and reaches a minimum inside

the canopy. In the roughness sublayer just near the top of the canopy where the Reynolds stress is larger, the turbulence generation probably takes place at frequencies typical of the length scales between tree crowns and tree elements. The Fourier analysis of the canopy surface described previously indicates a length scale of about 6 m for the canopy. Turbulent eddies generated at this scale would have frequencies between .4 and 1.2 Hz at the wind speeds in these runs. This could explain the shift of the inertial subrange to higher frequencies.

Another phenomenon often observed in our measurements in the near canopy and inside canopy spectra, but not in the above canopy spectra (see Figure 5.5), is the occurrence of an oscillating plateau between .5 and 1 Hz. This implies that the canopy tends to filter out the mid-range frequencies and passes the energy of relatively large eddies above the canopy to small eddies inside the canopy in a rapid step change.

Figure 5.6 shows a vertical profile of uw cospectra calculated from the data in Figure 5.5 at 20 m, 14 m, 11 m and 7.6 m. The cospectra show a shift of the frequencies of peak correlation to higher frequencies in the zone near the canopy top. Below the canopy the frequencies of maximum correlation were back to the same as in the air above the canopy. This frequency shift at different levels across the top of this canopy reflects a larger turbulent length scale above the canopy and in the trunk space inside the canopy. The wider region of oscillating peaks near the top of the canopy in the momentum spectra indicates a spread of eddy sizes at that level.

Figure 5.6 also shows a sign change in the uw cospectra in the top half of the canopy from + to - in the lower frequency range with the largest correlation. In the lower region of the canopy it

returns to +, implying a momentum sink inside the canopy.

Conditional Analysis of the Momentum Flux Over and Inside the Forest

Canopy

In recent years, a number of studies have been conducted to study the turbulence transport process over and inside plant canopies by the method of conditional analysis, e.g. Finnigan (1979) in wheat and Shaw et al. (1983) in corn. Shaw (1985) pointed out that there has been no such analysis performed on a forest canopy. He discussed its implication in understanding the turbulent transport process in relation to field observations and to higher-order closure problems for mathematical models.

The conditional analysis of the Reynolds stress is carried out by dividing the hodograph plane (u, w) into five regions: four quadrants and a hyperbolic hole. An indicator function can simply be represented by $\delta_{ij} = 1$ when $i=j$ and otherwise zero, where j indicates one of these regions, such that

$$j = \begin{cases} 0 & ; & |uw| \leq H |\overline{uw}| & \text{(the hole)} \\ 1 & ; & u \geq 0, w \geq 0 & \text{(outward interaction)} \\ 2 & ; & u < 0, w \geq 0 & \text{(ejection or bust)} \\ 3 & ; & u < 0, w < 0 & \text{(inward interaction)} \\ 4 & ; & u \geq 0, w < 0 & \text{(sweep or gust)} \end{cases} \quad (5.1)$$

where H is the size of the hole. Then, the stress-fraction function can be defined by

$$S_{i,H} = |\overline{uw}|^{-1} \lim_{T \rightarrow \infty} \frac{1}{T} \int_0^T uw \delta_{ij}(t;H) dt \quad (5.2)$$

and the time-fraction

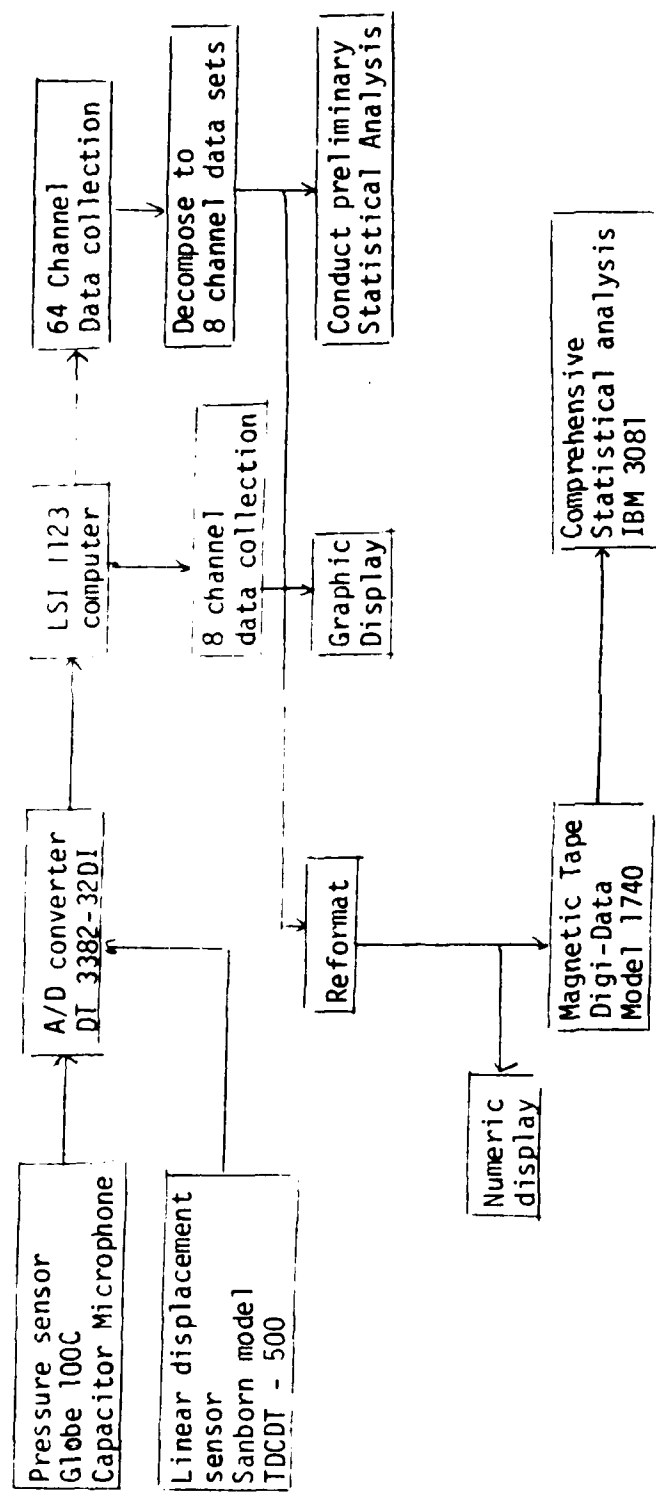
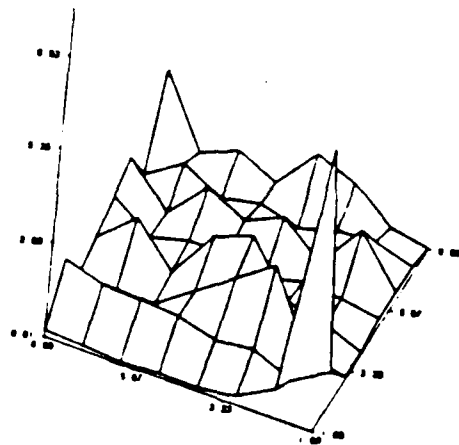
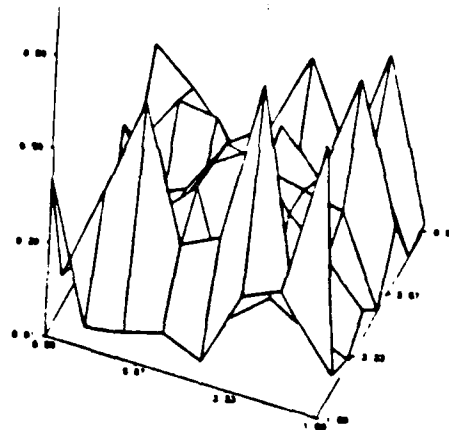


Figure 3.1. Flow diagram outlining the recording and data reduction steps for the pressure and linear tree displacement sensors.

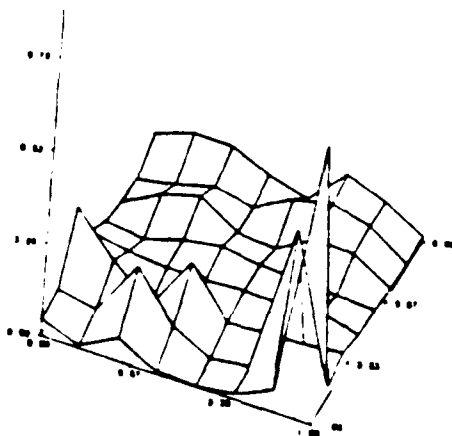
LAI SPECTRUM (5-10M)



LAI SPECTRUM (0-5M)



LAI SPECTRUM (10-15M)



LAI SPECTRUM (15-17M)

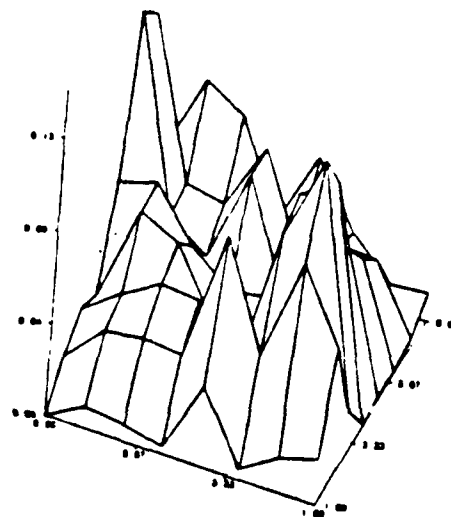


Figure 2.10. Two dimensional power spectra for LAI distributions in four different layers in the canopy.

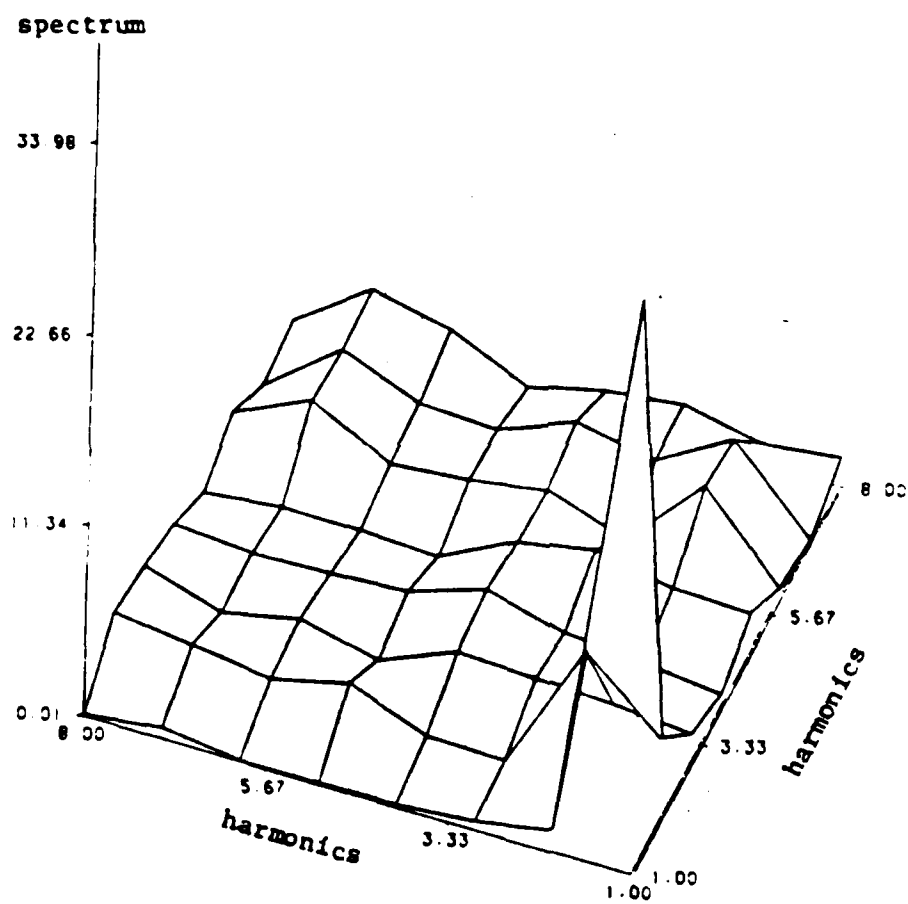


Figure 2.9. The two dimensional power spectrum for the LAI distribution.

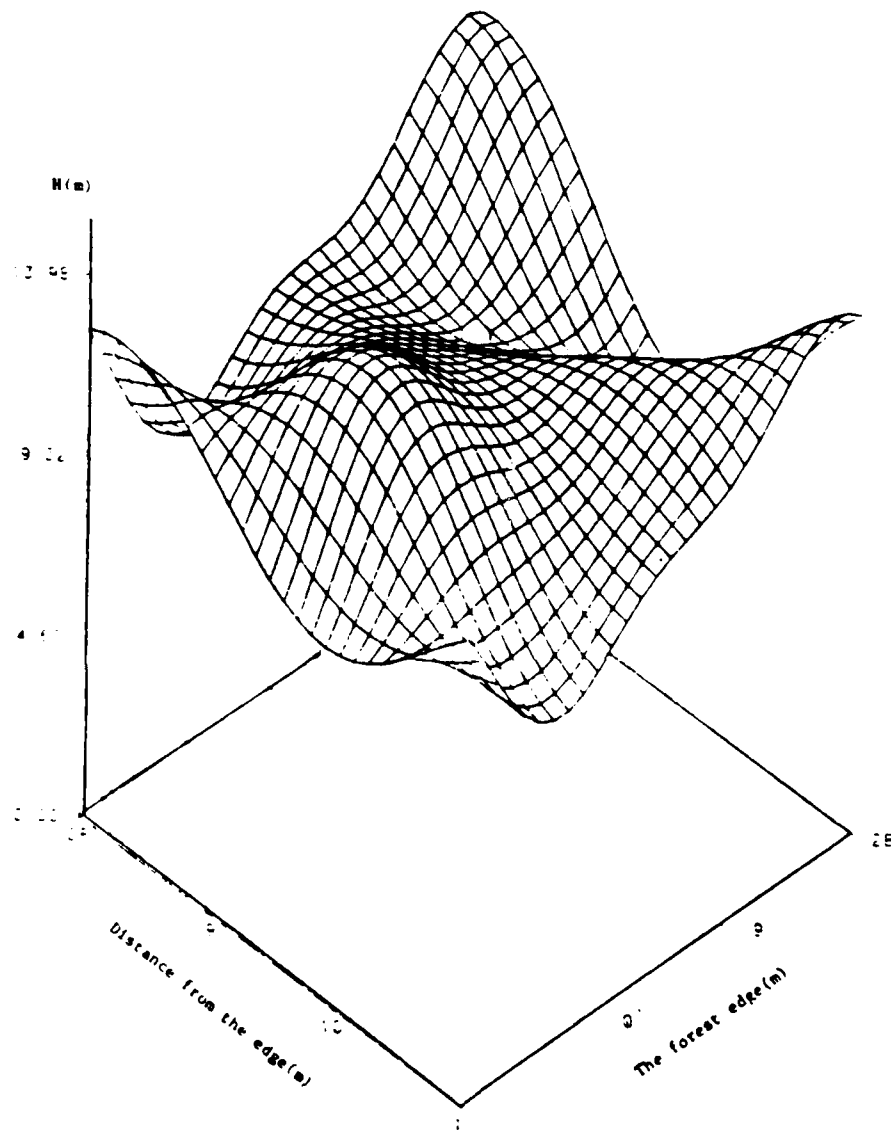


Figure 2.8. The smoothed canopy surface reconstructed from the significant harmonics.

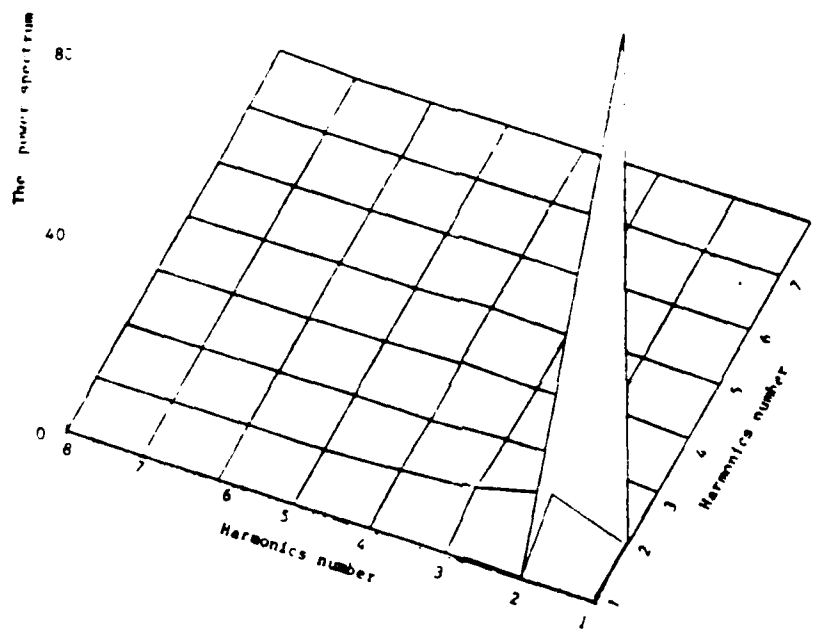


Figure 2.7. The two dimensional power spectrum for the canopy Surface.

CANOPY SURFACE

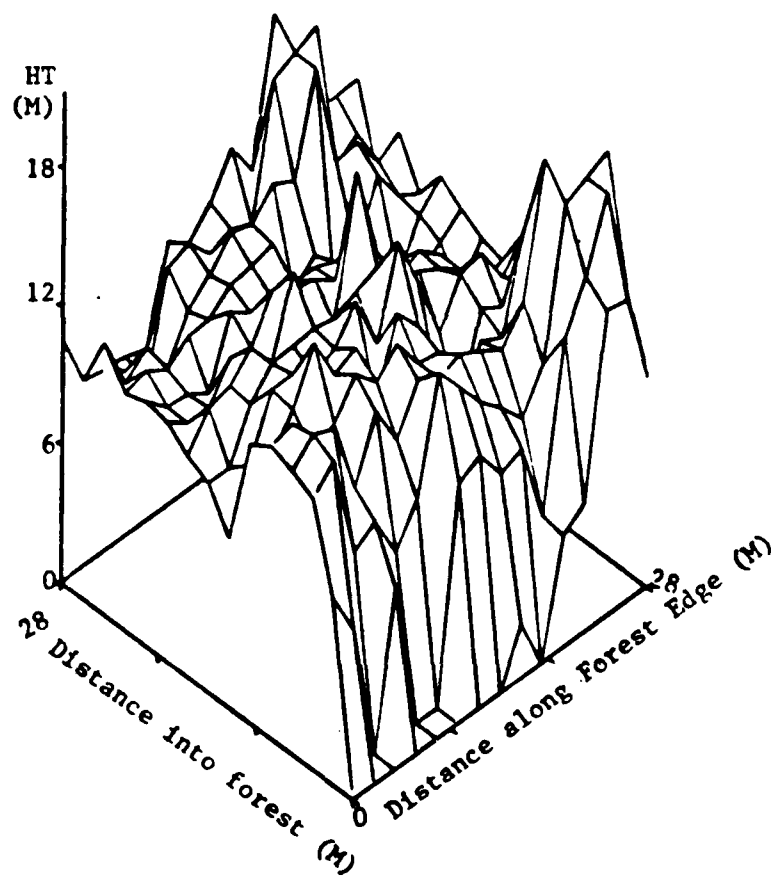


Figure 2.6. Three dimensional plot of the canopy surface.

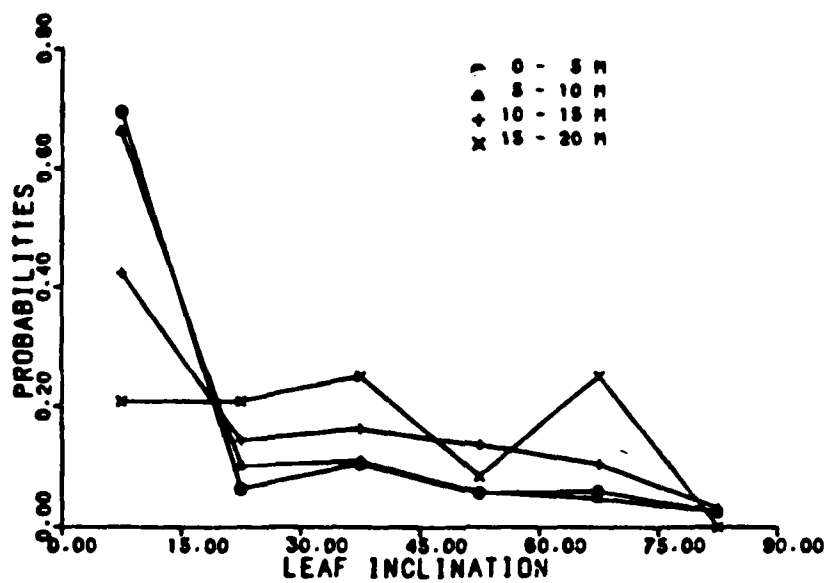


Figure 2.4. Leaf inclination angle distribution for Red Maple.

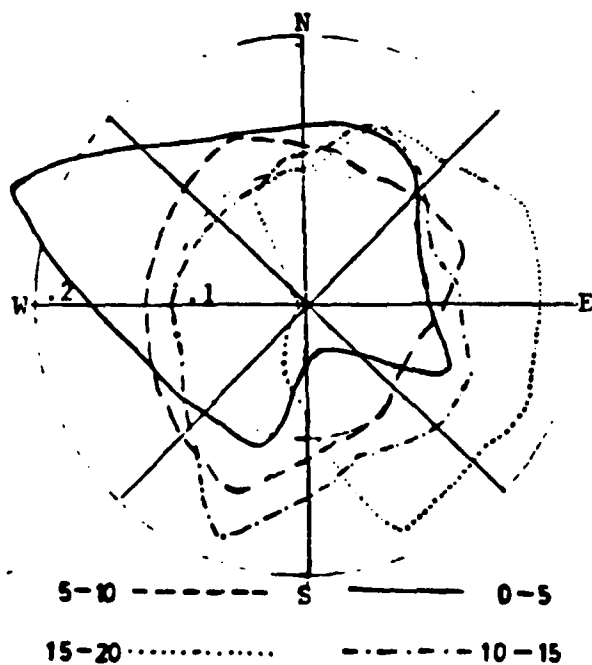


Figure 2.5. Leaf azimuth angle distribution for Red Maple.

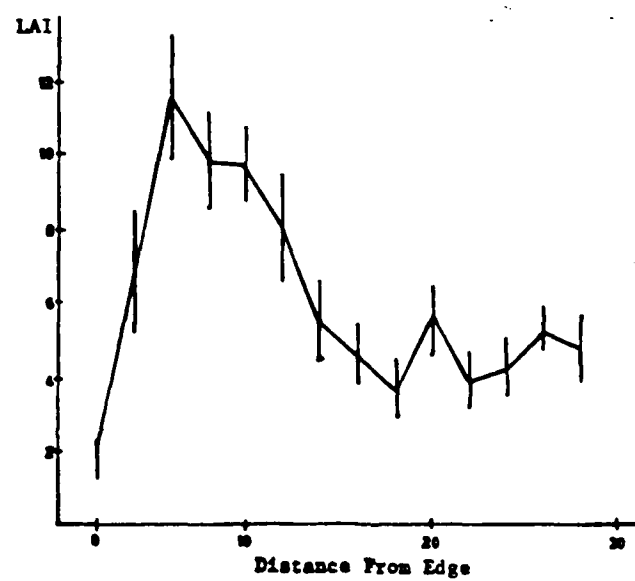


Figure 2.3. LAI variation from the stand edge to inside the stand.

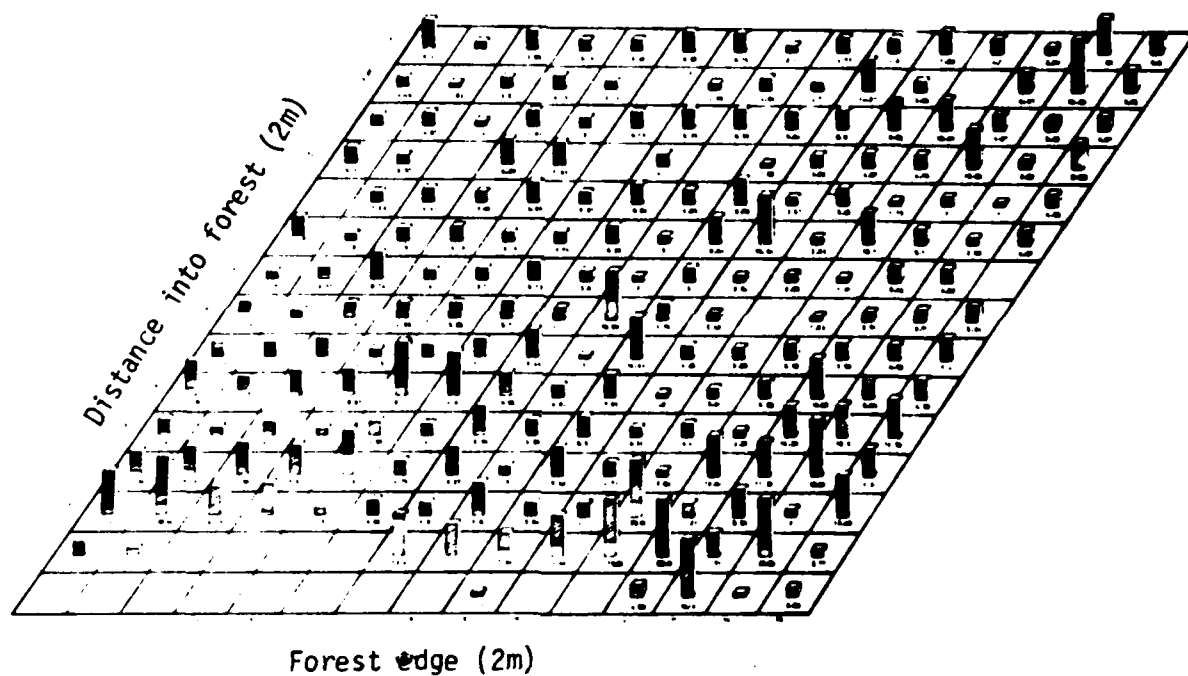


Figure 2.2. LAI distribution in the experimental plot.

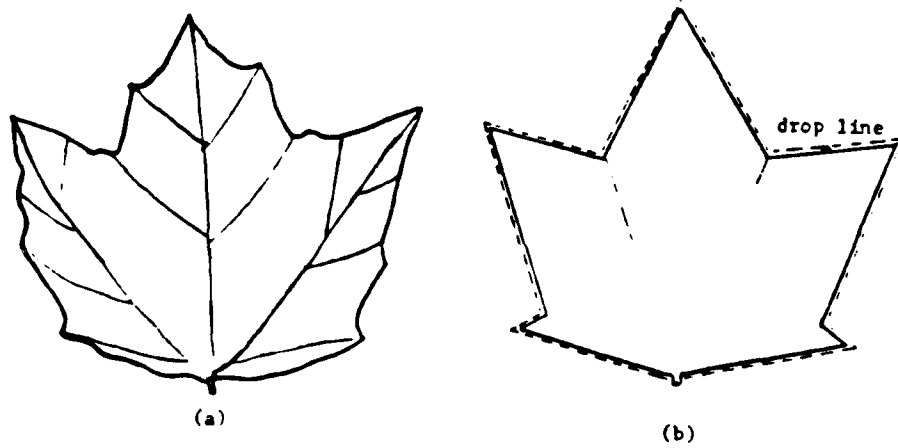


Figure 2.1 Average maple leaf (a) and idealized maple leaf (b). 75% of actual size.

LITERATURE CITED

- Finnigan, J.J., 1979. Turbulence in Waving Wheat, II. Structure of Momentum Transfer. Bound. Layer Meteorol. 16:213-236.
- Fox, R.D., R.D. Brazee, W.R. Alvey, W.R. Boyers, and A.W. Swank, 1980. A Data Management System for Studying Wind Profiles in Orchard and Field Crops. Trans. ASAE 23(4):578-984.
- Horst, T.W., 1973. Corrections for Response Errors in a Three-Component Propeller Anemometer. J. of Appl. Meteorol., 12:716-725.
- Jorgensen, F.E., 1982. Characteristics and Calibration of a Triple-Split Probe for Reversing Flows. DISA Information No. 27, pp. 15-22.
- Larsen, S.E. and N.E. Busch, 1974. Hot-Wire Measurements in the Atmosphere. Part I. Calibration and Response Characteristics. DISA Information No. 12, pp. 15-34.
- Lin, J.D., D.R. Miller, Z.J. Li and S.F. Sun, 1985. Three-Dimensional Hot Film Sensors for Turbulent Flow Measurements in Plant Canopies. 17th Conf. Agr. and Forest Meteorology, American Meteorological Society, Scottsdale, Ariz., pp. 183-184.
- Lumley, J.L. and H.A. Panofsky, 1964. The Structure of Atmospheric Turbulence. J. Wiley, N.Y.
- Miller, D.R. and J.D. Lin, 1985. Canopy Architecture of a Red Maple Edge Stand Measured by a Point Drop Method. In: ed. by Hutchison, B.A. and B.B. Hicks. The Forest-Atmosphere Interaction, pp. 55-70. D. Reidel Co.
- Shaw, R.H., J. Tavanger and D.P. Ward, 1983. Structure of the Reynolds Stress in a Canopy Layer. J. Clim. Appl. Meteorol., 22:1922-1931.
- Shaw, R.H., 1985. On Diffusive and Dispersive Fluxes in Forest Canopies. In: the Forest Atmosphere Interaction, ed. by B.A. Hutchison and B.B. Hicks, pp. 407-419.
- Wang, Y.S., 1985. Quantification of a Red Maple Forest Canopy. M.S. Thesis, Renewable Natural Resource Department, University of Connecticut, Storrs, CT 77 pp.
- Watson, G.S., 1971. Trend Analysis. J. Inter. Assoc. Mathemetical Geology. 3(3):215-226.

different levels and locations.

4. Make a survey of the flow pattern in the "stagnation" region in front of the leading edge and through the edge toward the interior region.
5. Measure the static pressure in front and inside the edge to correlate with the wind.

require extensive software support, but should give accurate field measurements at low wind velocities with high turbulence intensity inside the canopy.

4. The WOES has been calibrated and showed good responses at low wind velocities. Its compatibility with a tri-diagonal hot film probe is being evaluated.
5. The characteristic frequency of the site in velocity component spectra appears to be in the neighborhood of 1 Hz.
6. The conditional analysis shows that the ejection- sweeping mechanism of turbulent transport exists in the forest stand as observed in wind tunnels and in crops. However, this mechanism is considerably modified due to forest canopy structure, especially in the edge region when the wind enters the edge as indicated by the results from the corn-field fetch.
7. The energy spectra suggest that the canopy acts to filter out the mid-range turbulent eddies.
8. The uw cospectra show the expected momentum sink in the crown region.

The following programs are planned for this year:

1. Continue to survey the turbulence characteristics in the roughness sublayer over the canopy for a larger range of wind speeds for both the corn- field fetch and forest fetch cases.
2. Obtain more thorough samples of vertical profiles inside the canopy using an array of the 3-D sensors.
3. Sample horizontally and vertically inside the canopy with sensor arrays to determine the spatial variability at

$$T_{i,H} = \lim_{T \rightarrow \infty} \int_0^T \delta_{ij}(t;H) dt \quad (5.3)$$

Two sets of data were analyzed using the above equations. Figures 5.7a,b show $S_{i,H}$ is a function of H for the wind from the forest fetch at two levels above the canopy. Figures 5.8 a-e show data for the wind from the corn field fetch toward the edge at 5 levels above and inside the canopy. It is obvious that as the canopy is approached, the sweep or burst becomes dominant; however, it is much stronger than those in wheat and corn canopies as indicated by Finnigan (1979) and Shaw et al. (1983). With the corn field fetch, the presence of strong upward interaction might be due to the upward trend of the mean flow streamlines near the leading edge region in the canopy. Further investigations will be conducted when more data become available.

VI CONCLUSIONS AND FUTURE PLANS

For the purpose of this interim report, the following conclusions may be drawn for these preliminary studies:

1. The canopy surface geometry analysis indicates an overall characteristic length of about 6 m for the forest stand. The experimental plot consists of an edge region of 1 h, where the LAI is about double that of the interior canopy. The interior region has a fairly uniform LAI of 5.5.
2. The x-hot film sensors used in conjunction with a vane can give reasonable results of 3-D velocity components as long as the sensors are not too far away from the vane. This configuration may be useful in the region above the canopy.
3. The dual triple-split hot films are tedious to calibrate and

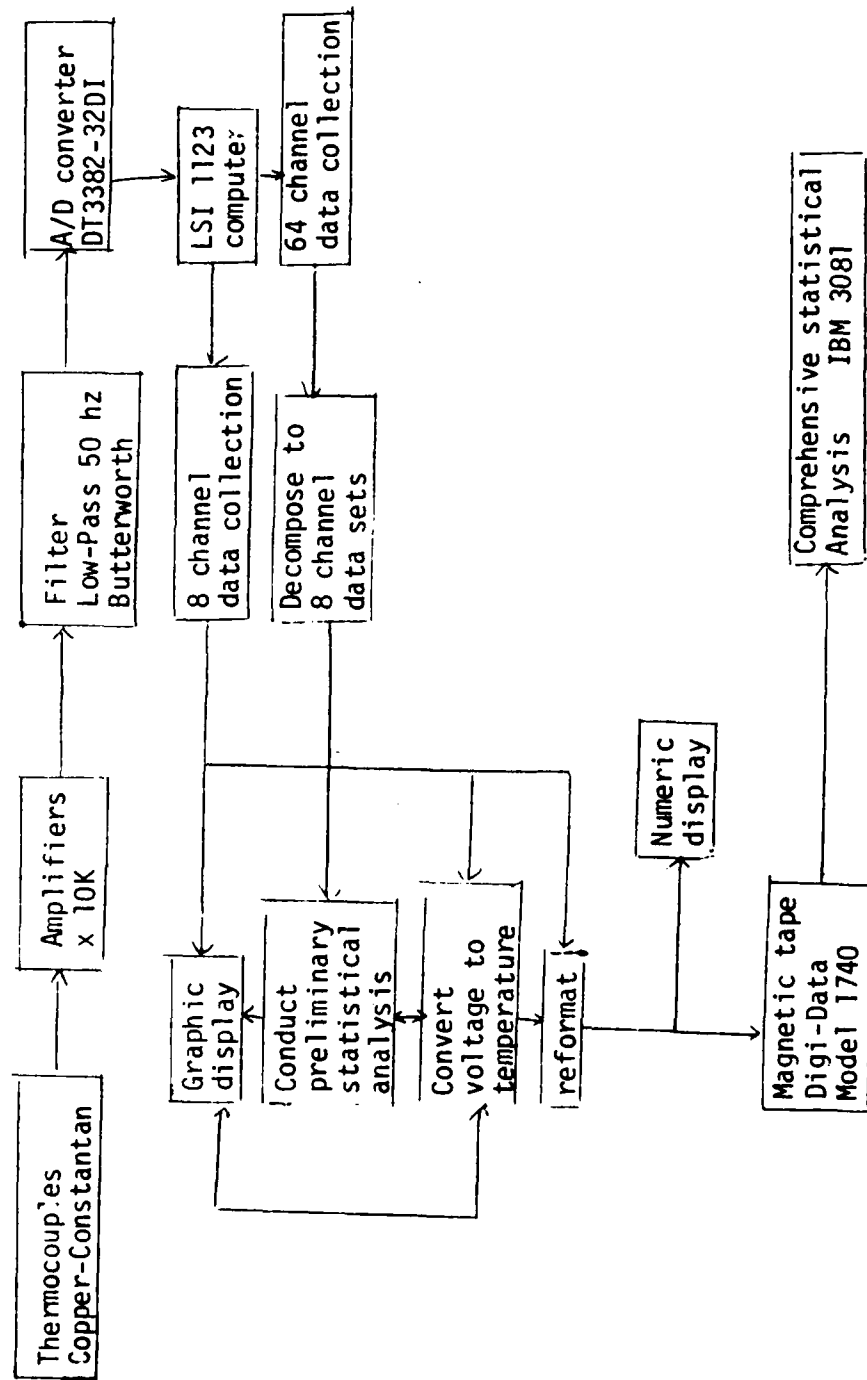


Figure 3.2. As figure 3.1 for the temperature sensor data.

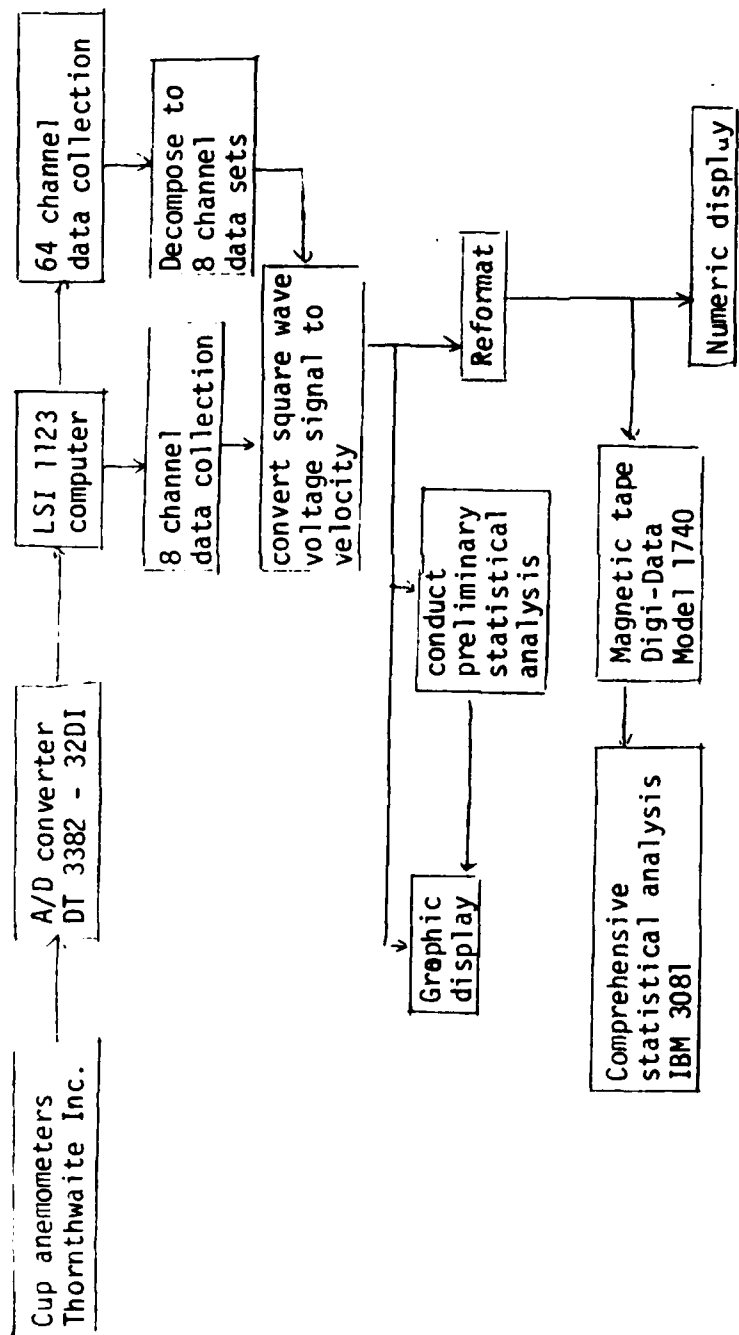


Figure 3.3. As figure 3.1 for the cup anemometers.

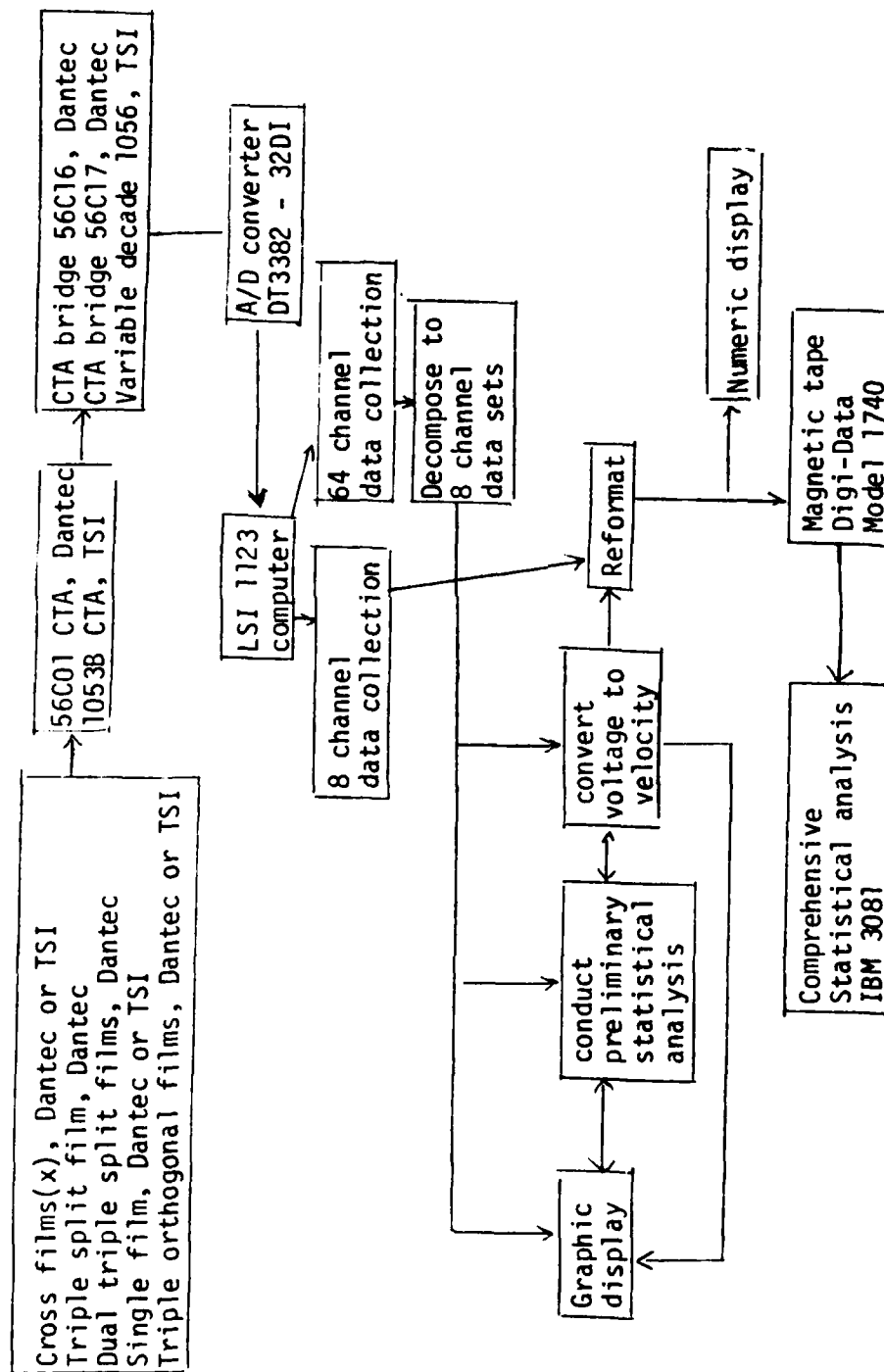


Figure 3.4. As figure 3.1 for the thermal anemometers.

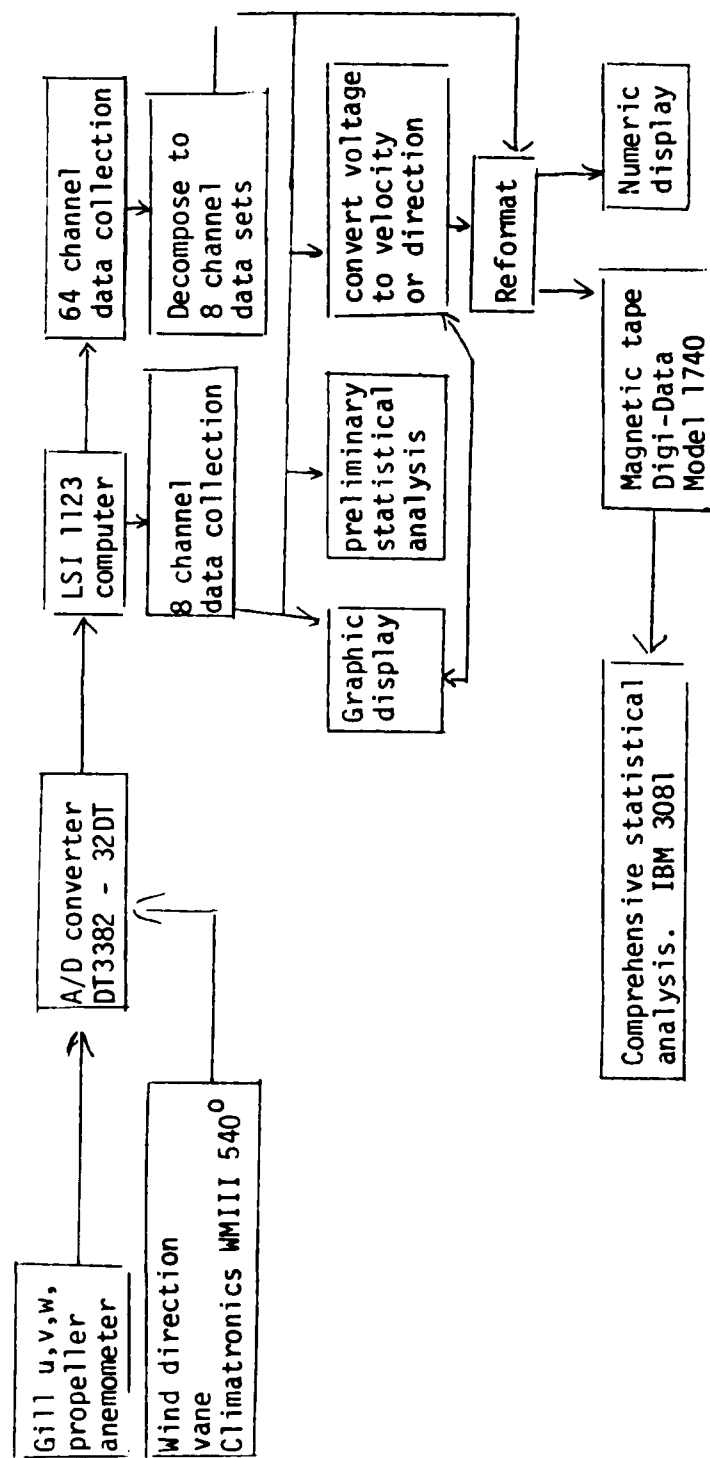


Figure 3.5. As figure 3.1 for the wind direction vane and the propeller anemometers.

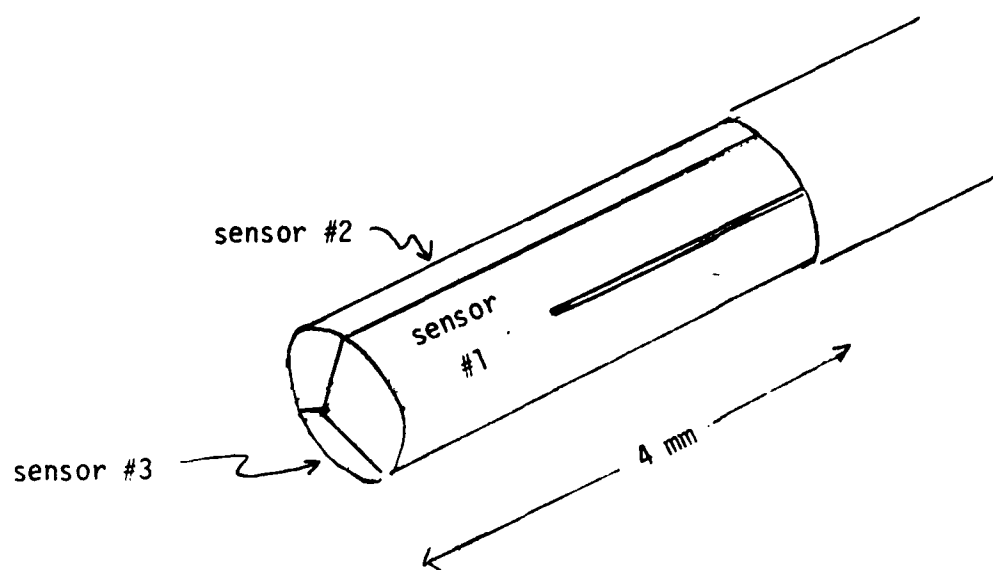


Figure 4.1. Triple-split hot film anemometer.

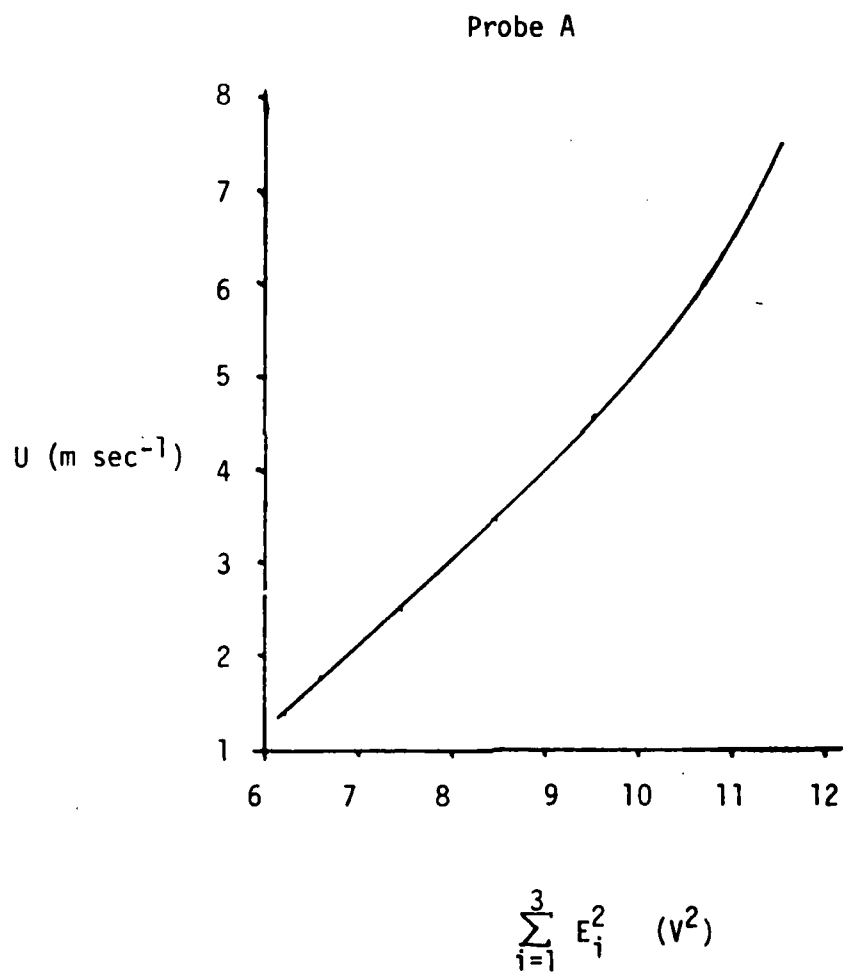
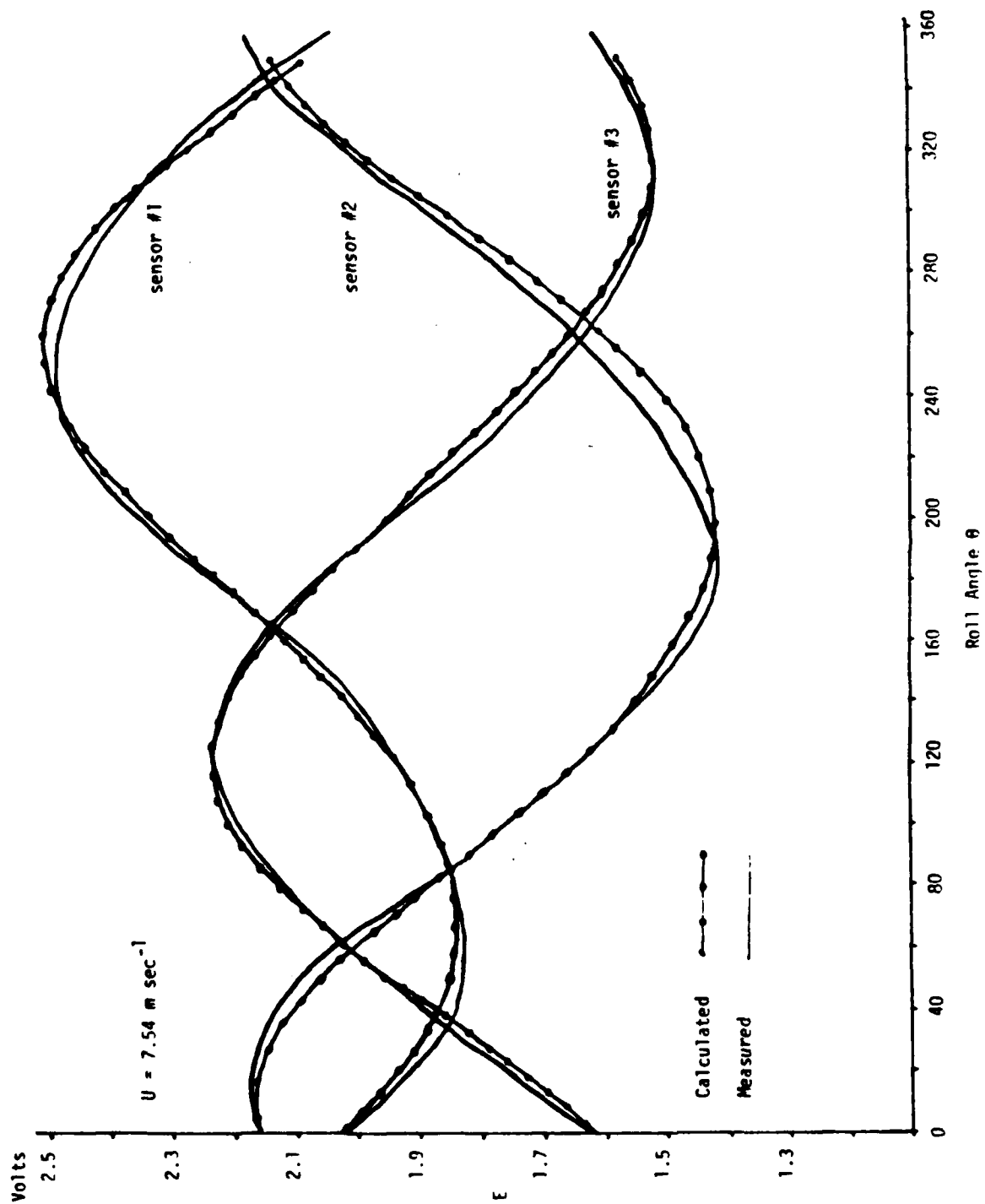


Figure 4.2. Sum of the squared sensor voltages as a function of wind speed for probe b.

Figure 4.3. Roll angle response of the three elements on probe b.



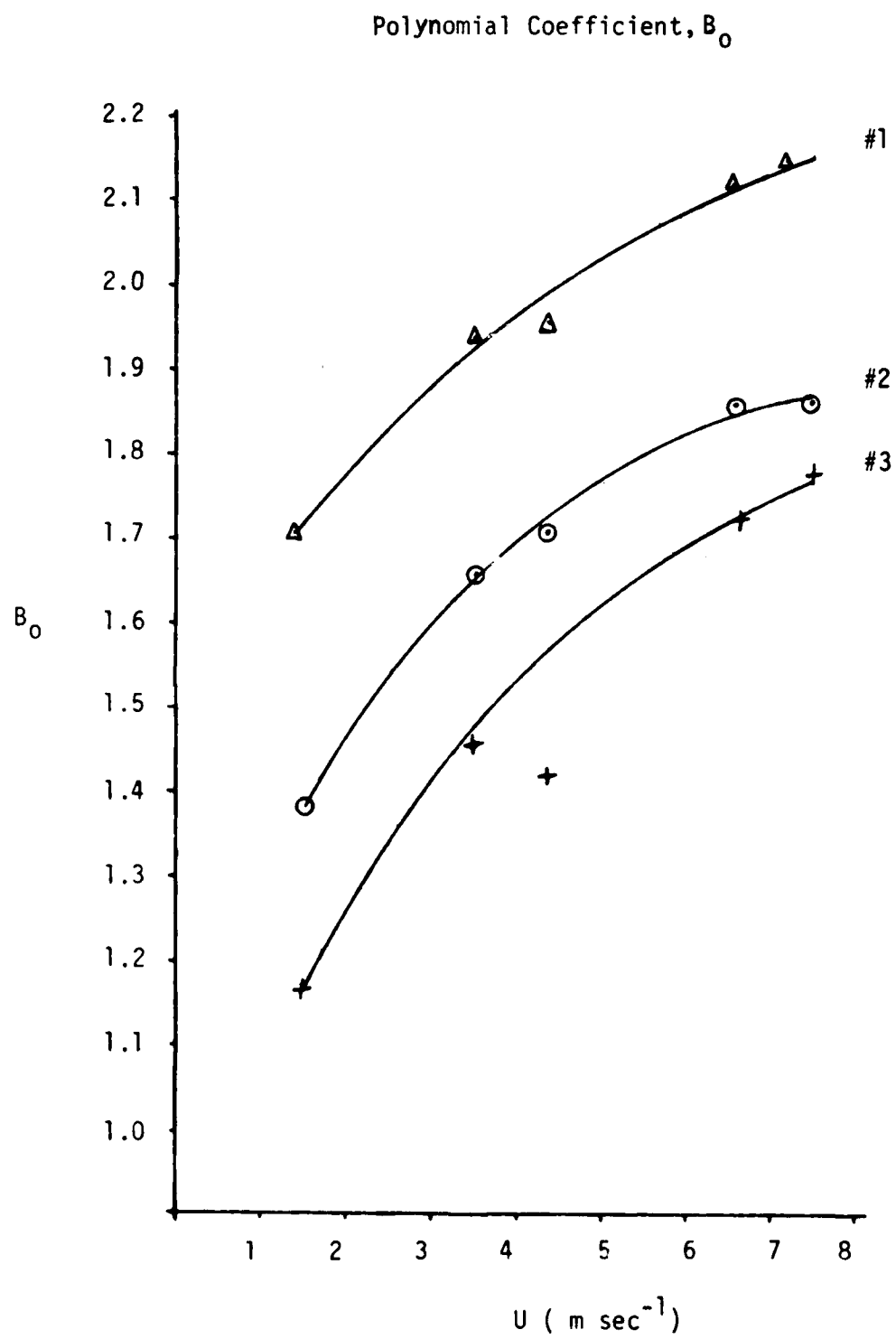


Figure 4.4 a. Polynomial coefficient B_0 as a function of wind speed.

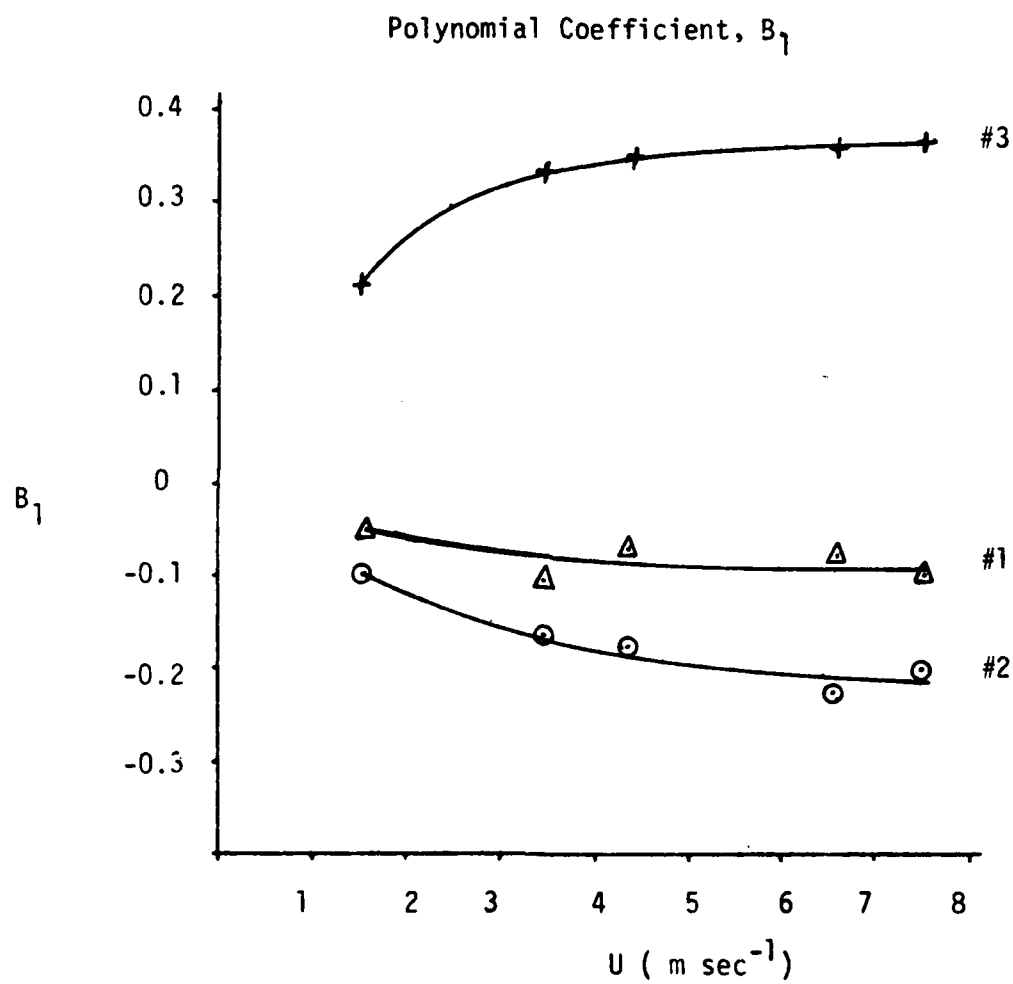


Figure 4.4 b. Polinomial coefficient B_1 as a function of wind speed.

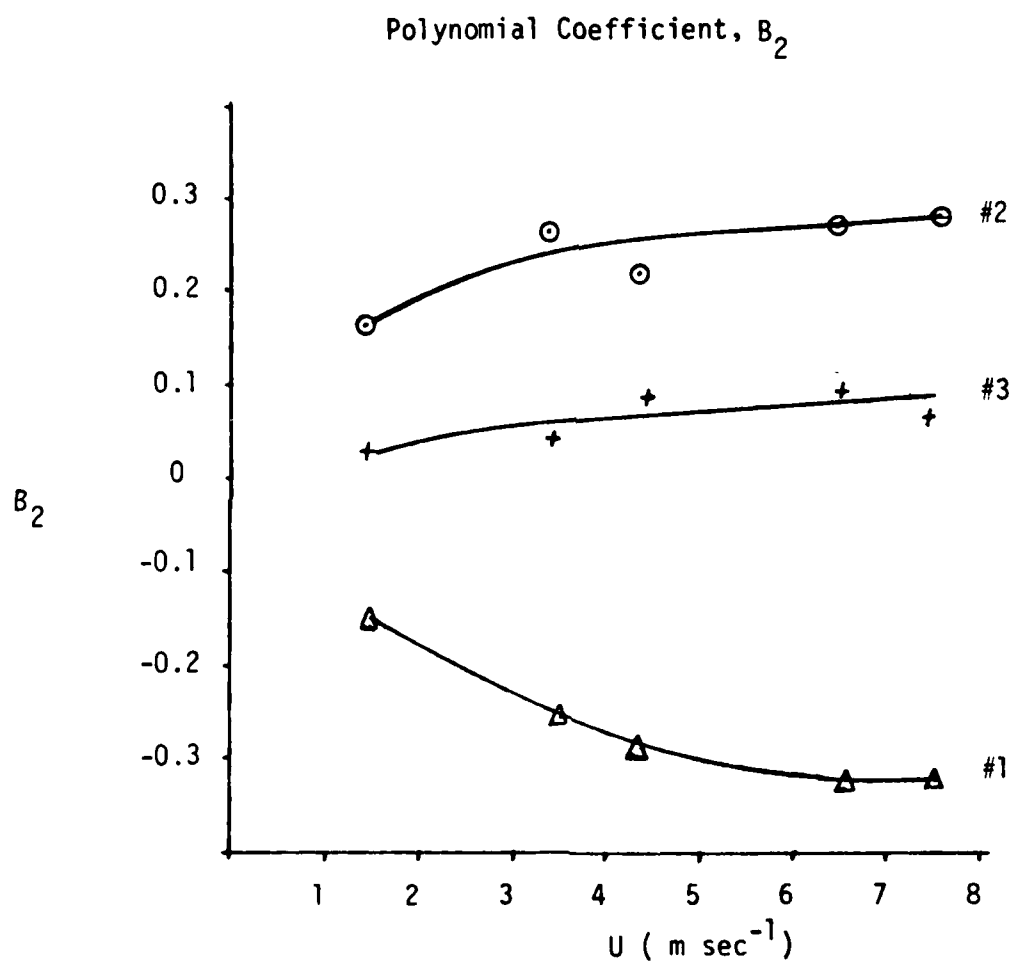


Figure 4.4 c. Polynomial coefficient B_2 as a function of wind speed.

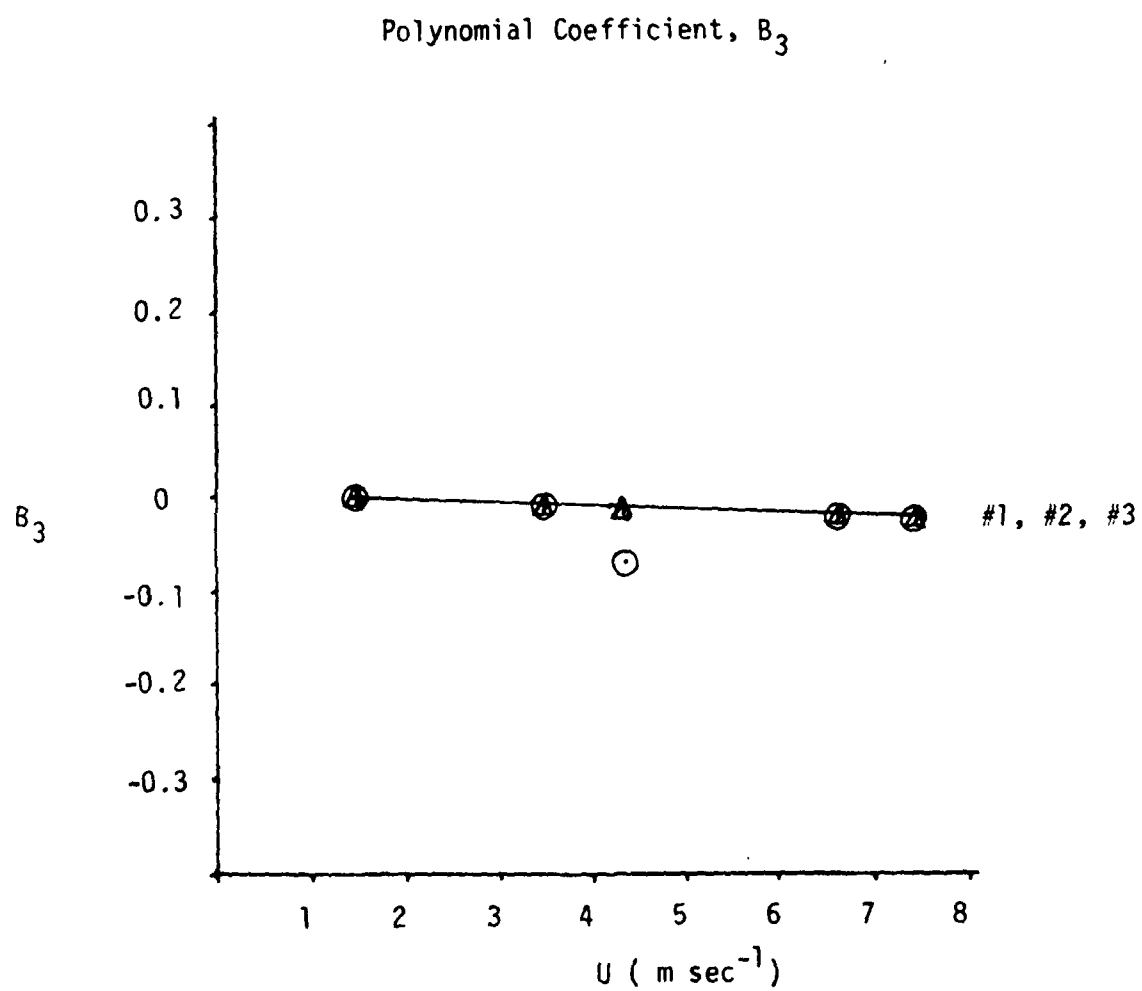


Figure 4.4 d. Polynomial coefficient B_3 as a function of wind speed.

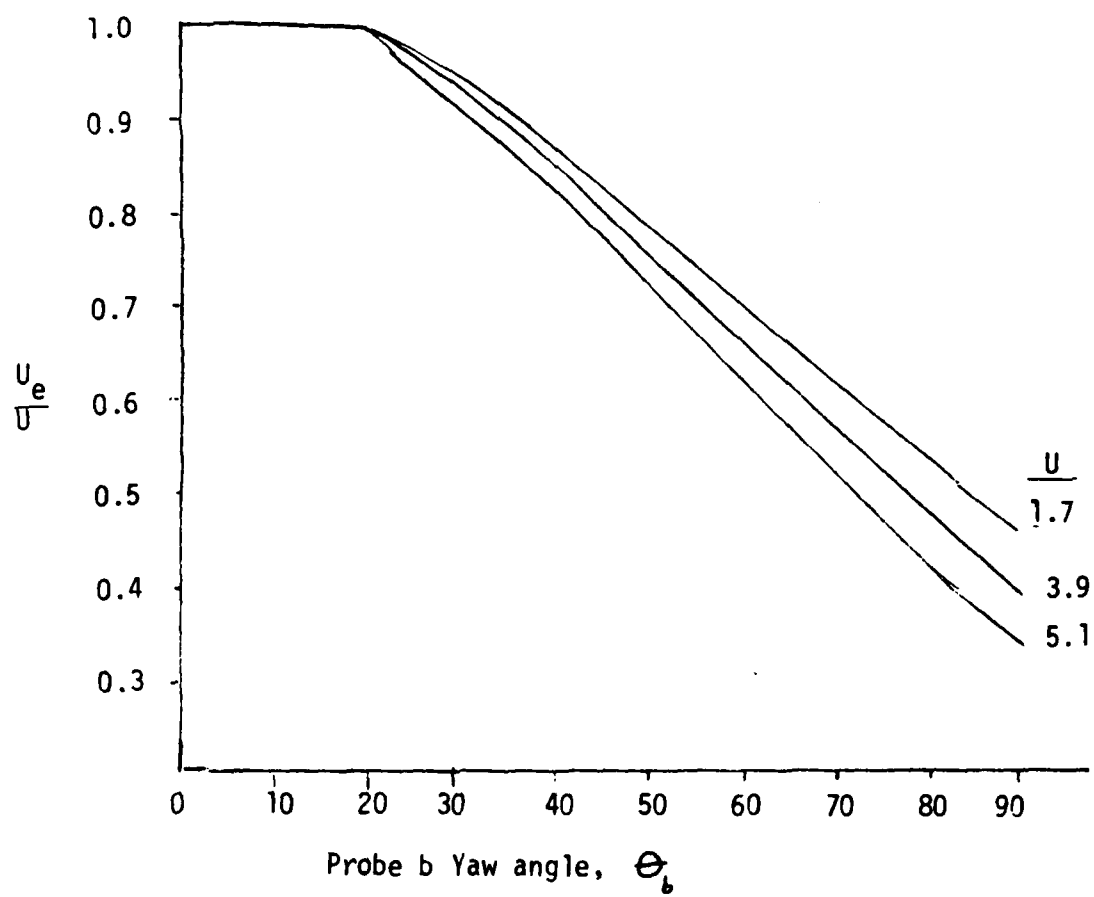


Figure 4.5. Yaw angle response of probe b.

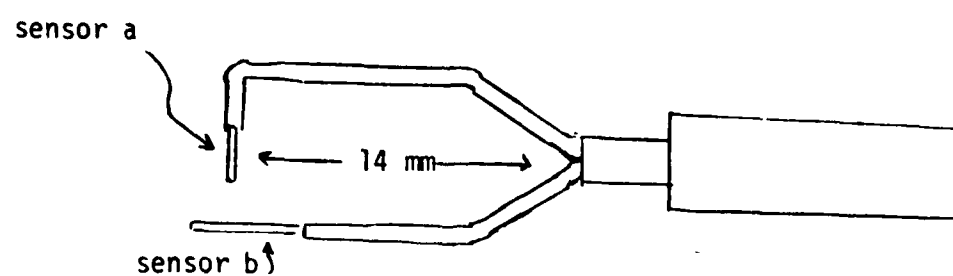


Figure 4.6. Two orthogonal triple-split hot film sensors mounted on a single holder.

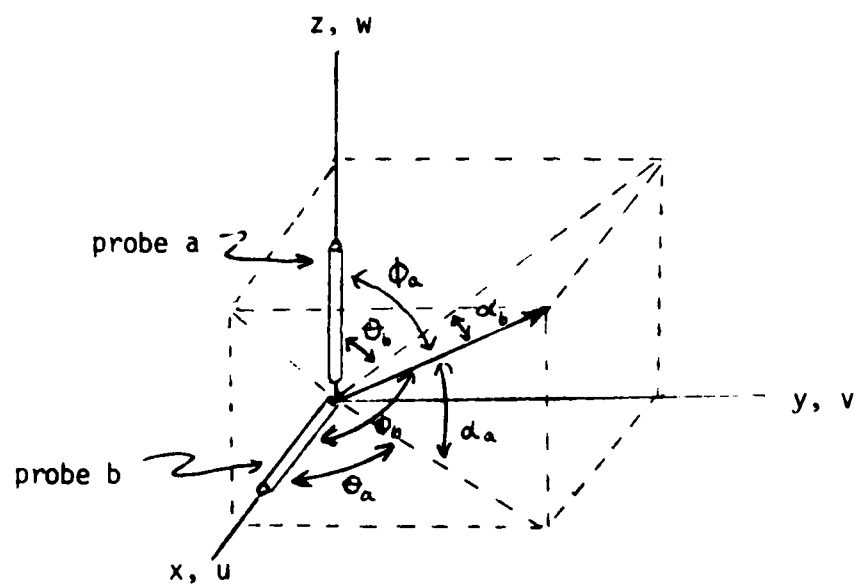


Figure 4.7. Coordinate system for dual triple-split hot films.

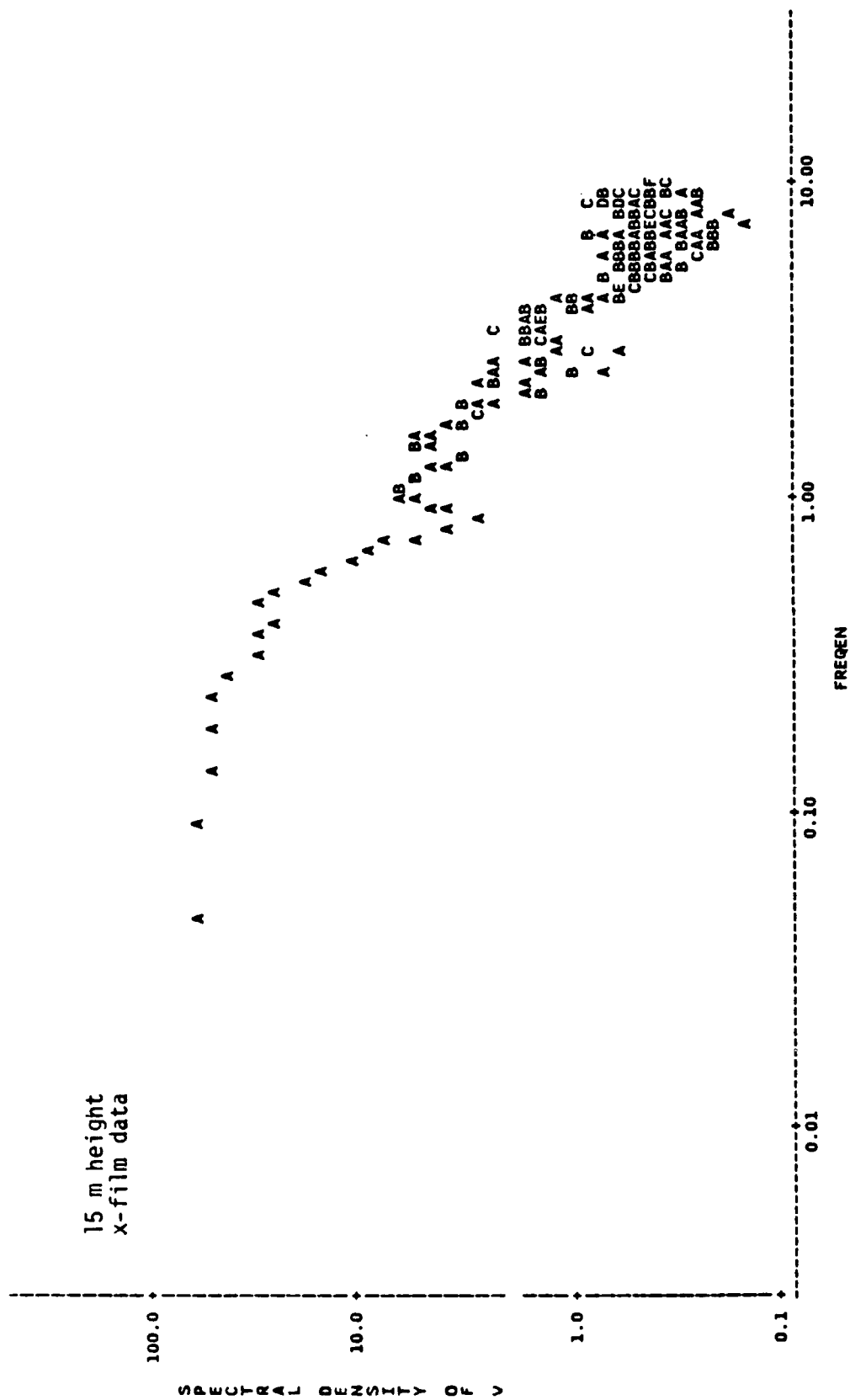


Figure 5.3. cont.

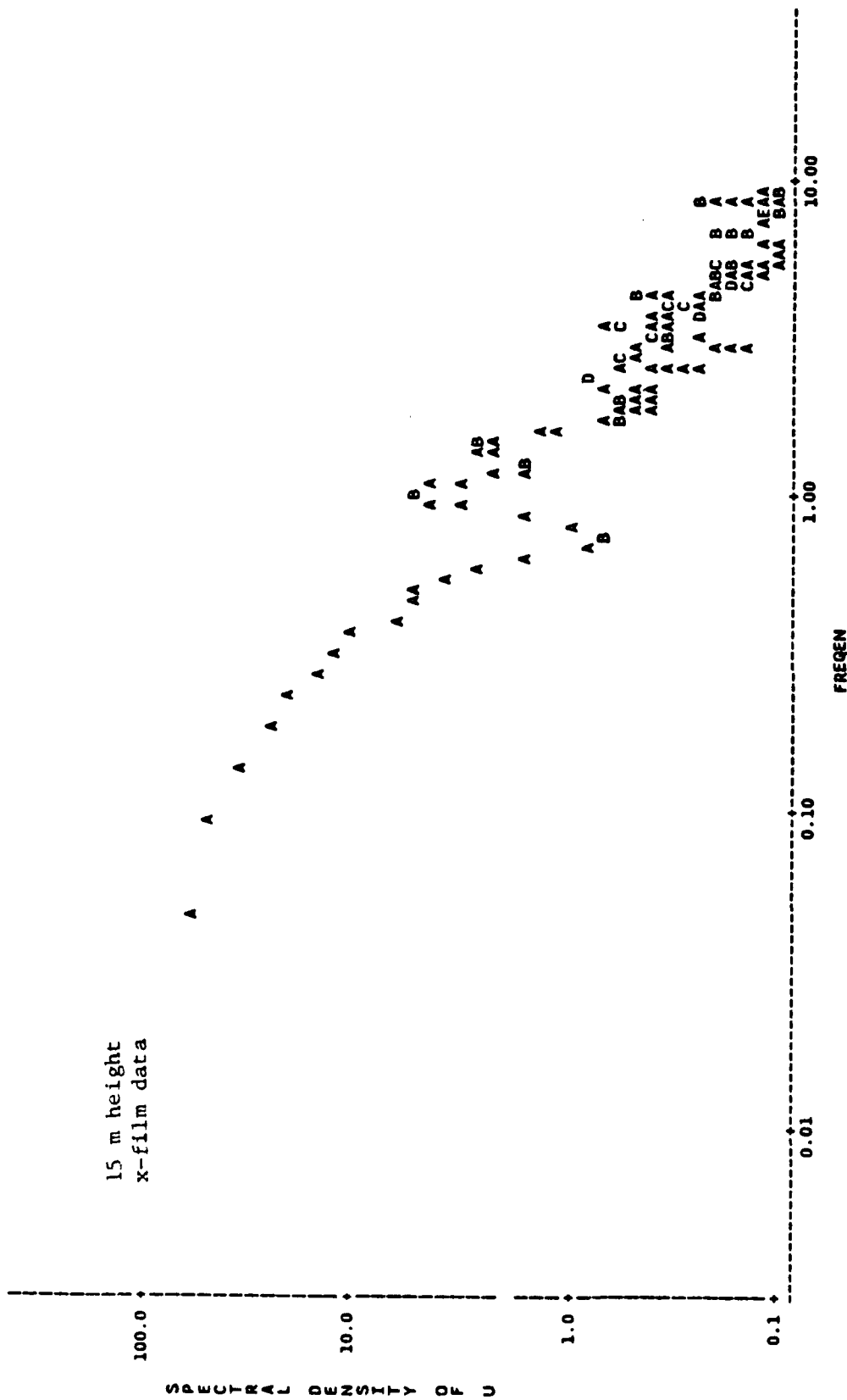


Figure 5.3 cont.

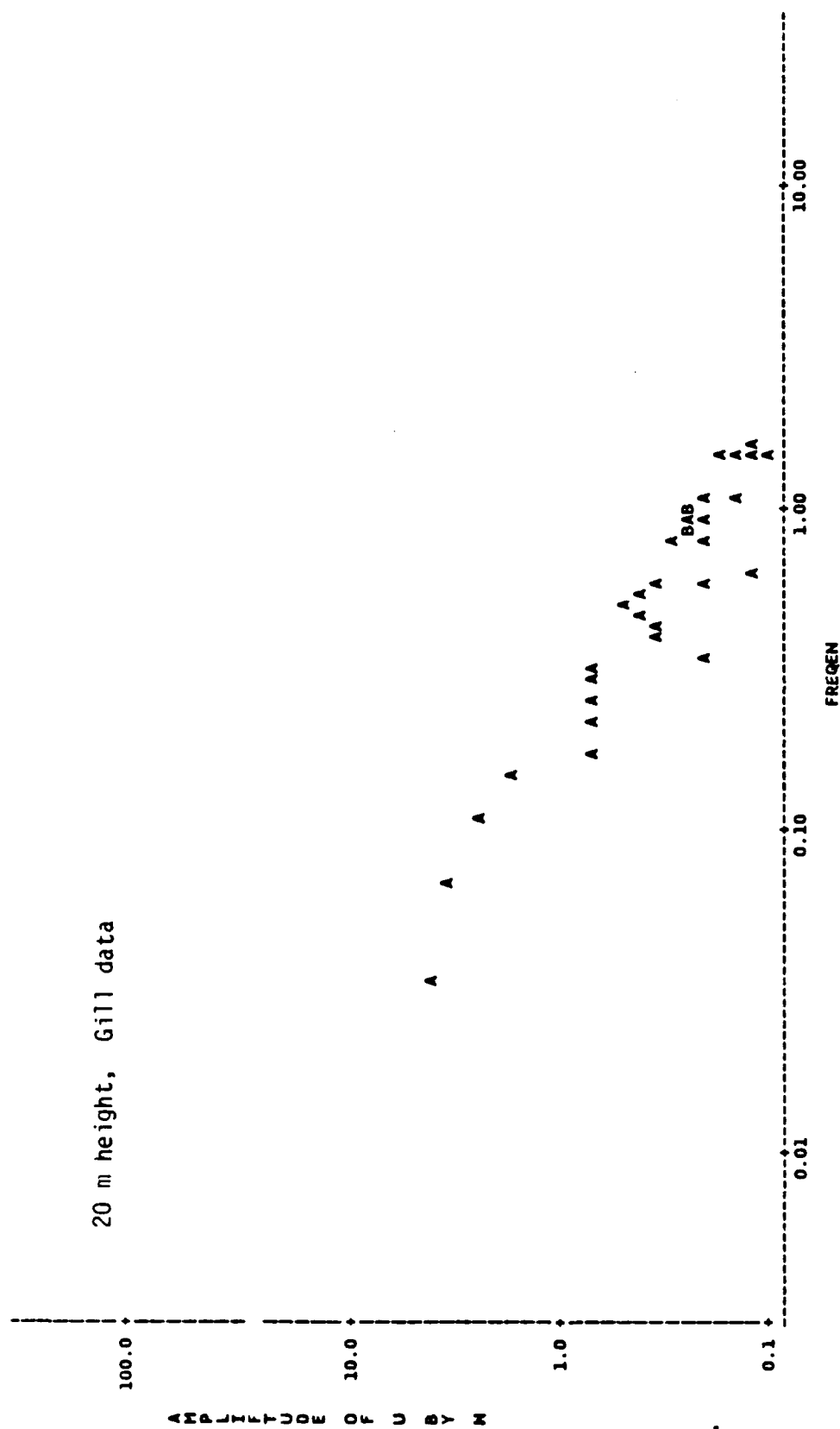


Figure 5.3. cont.

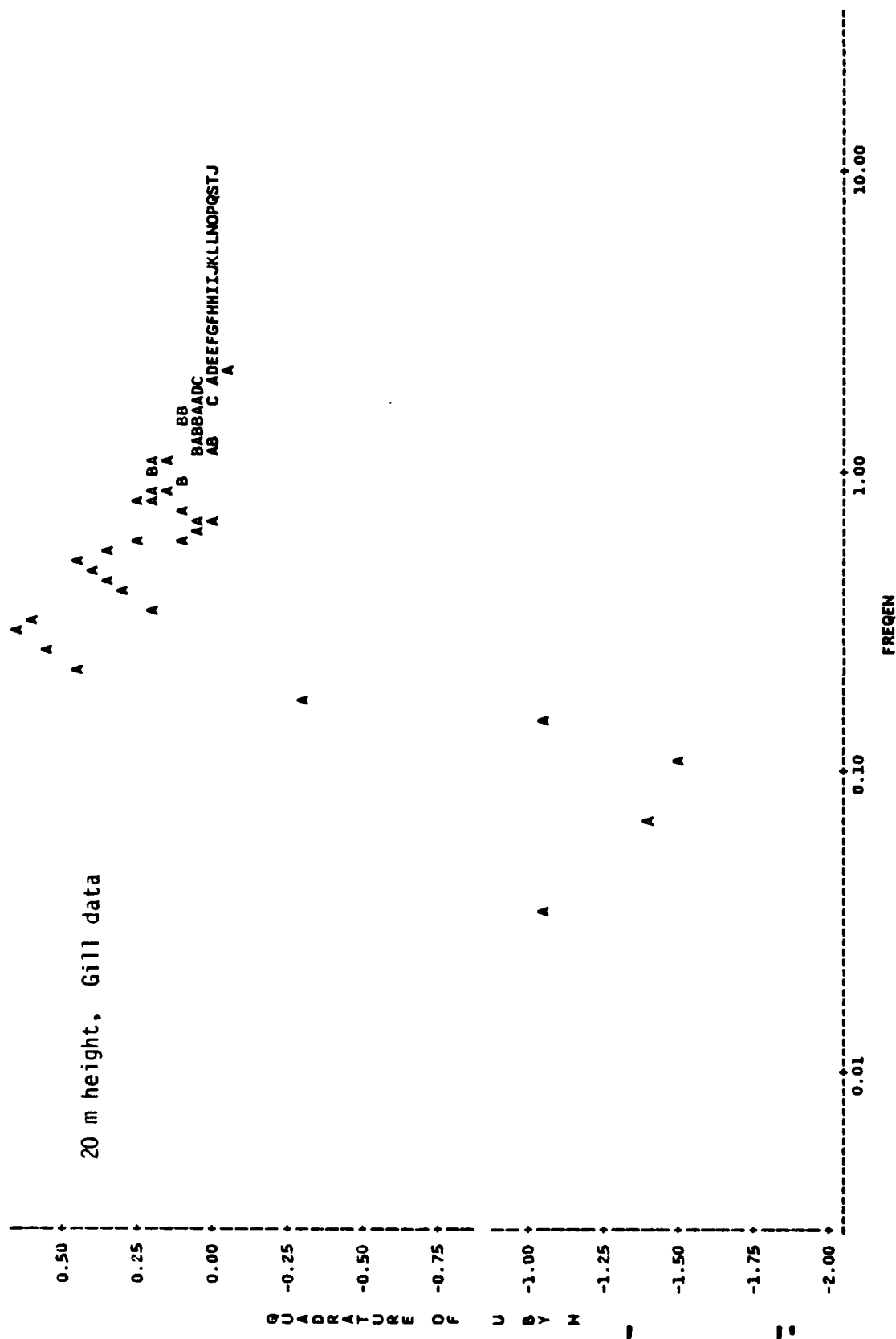


Figure 5.3. cont.

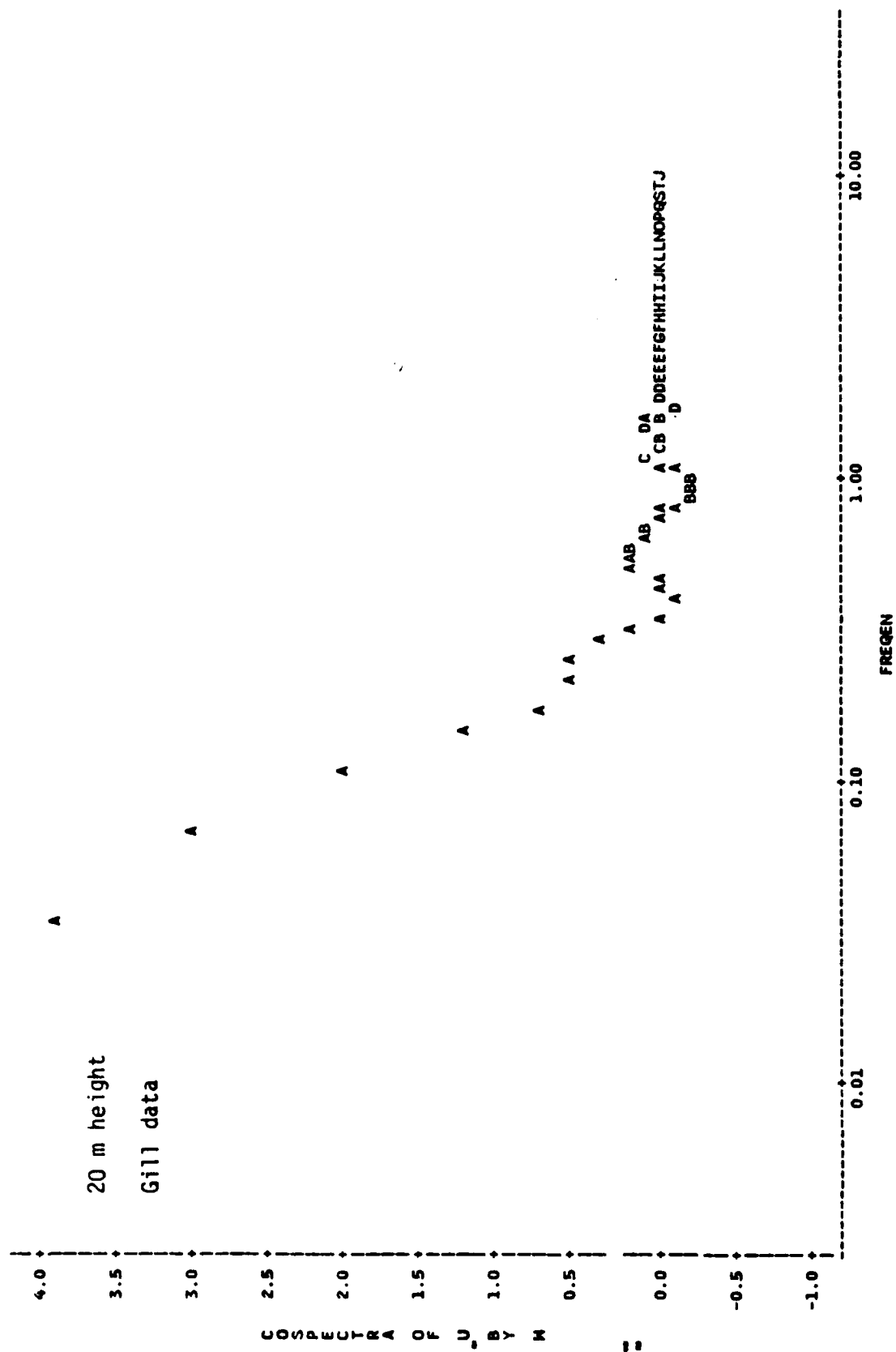


Figure 5.3. cont.

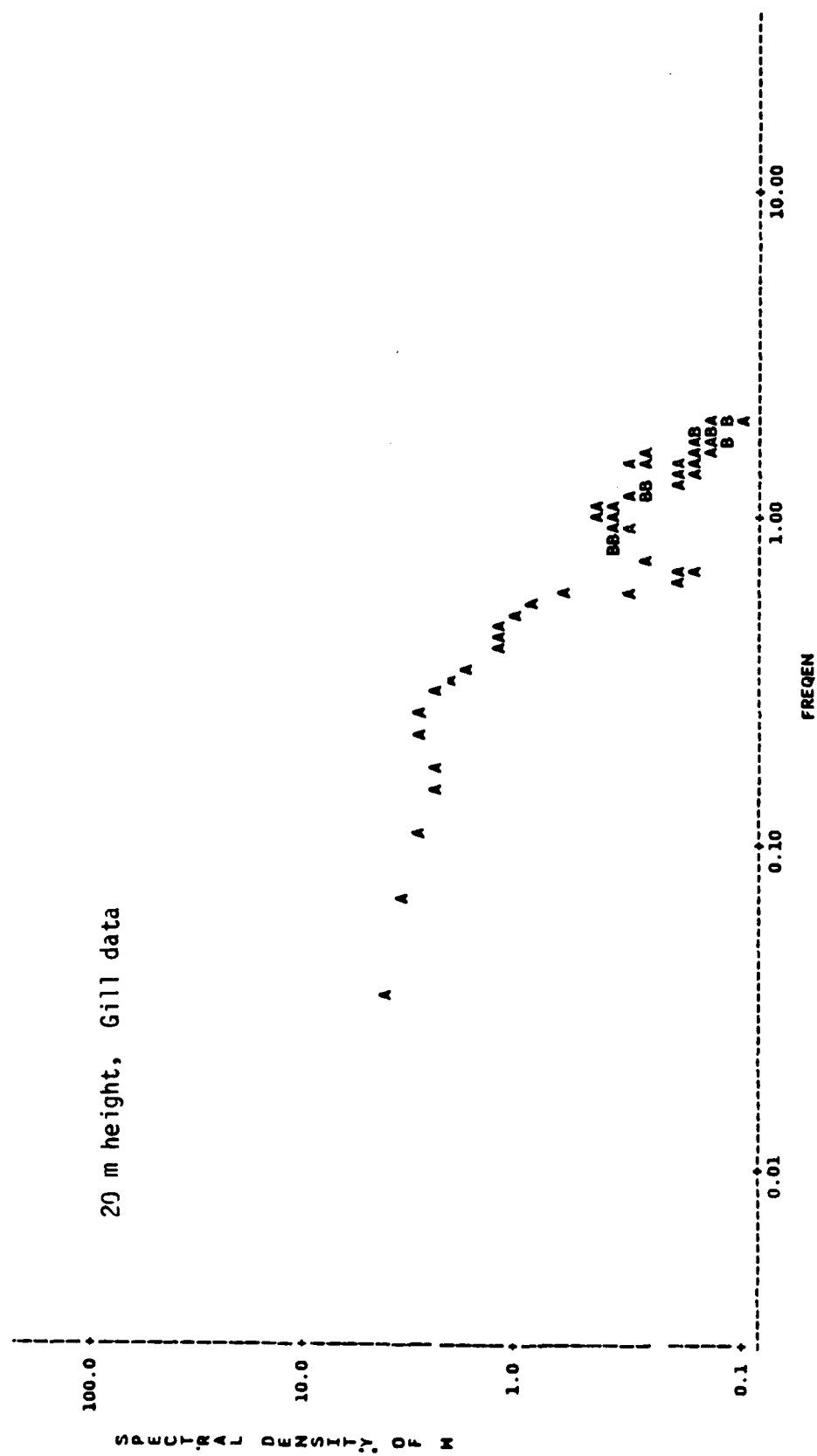


Figure 5.3. cont.

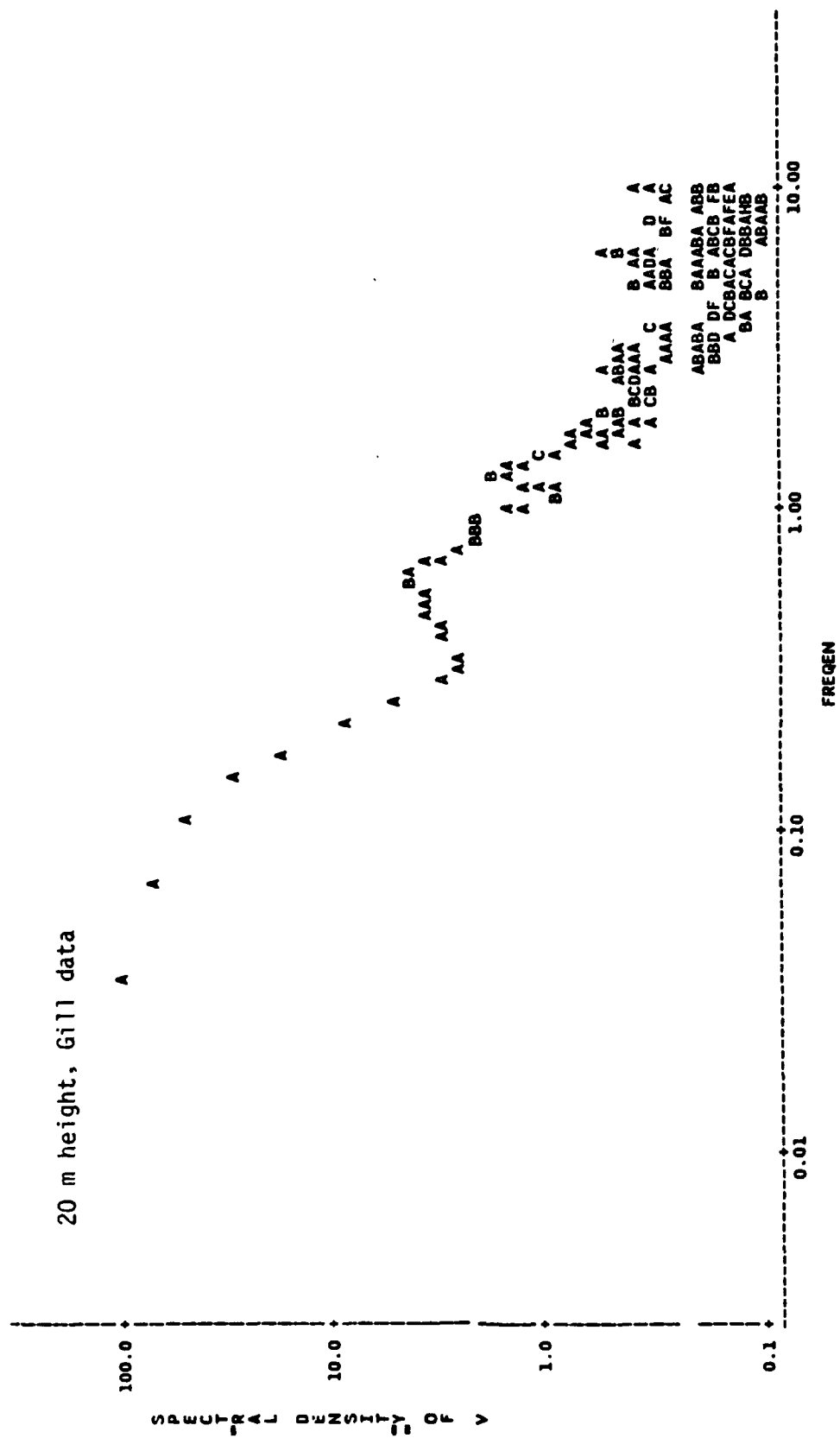


Figure 5.3. cont.

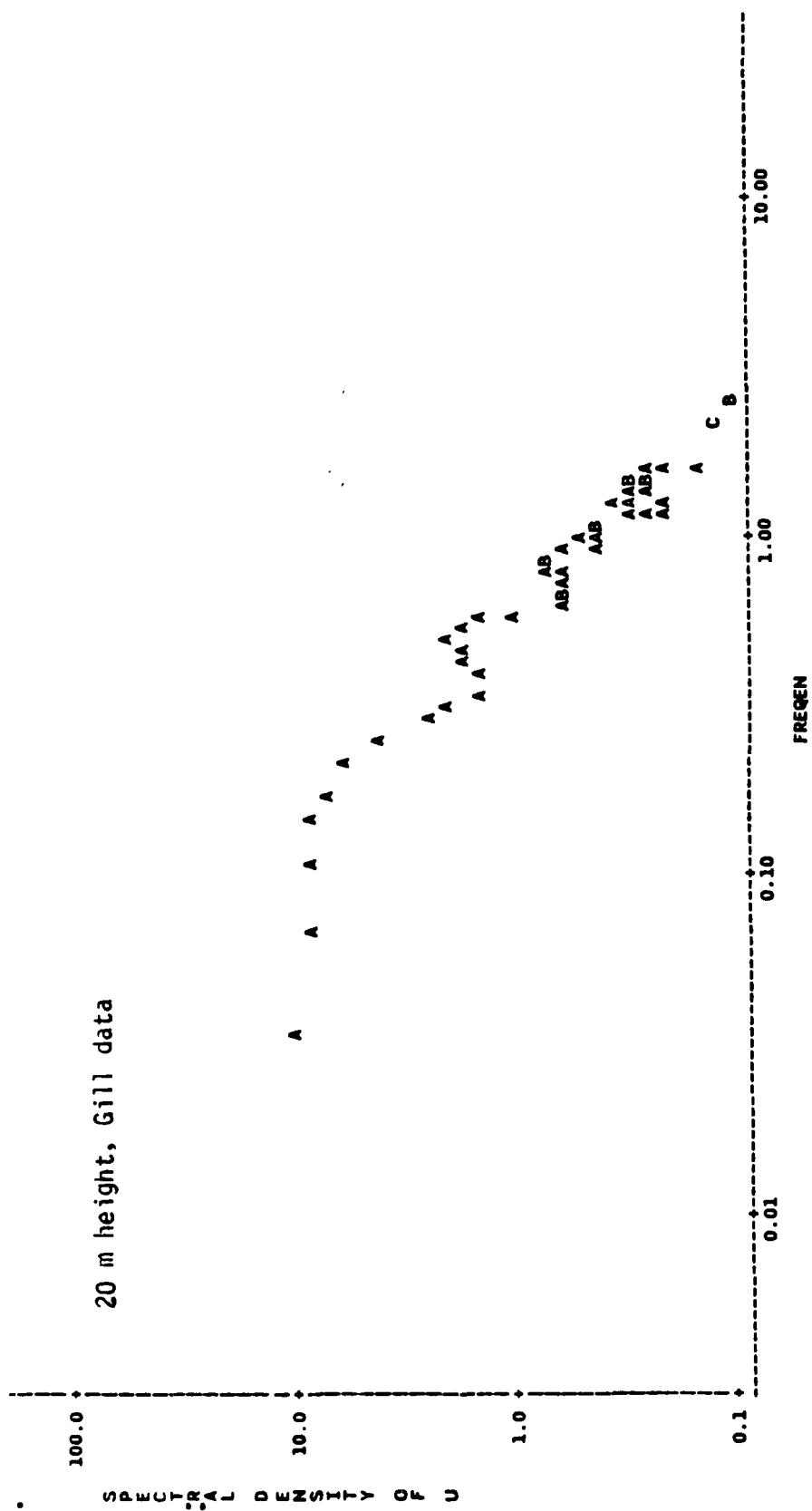


Figure 5.3. Spectra of the wind components, UW cospectra, UW quadrature spectra, and UW amplitude spectra from two levels above the canopy with the wind from a forest fetch.

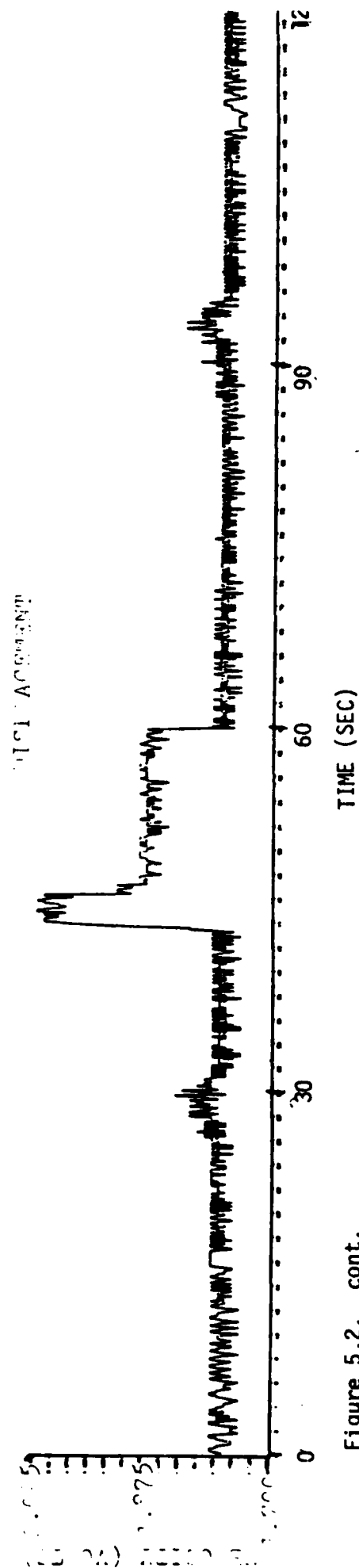
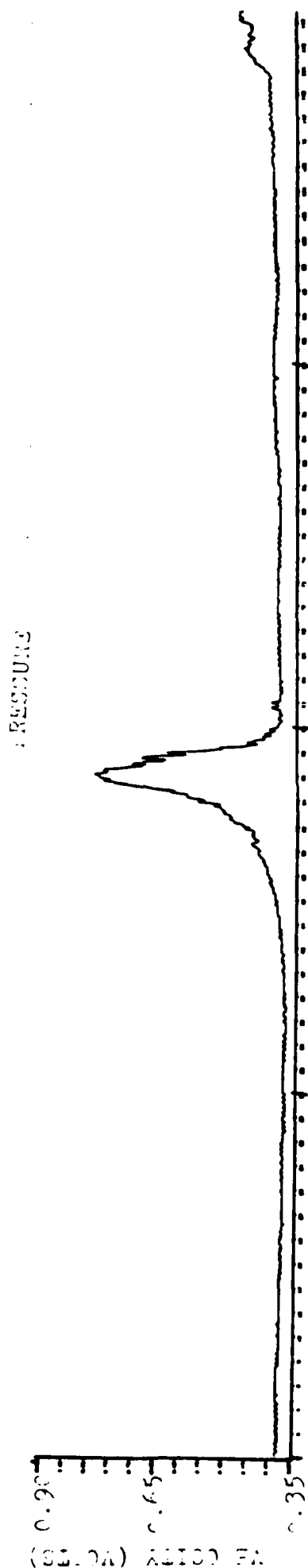
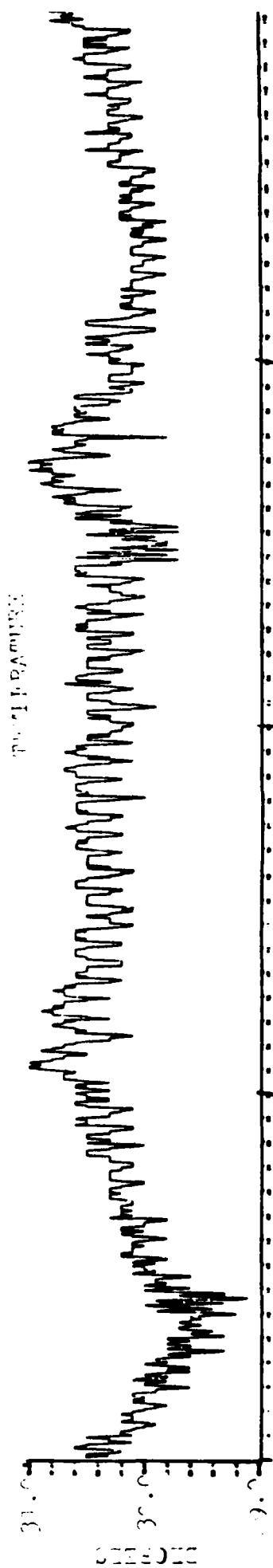


Figure 5.2. cont.

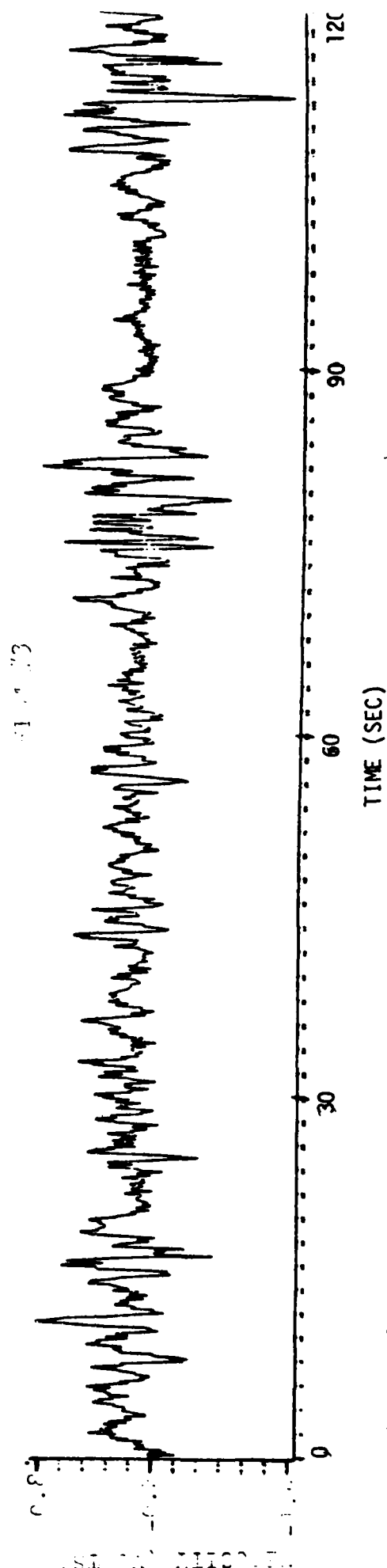
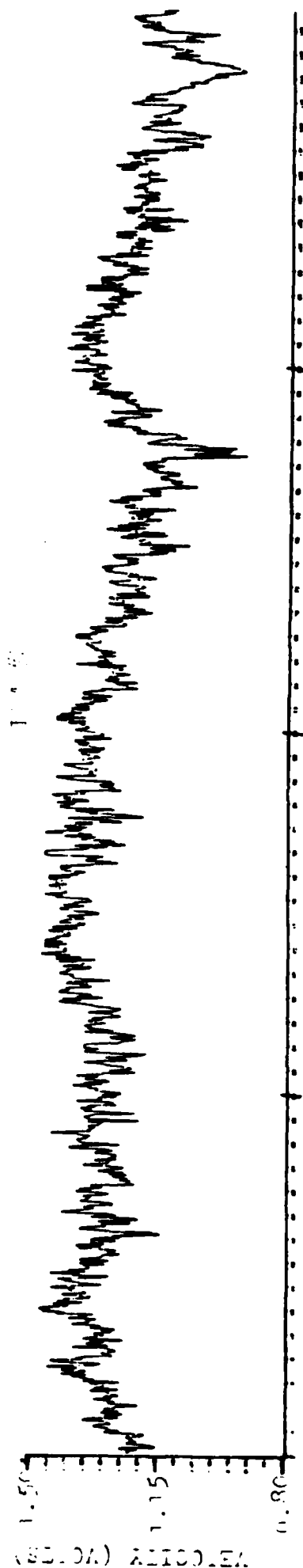
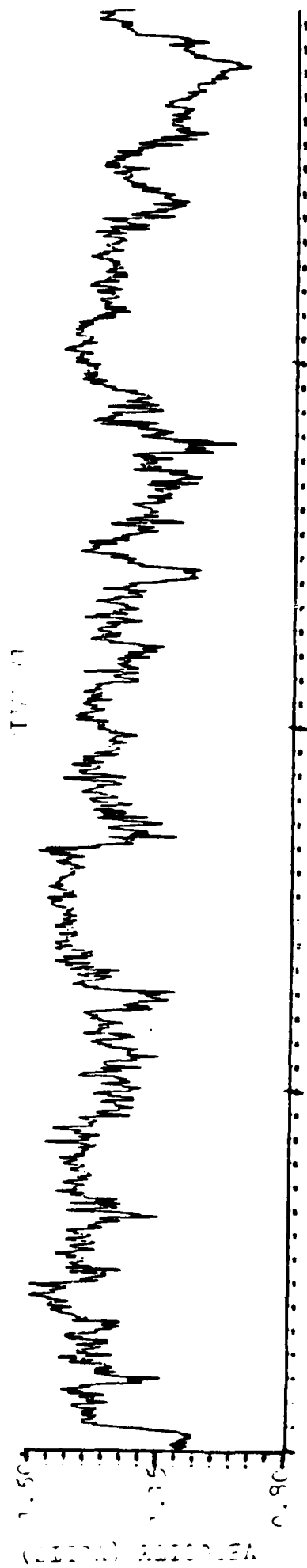


Figure 5.2. cont.

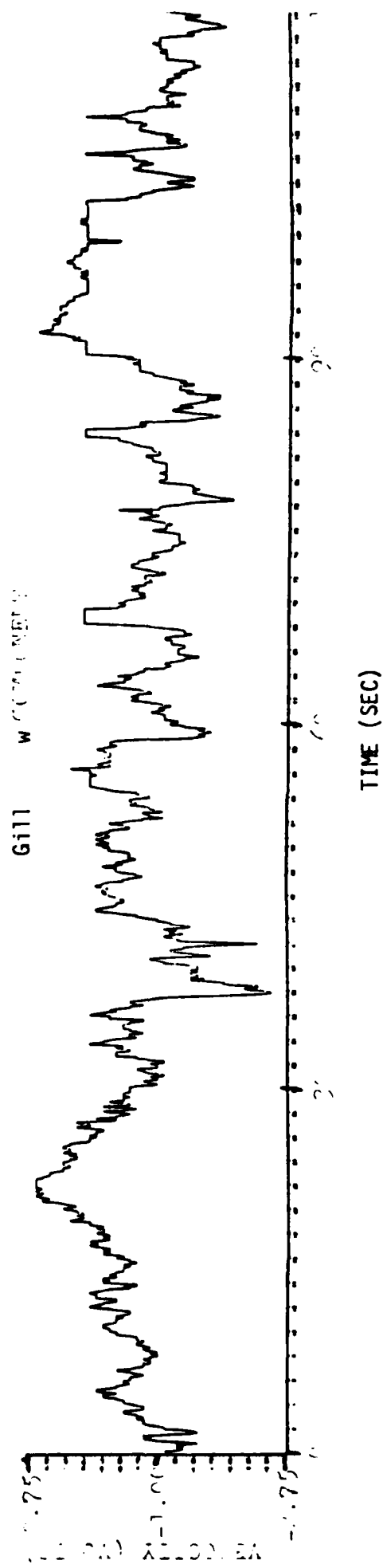
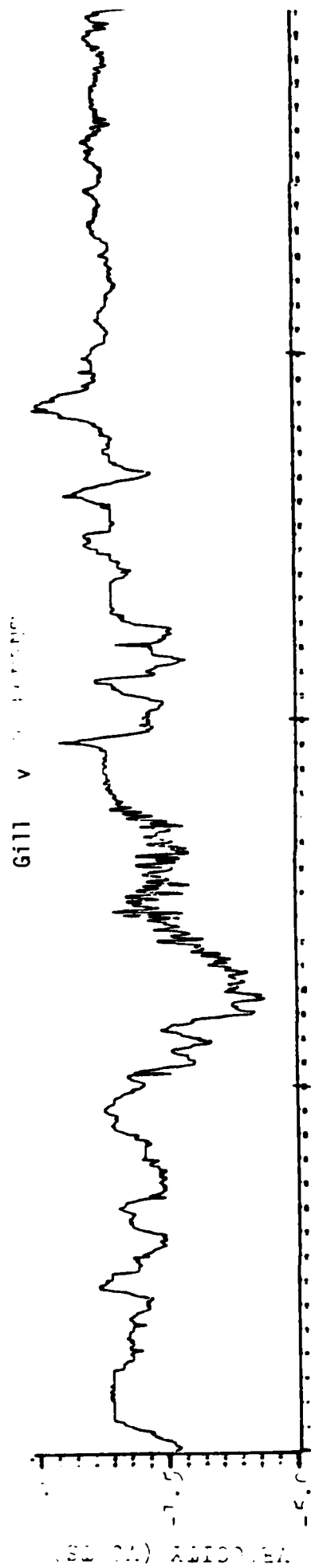


Figure 5.2. cont.

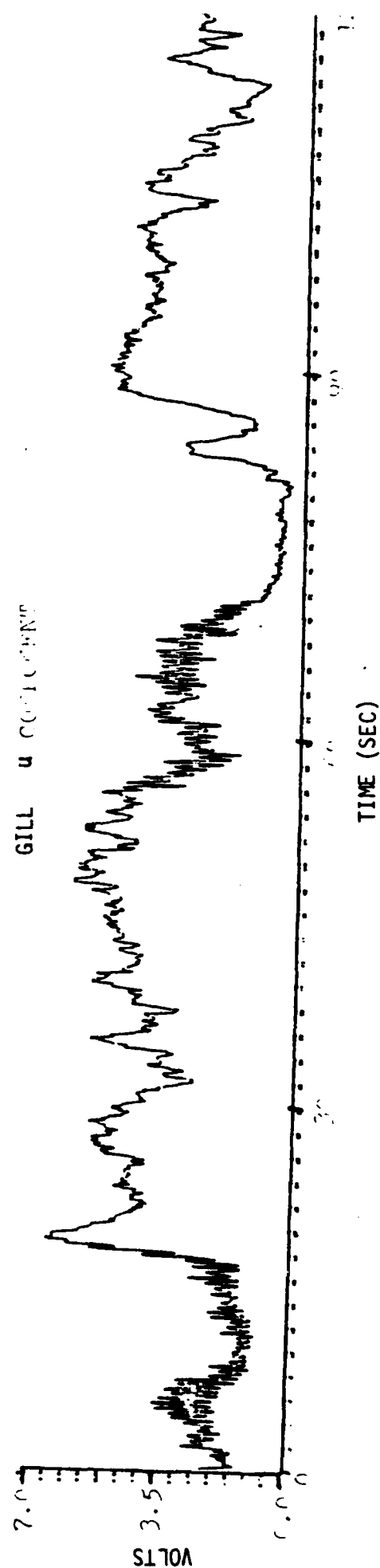
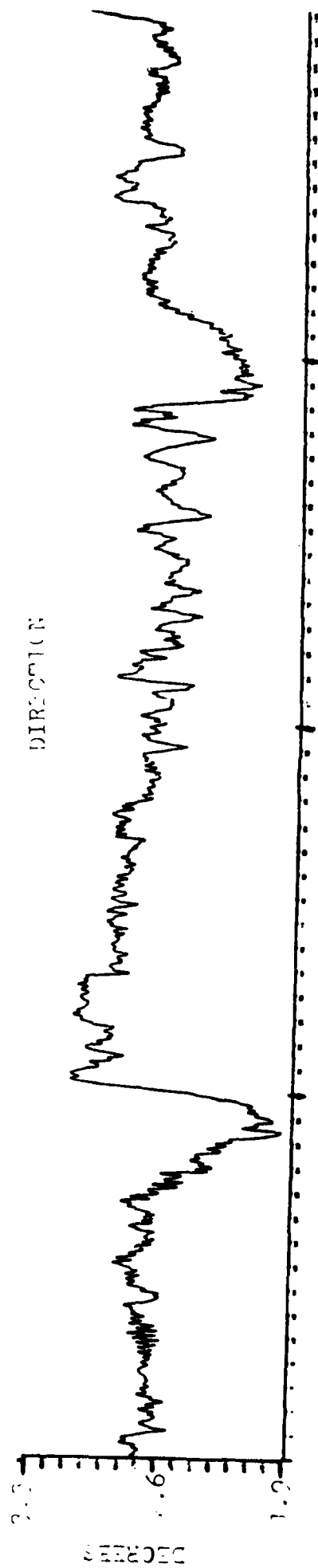


Figure 5.2. Raw voltage signals from a 120 sec run.

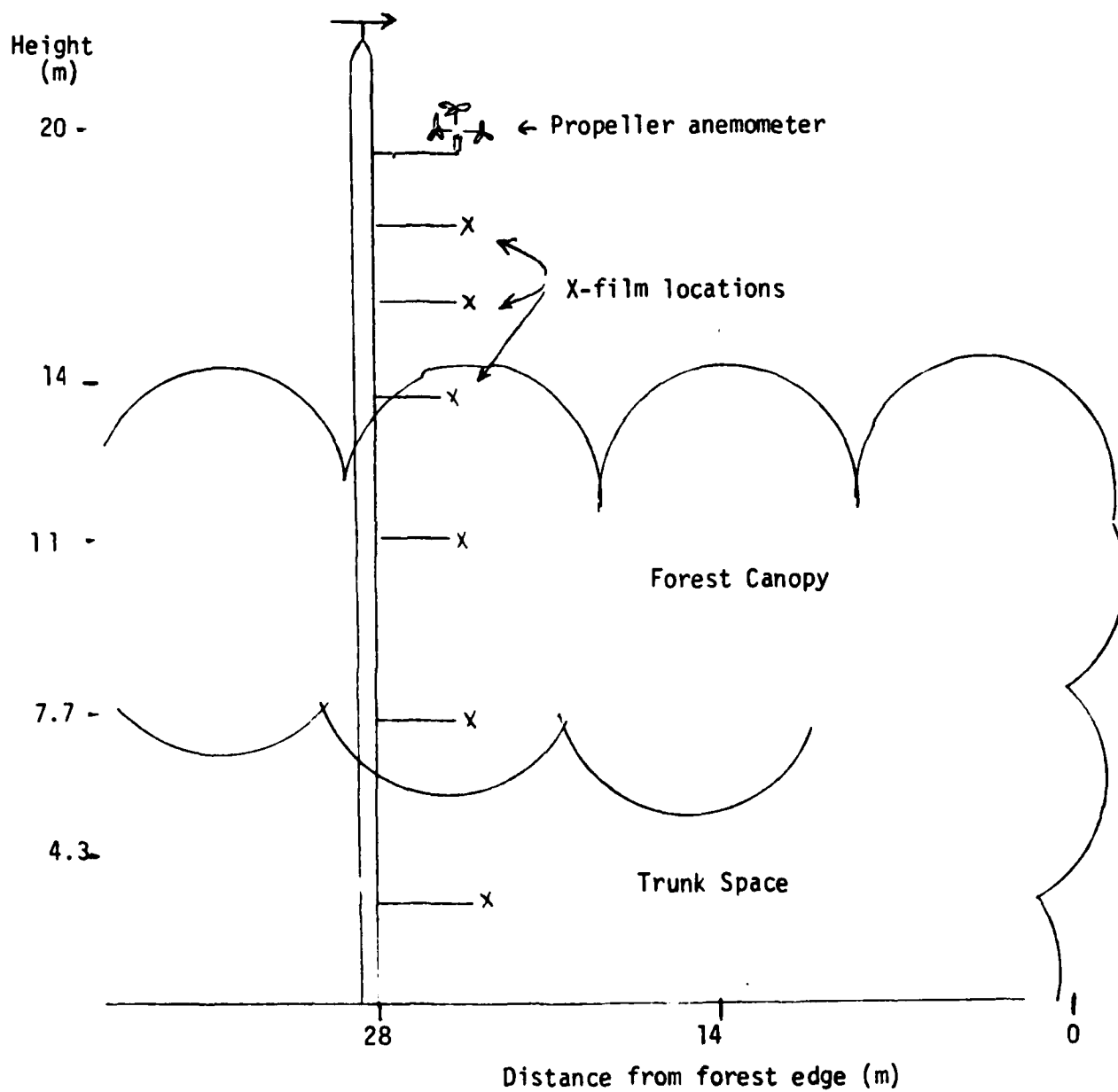


Figure 5.1. Tower and sensor arrangement in the experimental plot.

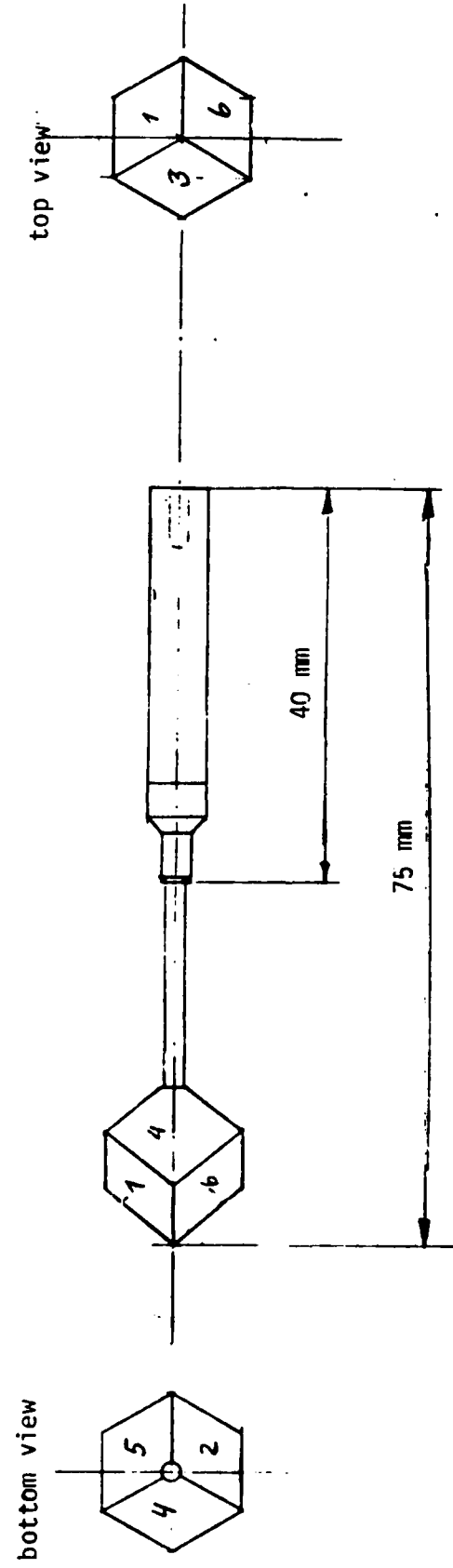


Figure 4.8. The wind octant electronic sensor (WOES).

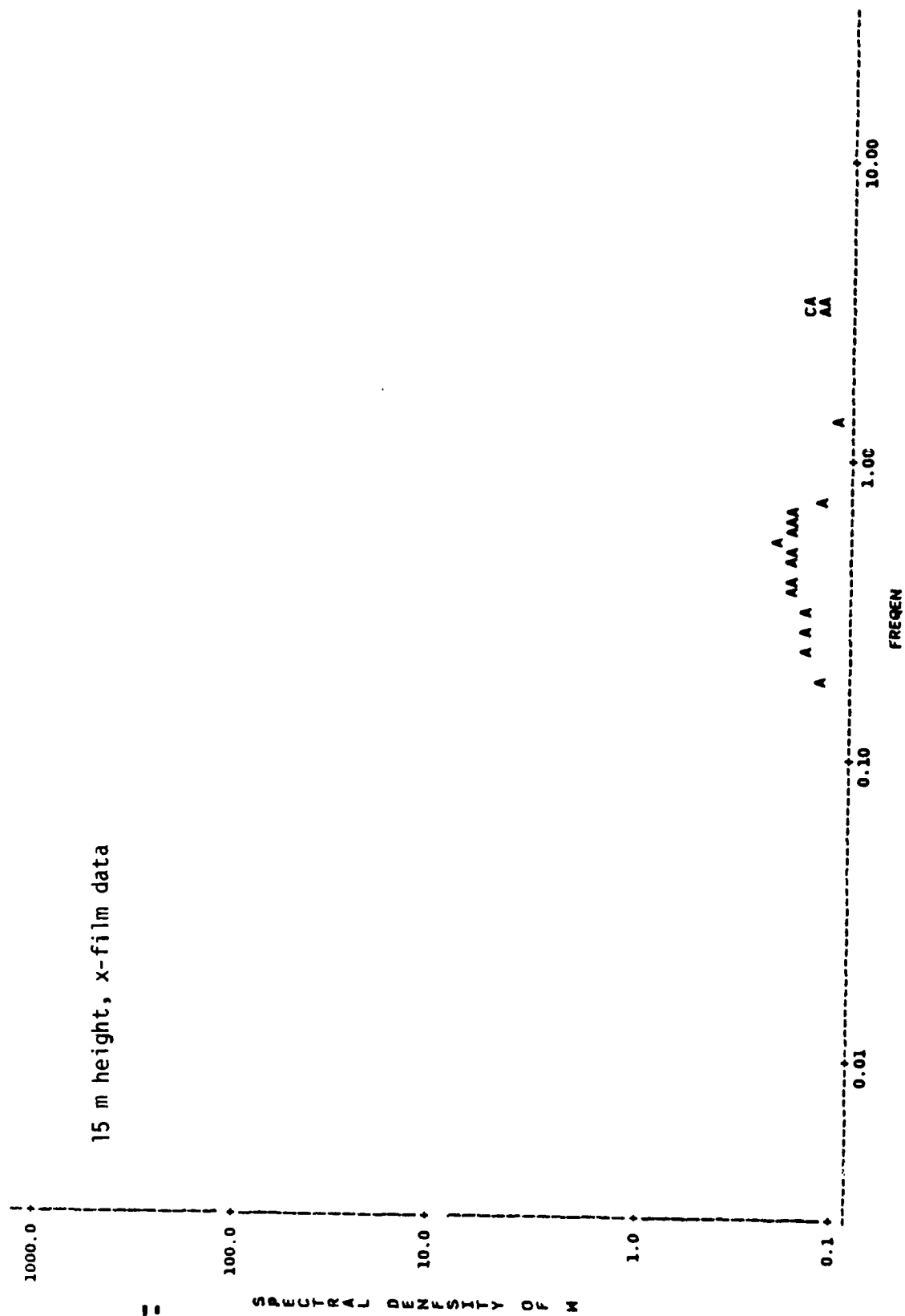
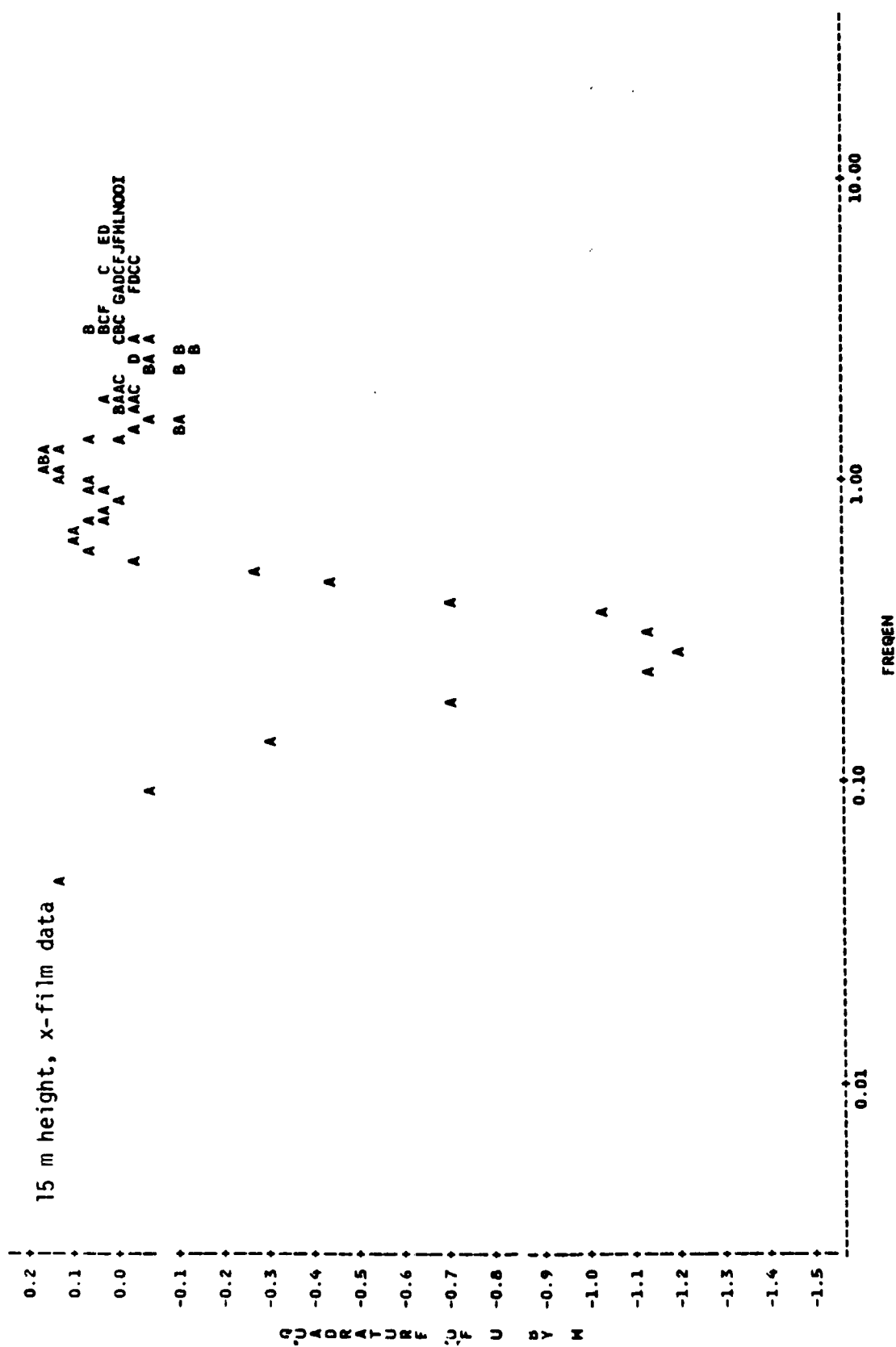


Figure 5.3. cont.



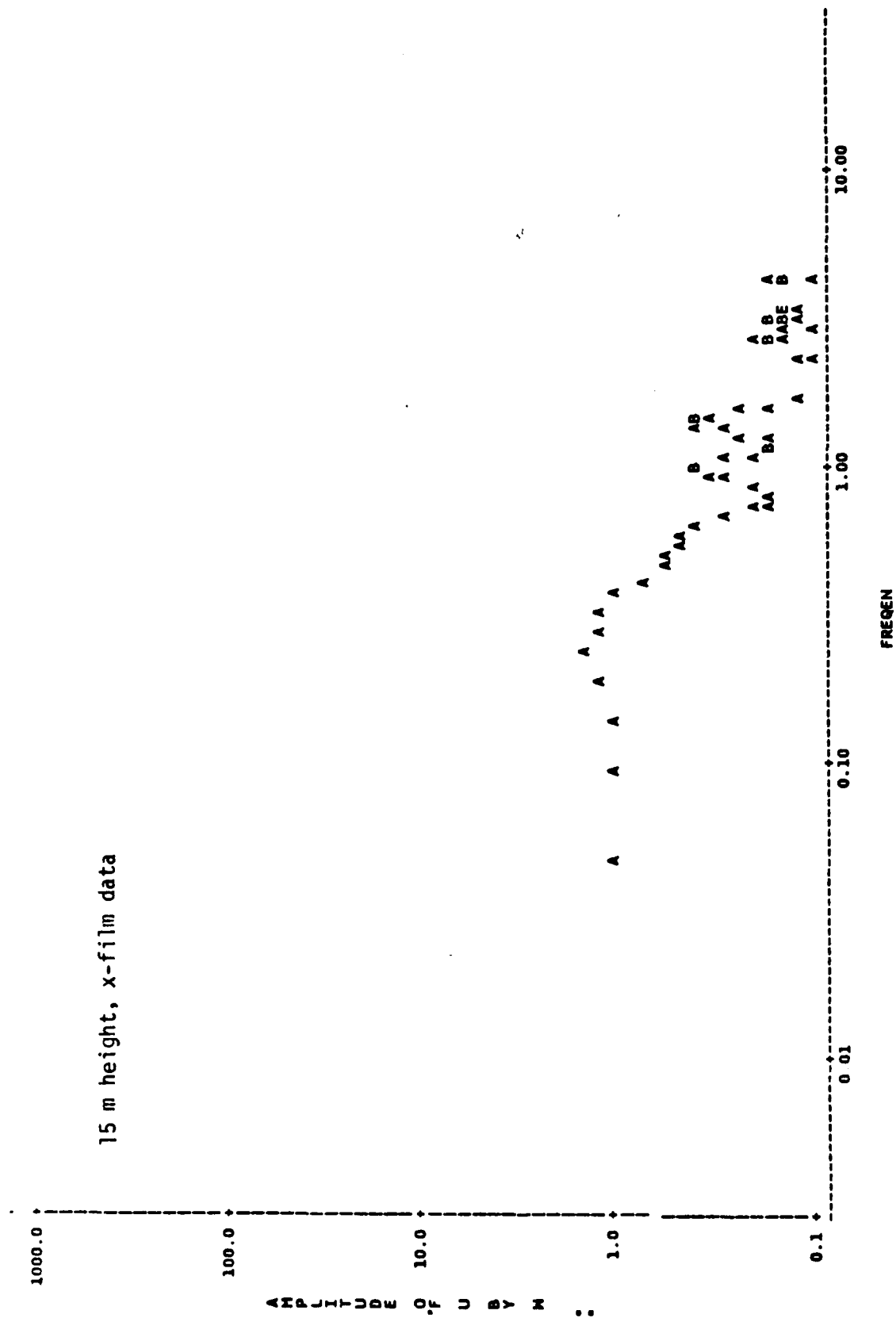


Figure 5.3. cont.

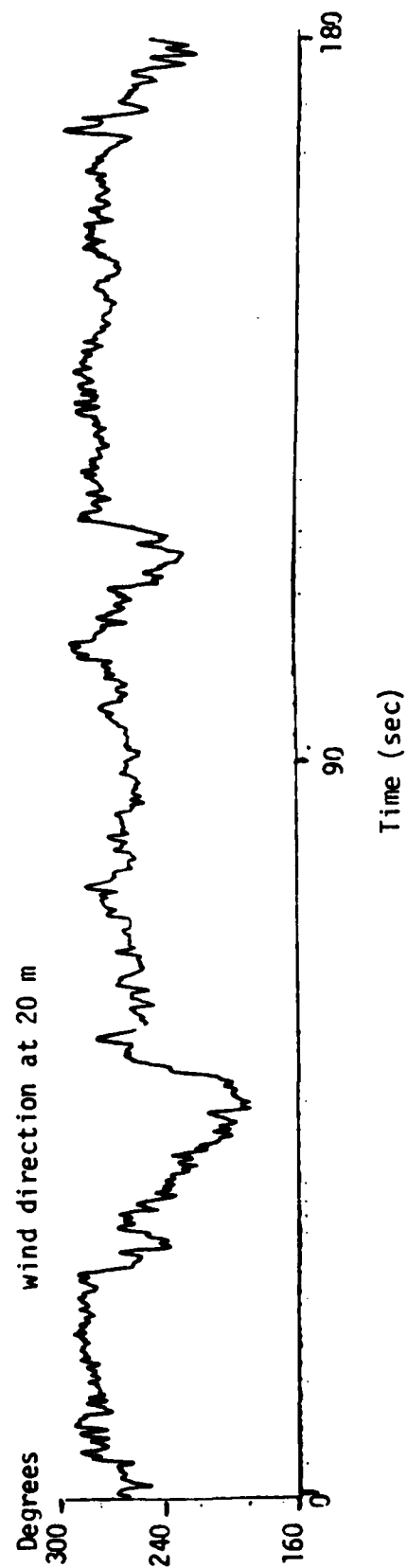


Figure 5.4. Time series of the wind components from the propeller anemometer at 20m and from the x-film at four different depths in the canopy.

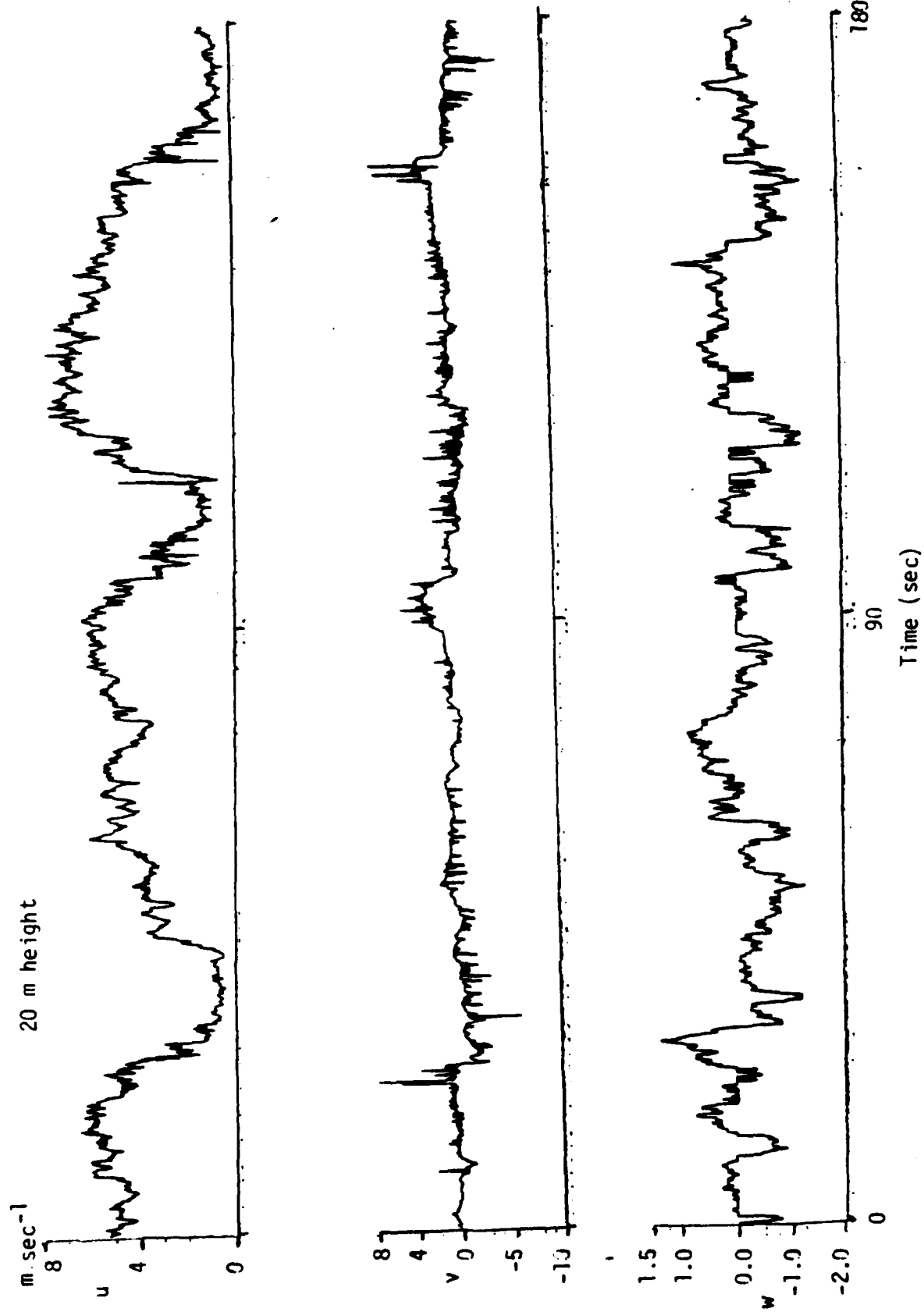


Figure 5.4. cont.

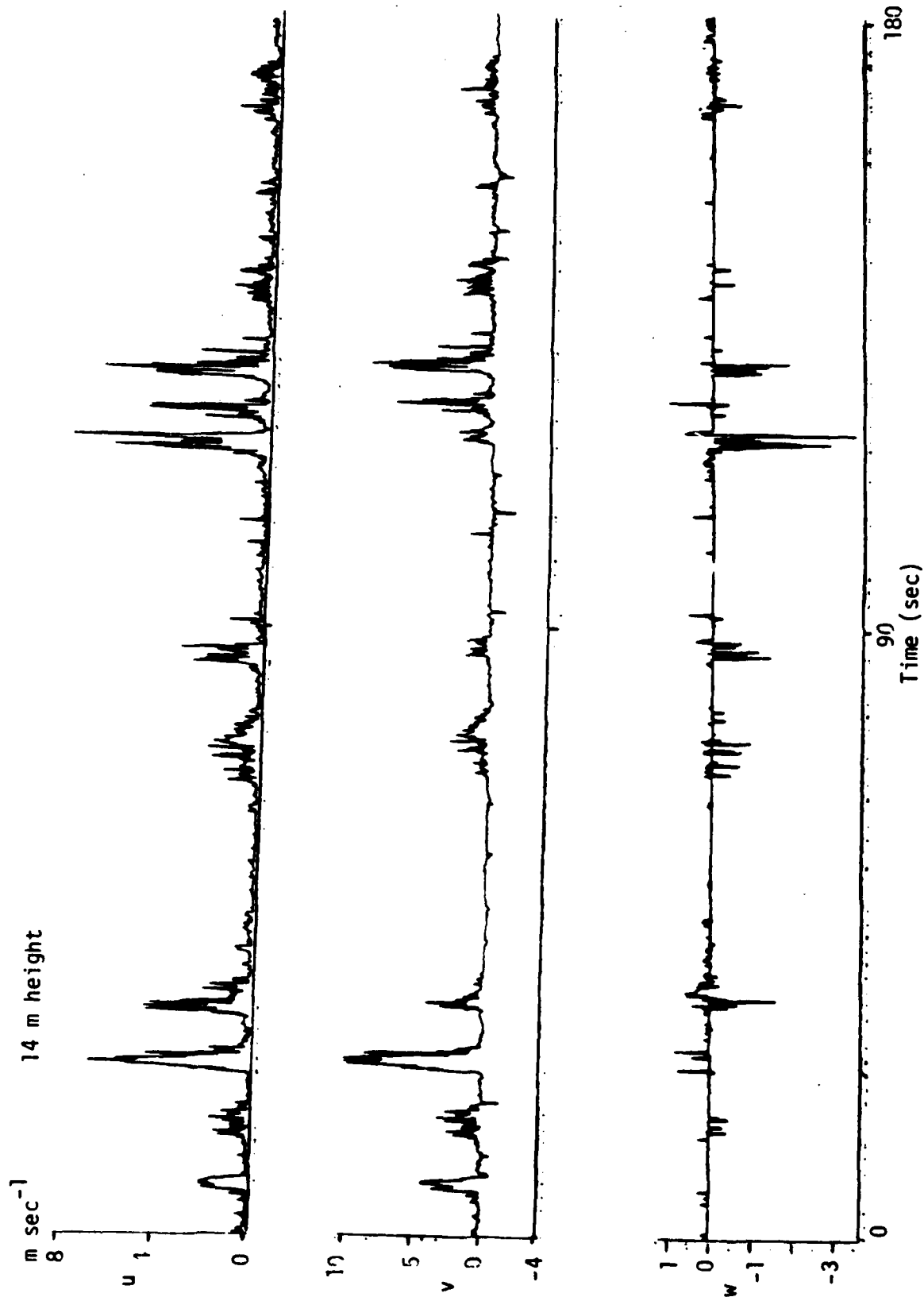


Figure 5.4. cont.

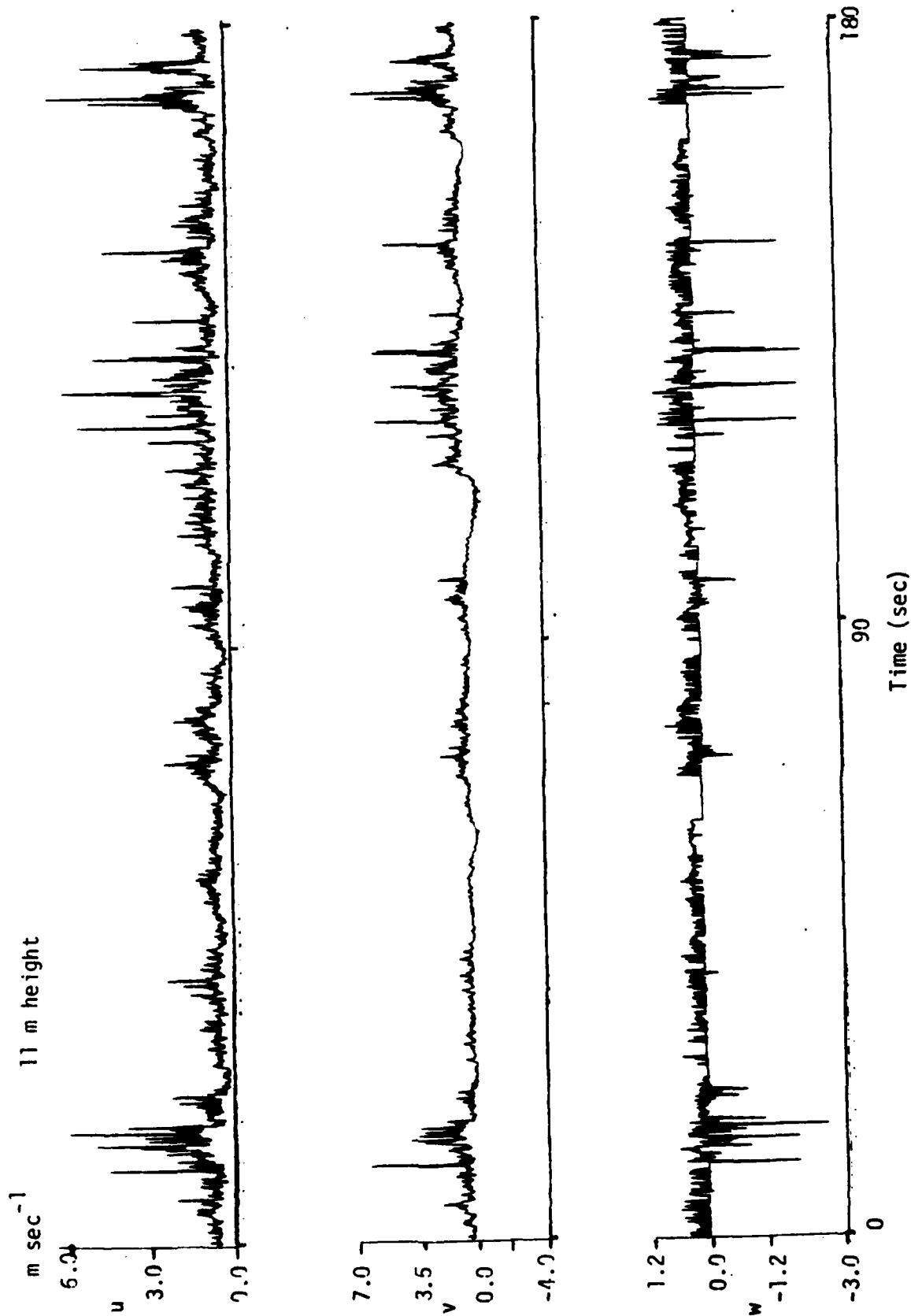


Figure 5.4. cont.

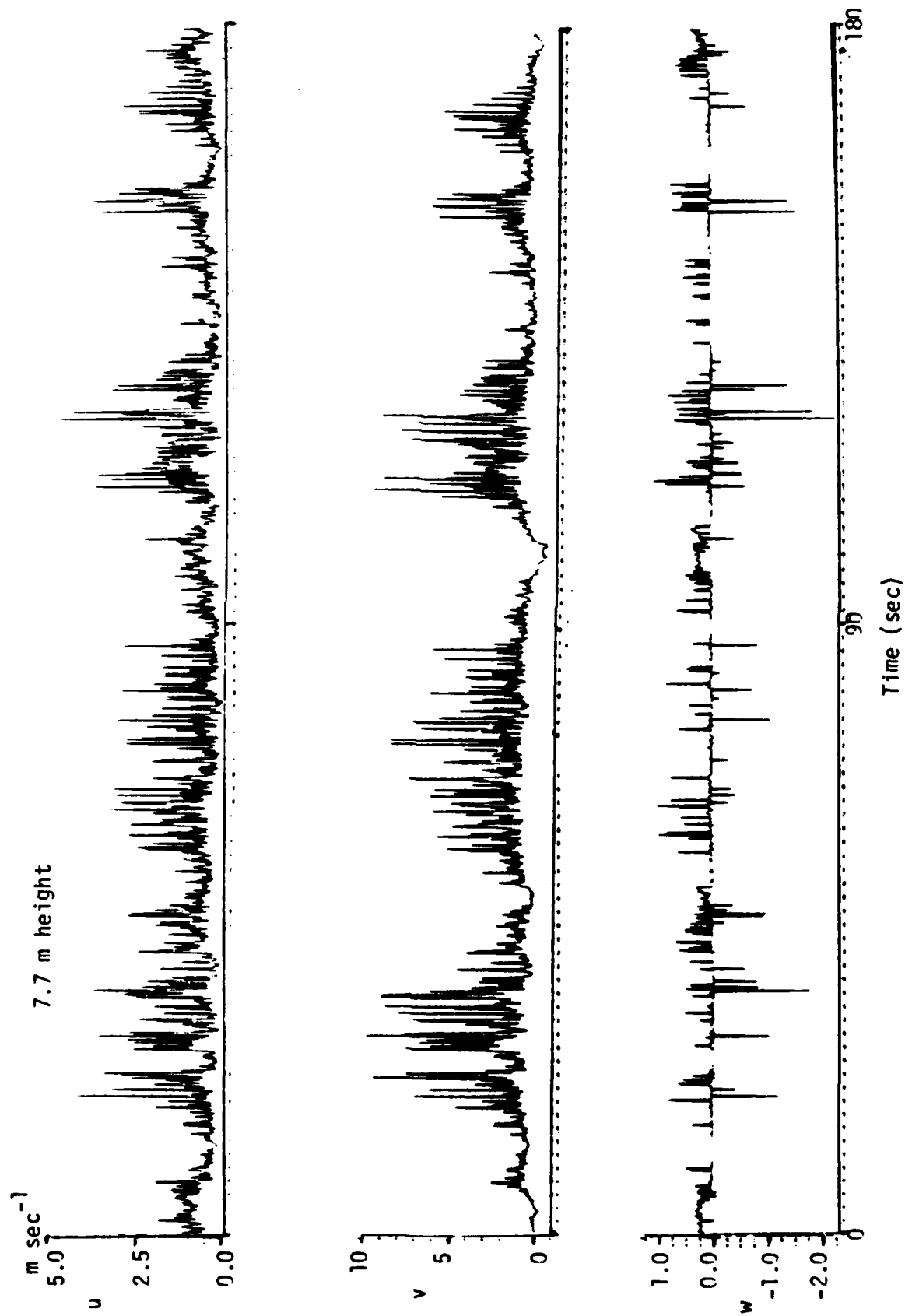


Figure 5.4. cont.

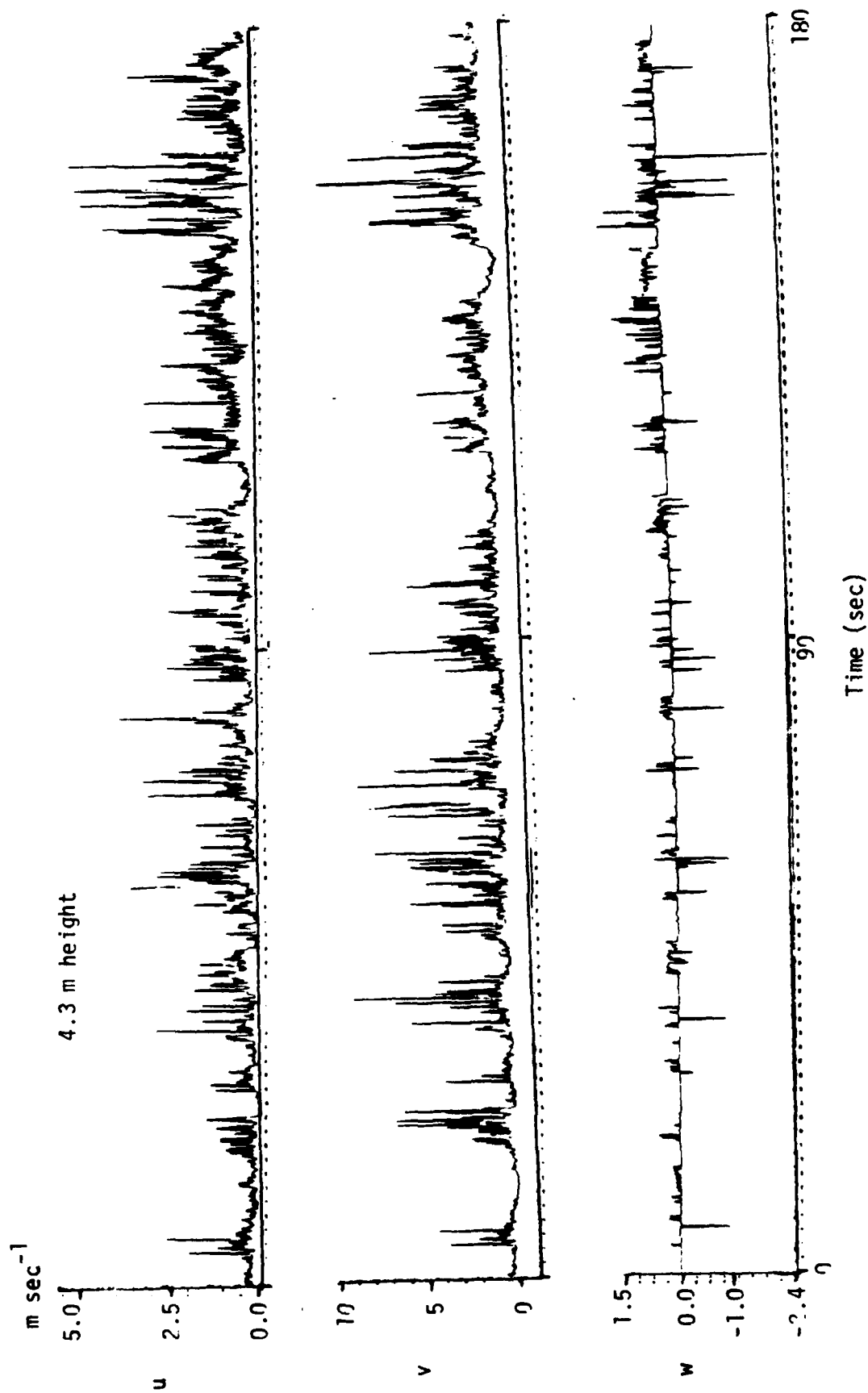


Figure 5.4. cont.

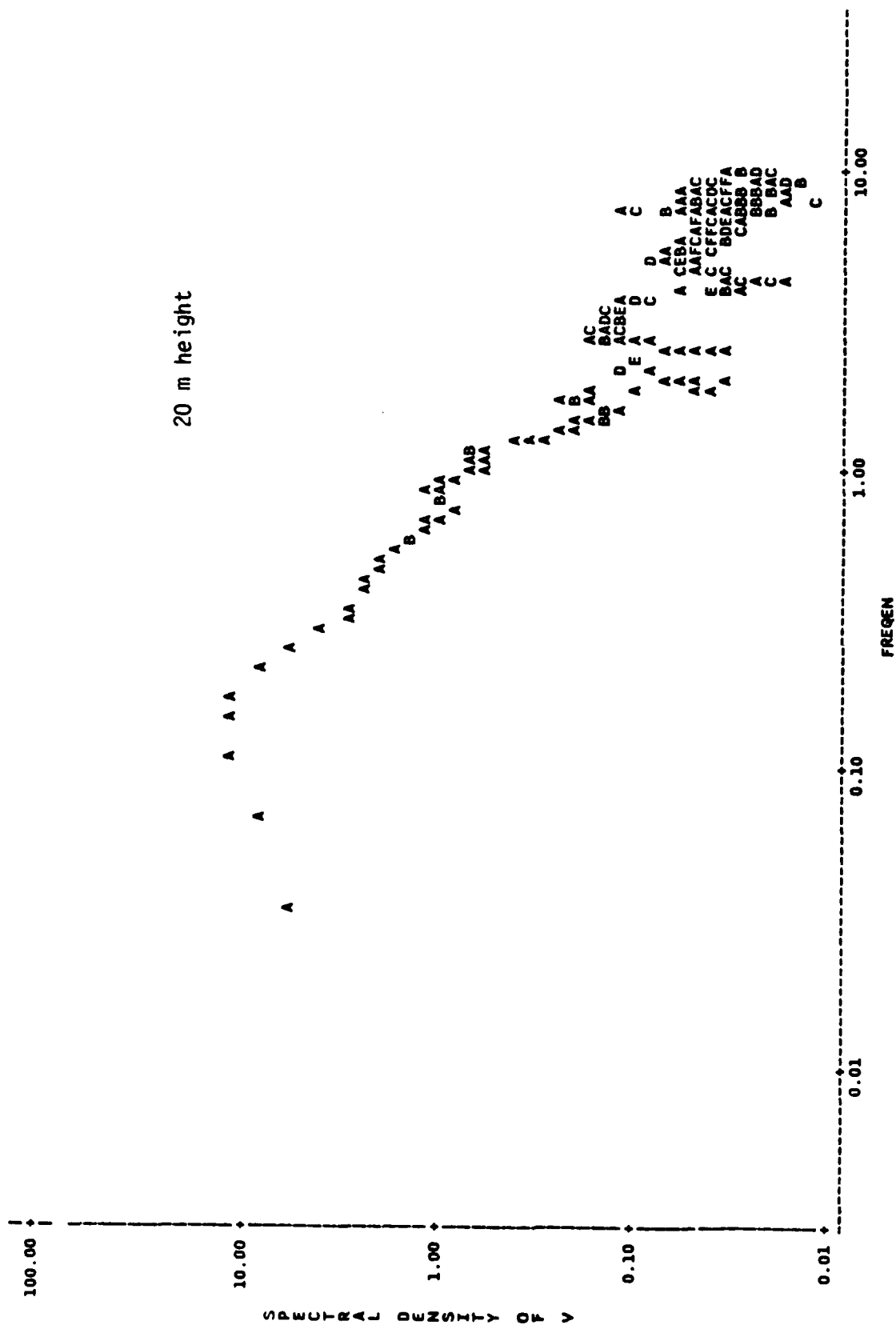


Figure 5.5. cont.

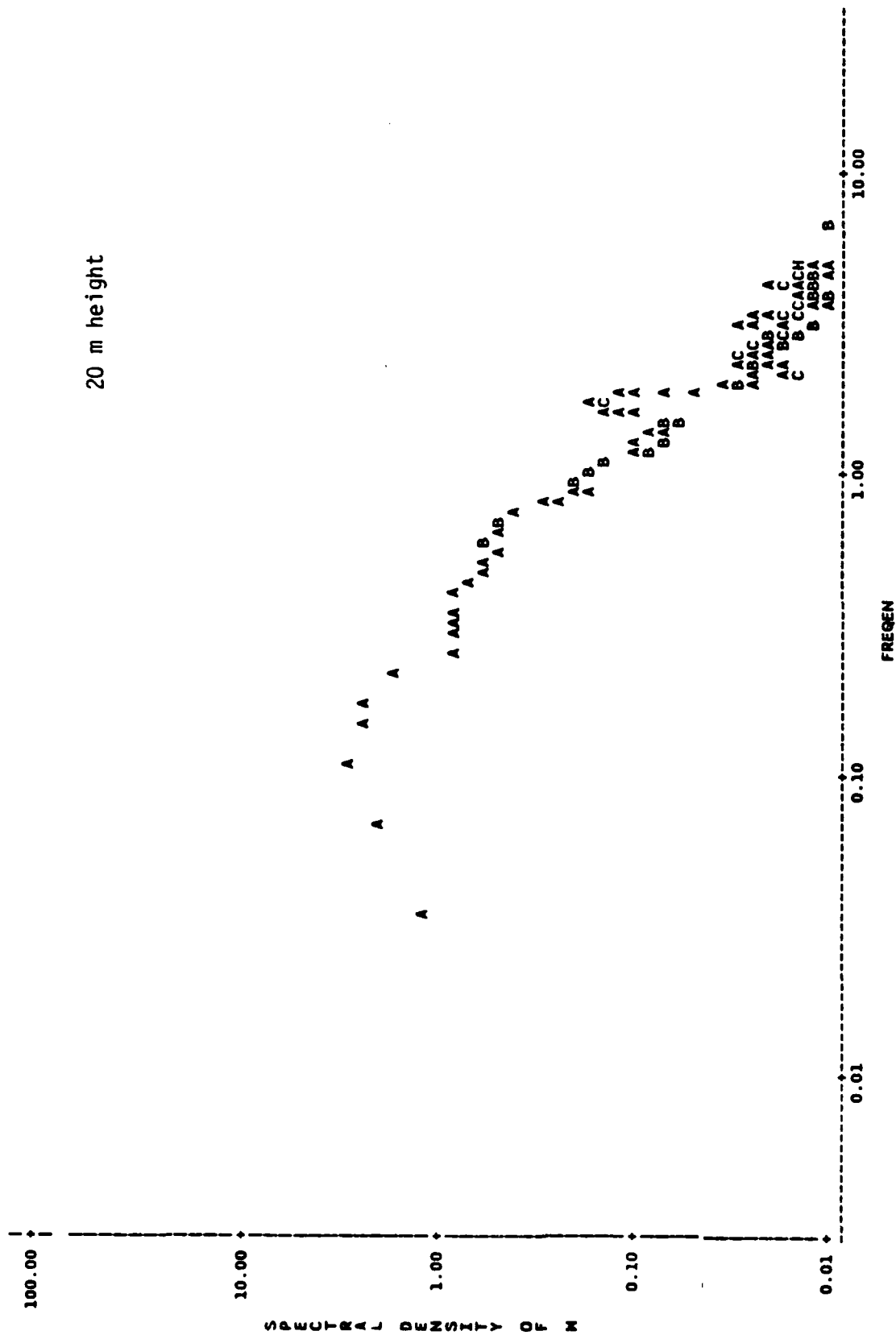


Figure 5.5. cont.

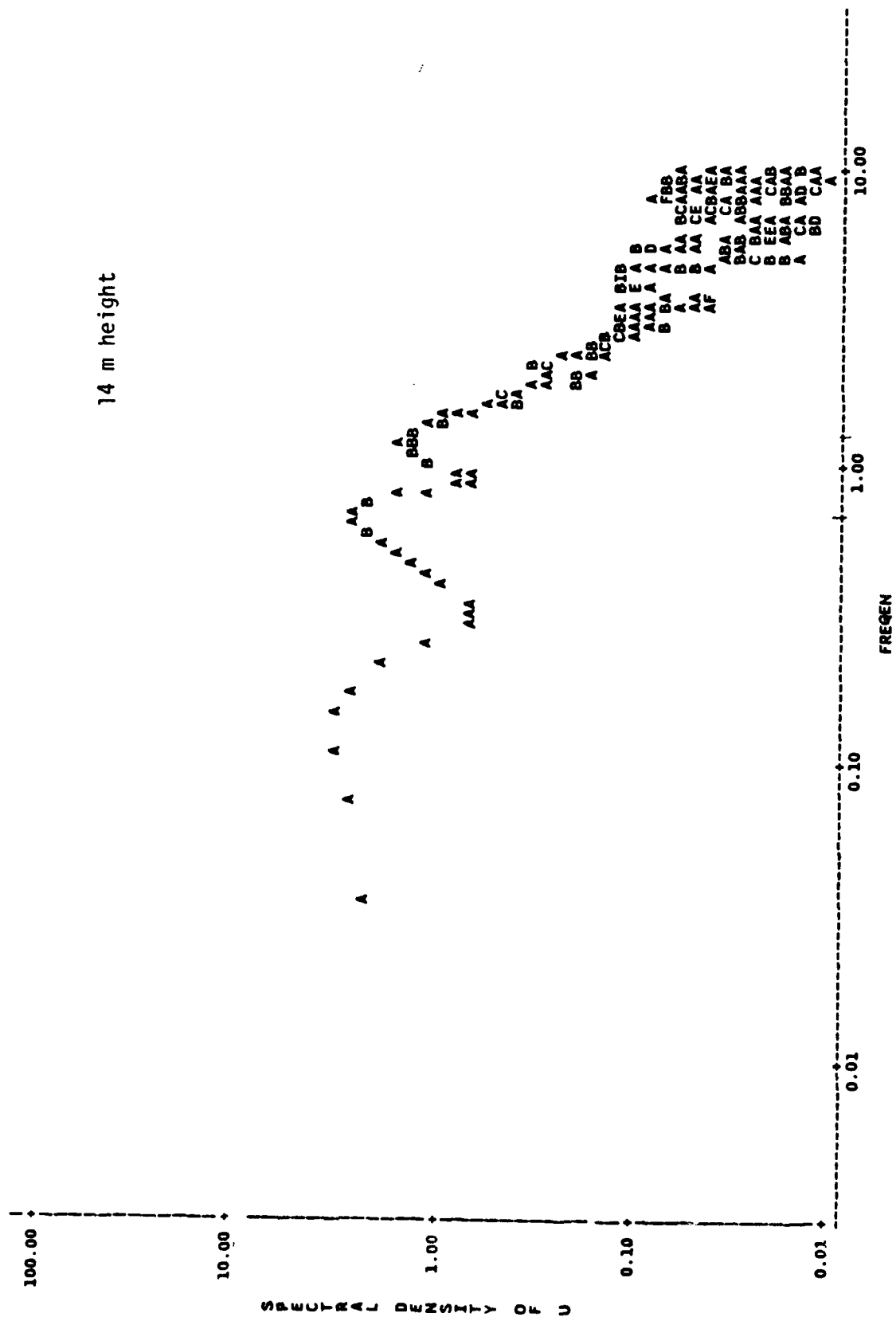


Figure 5.5. cont.

AD-A158 489

A PRELIMINARY FIELD STUDY OF TURBULENT FLOW OVER AND
INSIDE A FOREST EDGE(U) CONNECTICUT UNIV STORRS
J D LIN ET AL 01 JUL 85 ARO-21156.1-GS

2/8

UNCLASSIFIED

DAG29-84-K-0017

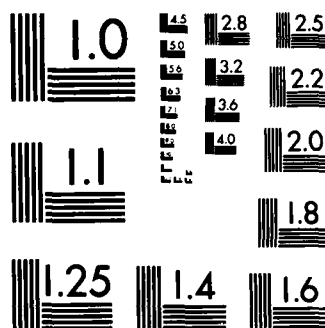
F/G 4/2

NL

END

FILED

STC



MICROCOPY RESOLUTION TEST CHART
NATIONAL BUREAU OF STANDARDS-1963-A

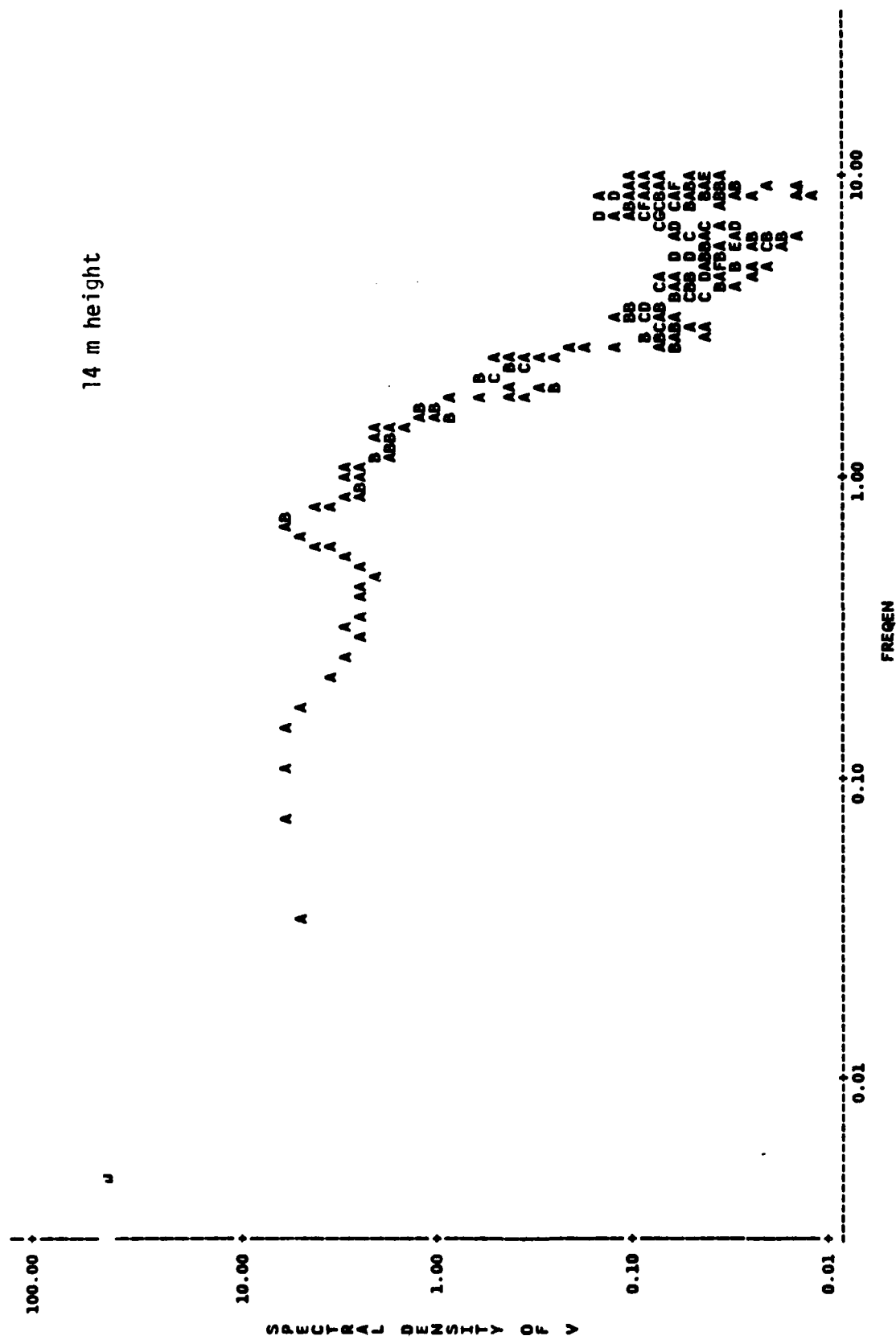


Figure 5.5. cont.

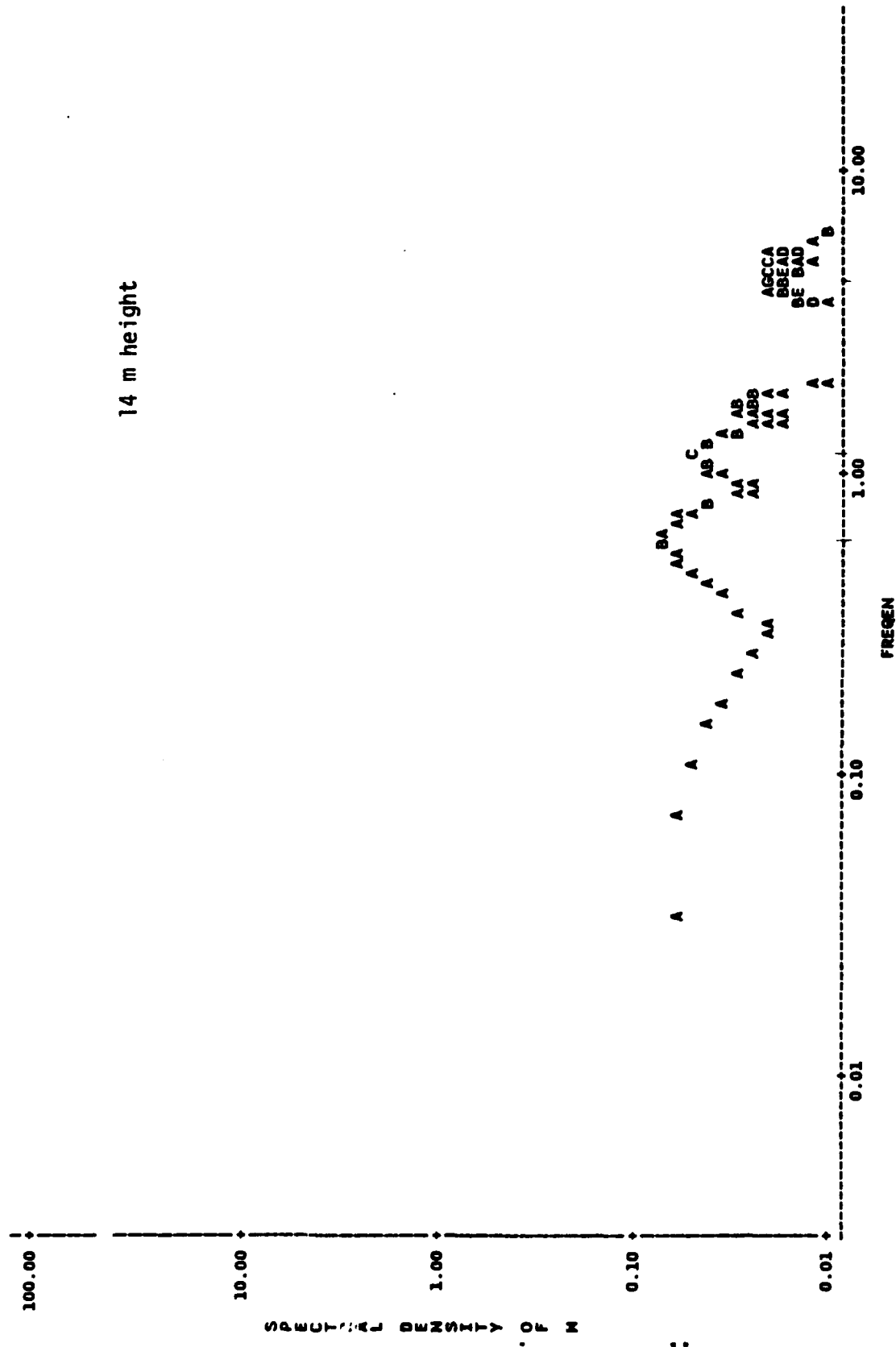
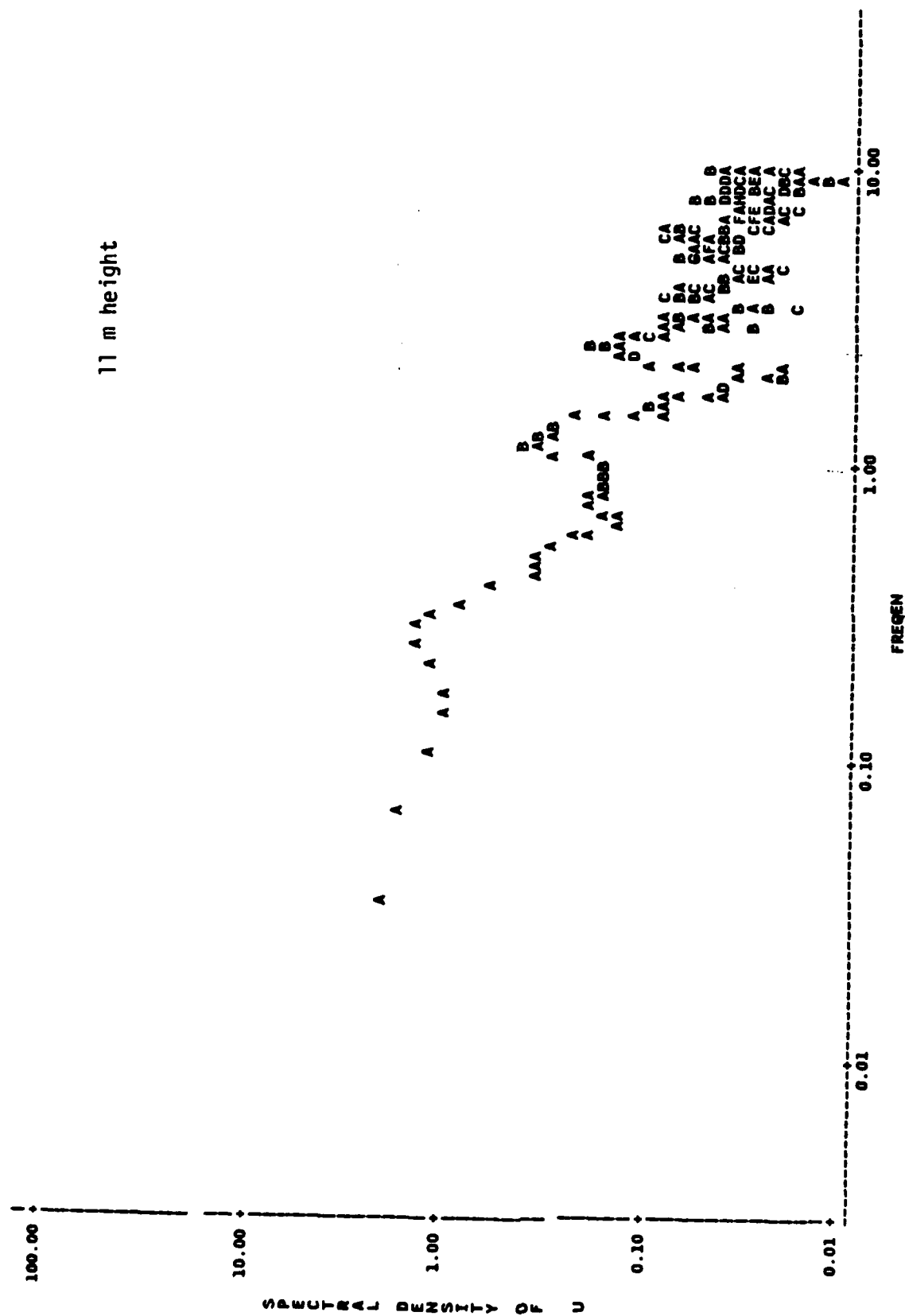


Figure 5.5 cont.



A spectral density plot titled "11 m height". The vertical axis is labeled "SPECTRAL DENSITY OF V" and has major tick marks at 0.01, 0.10, 1.00, 10.00, and 100.00. The horizontal axis is labeled "FREQN" and has major tick marks at 0.01, 0.10, 1.00, and 10.00. Both axes are logarithmic. Data points are represented by letters (A, B, C, D, E, I) scattered across the plot area. A dense cluster of letters is located between frequencies of 1.00 and 10.00 and spectral densities of 0.01 and 0.10. Other letters are more sparsely distributed at higher frequencies and lower spectral densities.

Figure 5.5. cont.

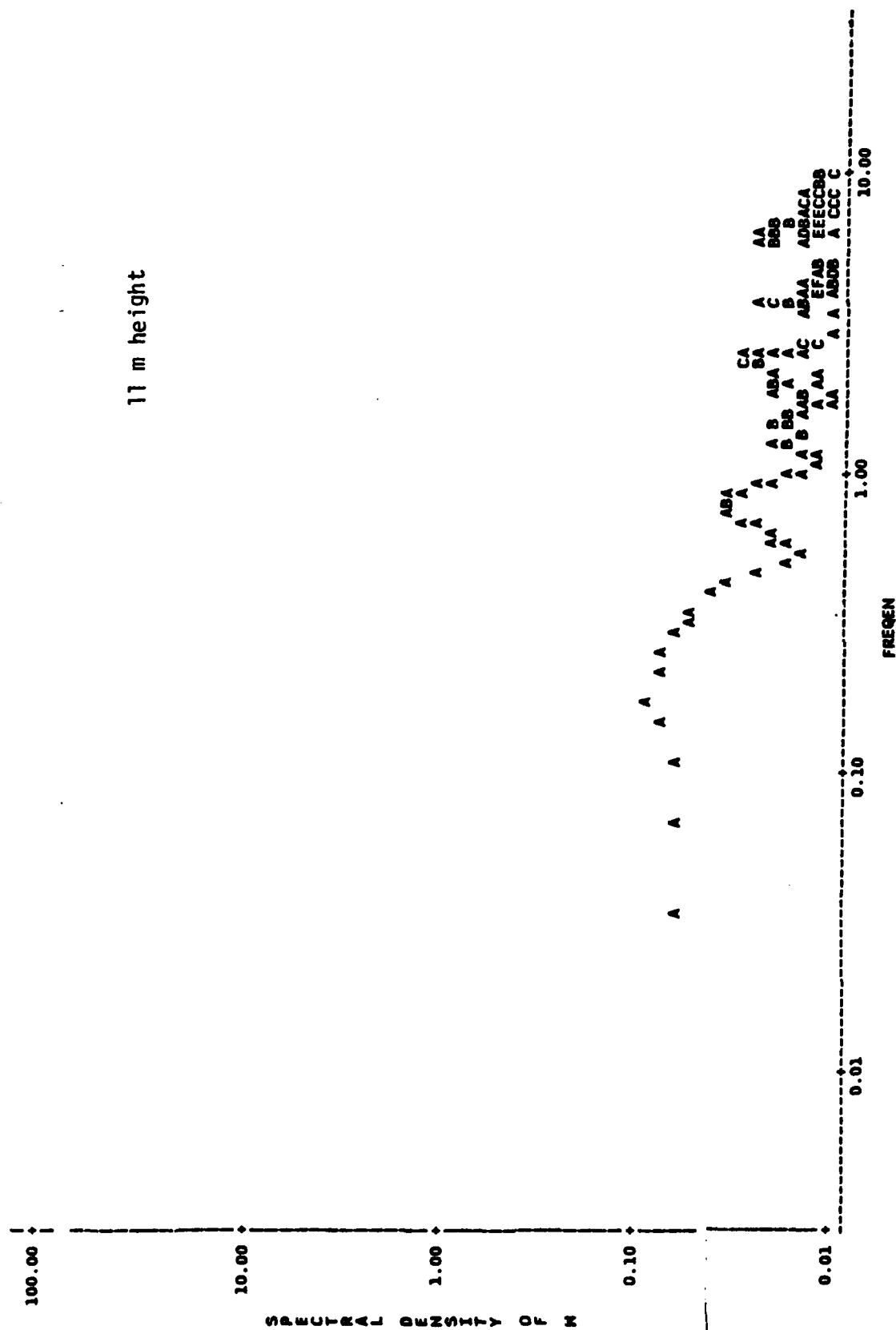


Figure 5.5. cont.

7.7 m height

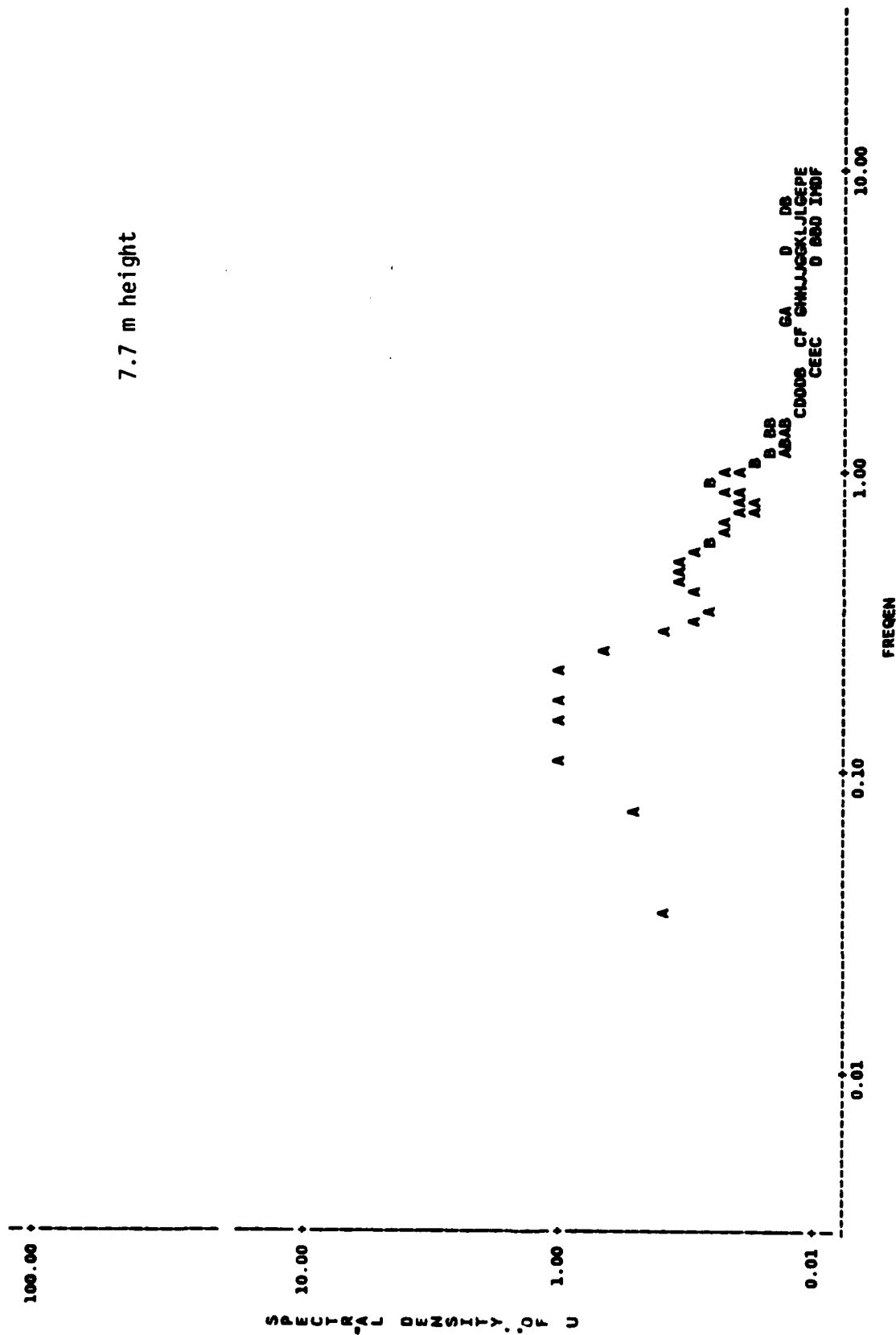


Figure 5.5. cont.

7.7 m height

SPECTRAL DENSITY OF V

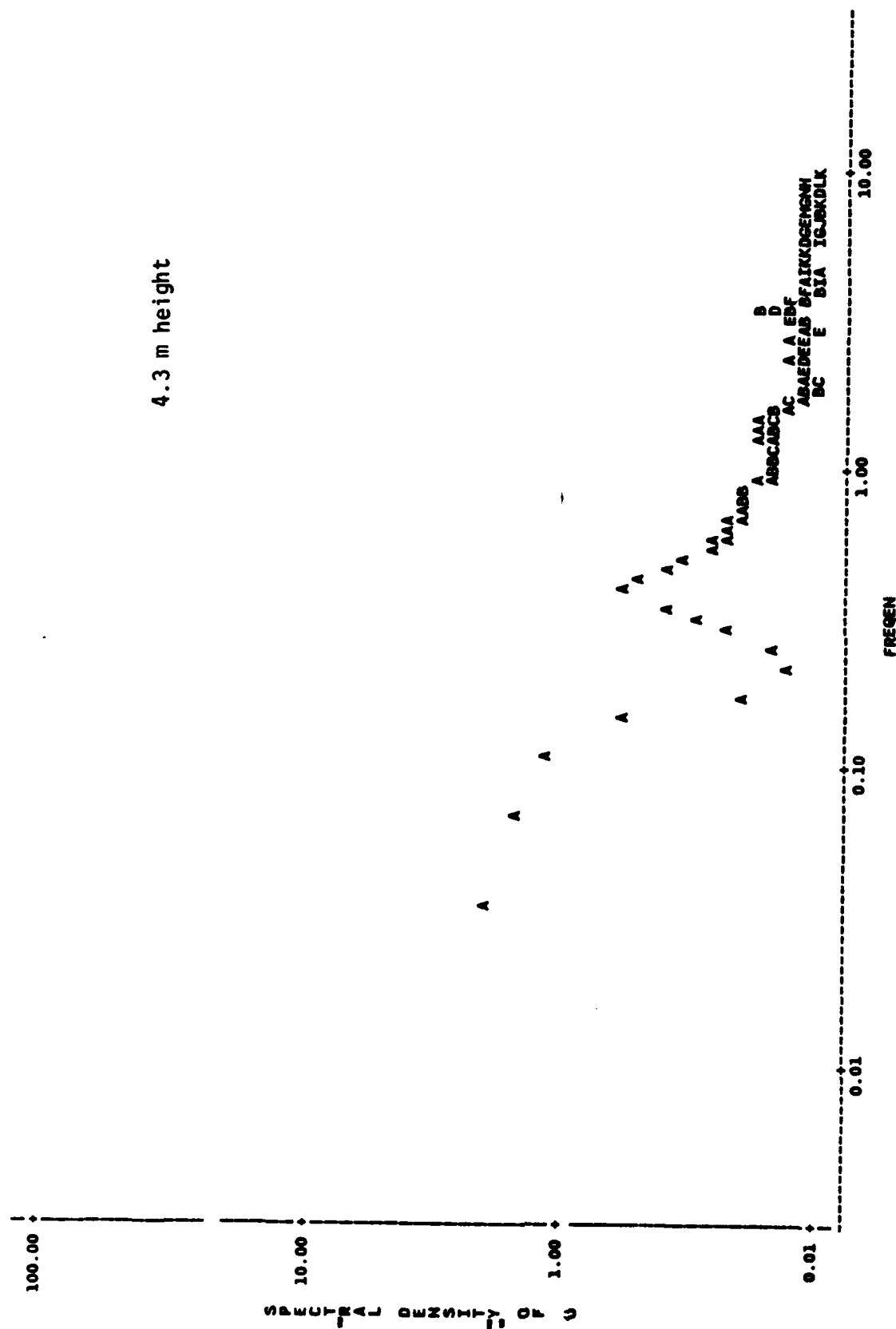
FREQUENCY

Figure 5.5. cont.

A log-log plot titled "7.7 m height". The vertical axis is labeled "S P E C T R A L D E N S I T Y O F W" and has major ticks at 0.01, 1.00, 10.00, and 100.00. The horizontal axis is labeled "F R E Q U E N C Y" and has major ticks at 0.01, 0.10, 1.00, and 10.00. The plot shows several peaks labeled with letters: 'A' at approximately 0.02 Hz, 'A A A A A' between 0.1 and 0.3 Hz, 'B A B' at approximately 0.6 Hz, 'C' at approximately 2.5 Hz, 'F' at approximately 4 Hz, and 'C' at approximately 8 Hz.

Figure 5.5. cont.

4.3 m height



4.3 m height

ACCELERATION

FREQUENCY

Figure 5.5. cont.

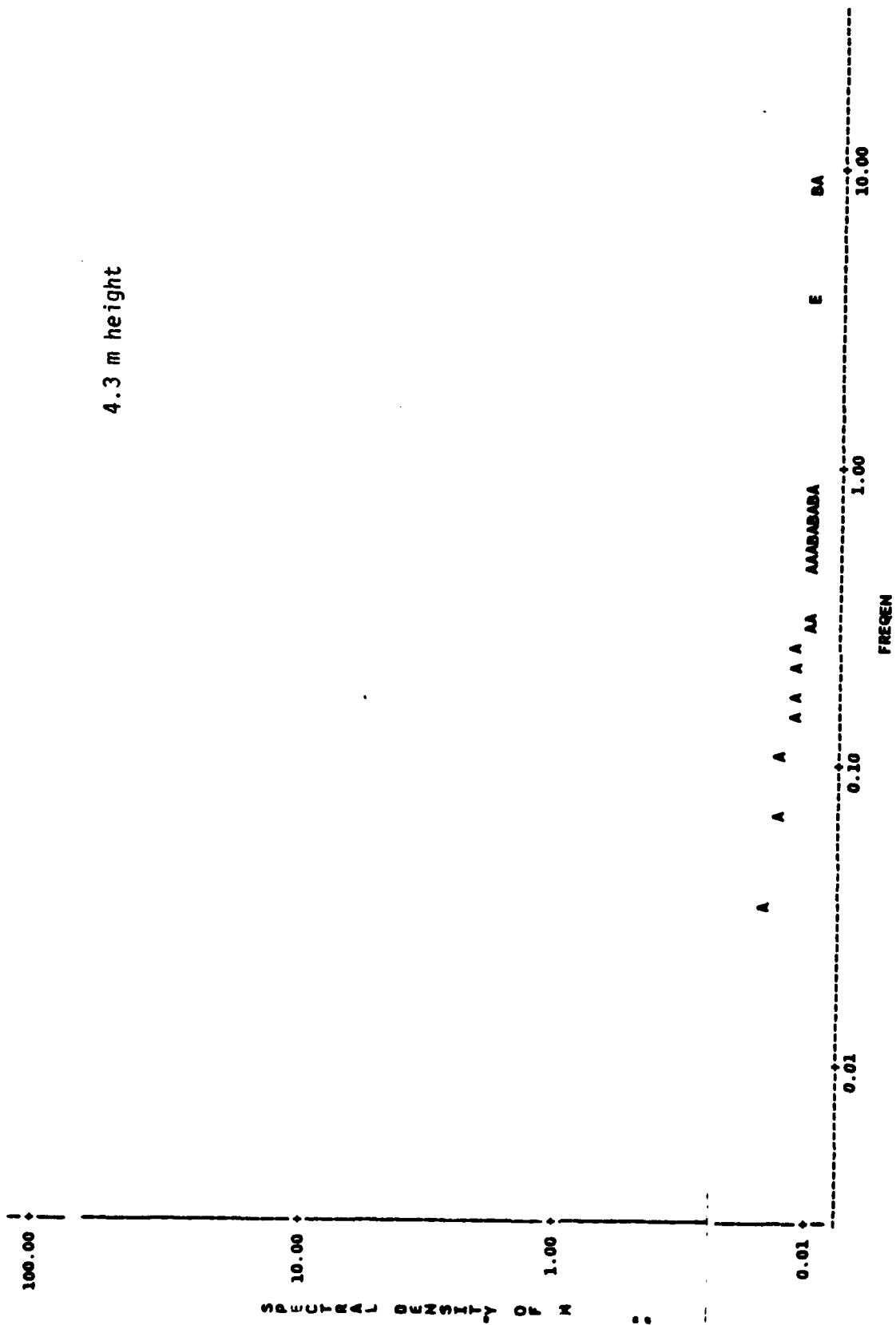
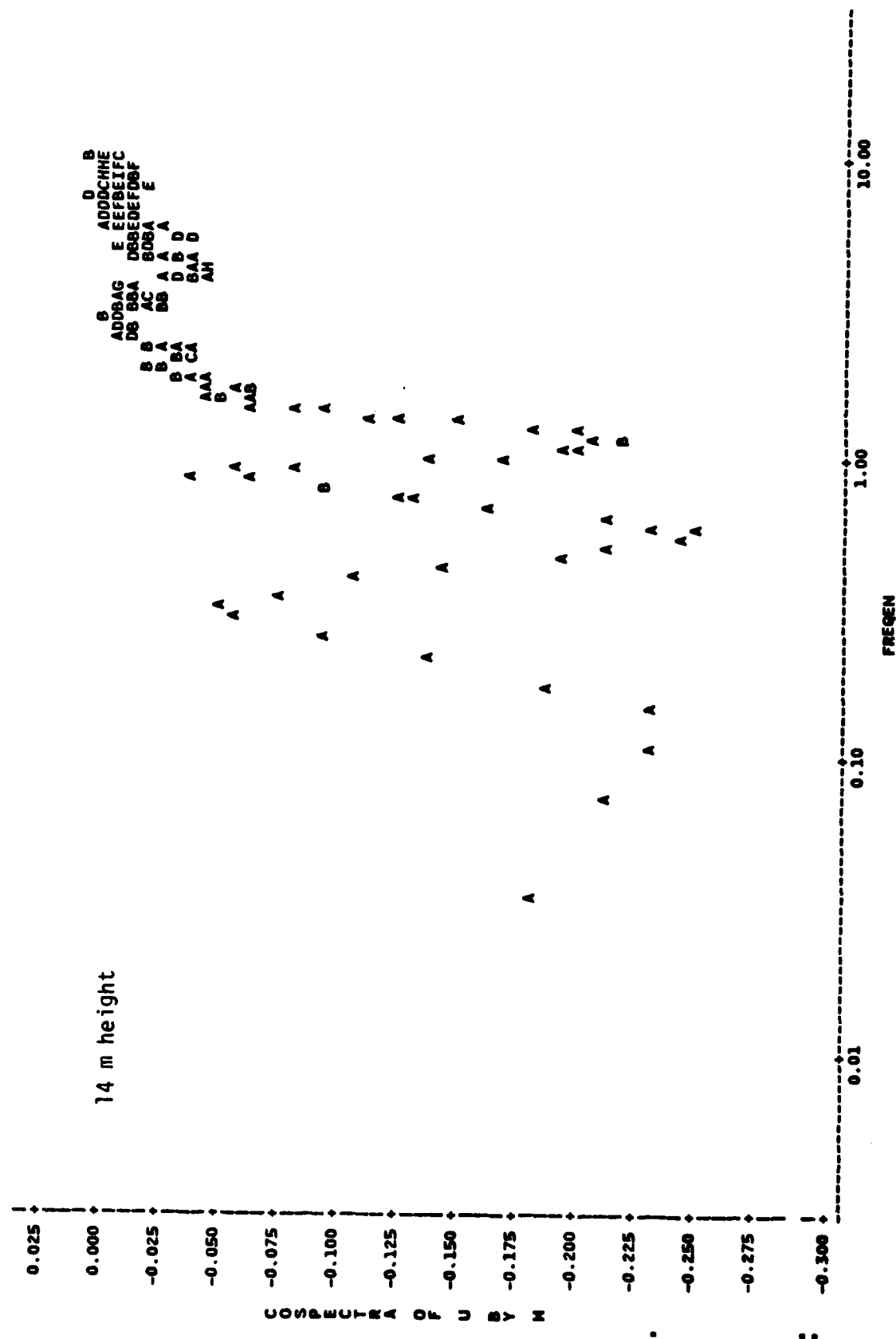


Figure 5.5. cont.



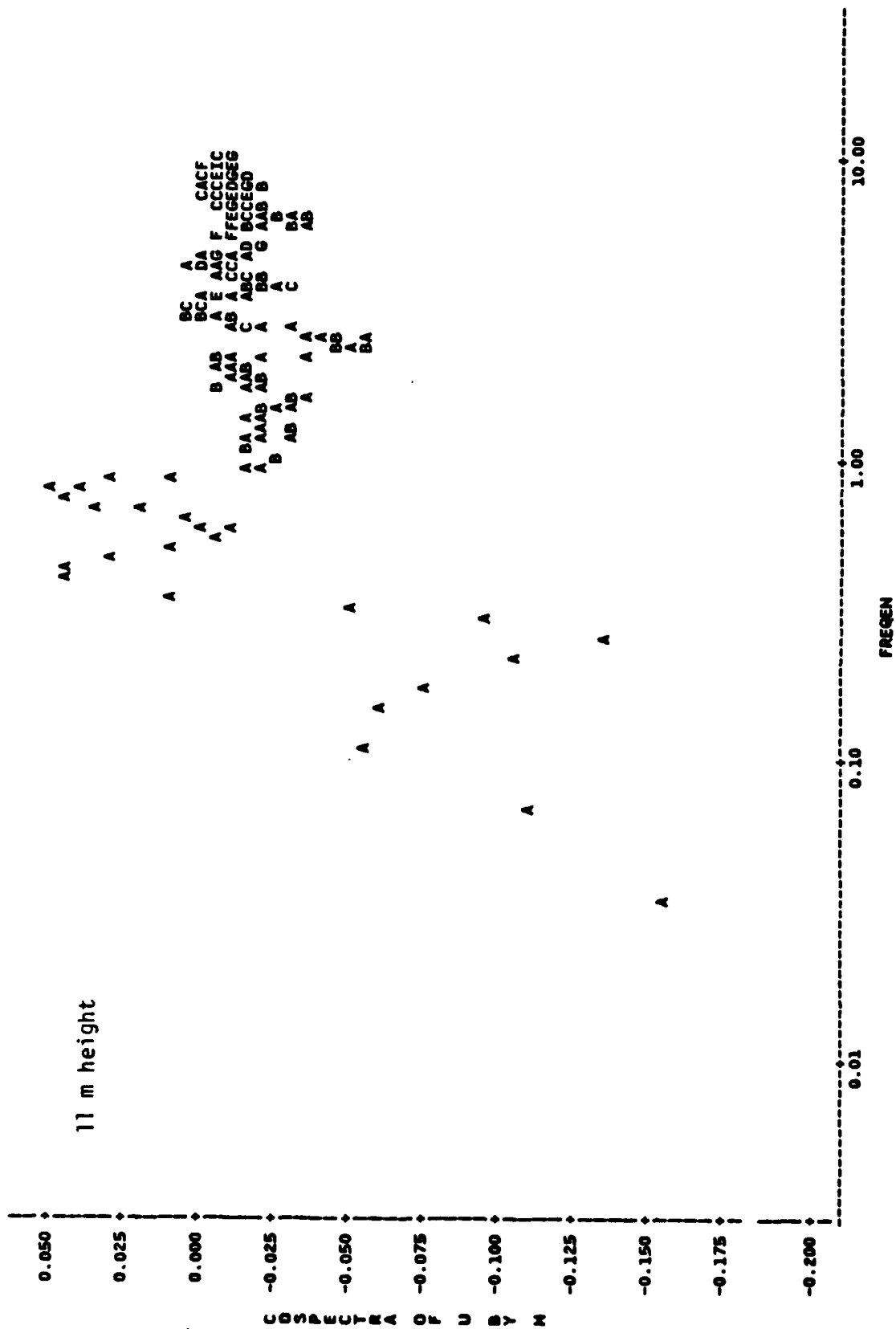


Figure 5.6c. *uw* cospectrum at the height of maximum foliage in the canopy.

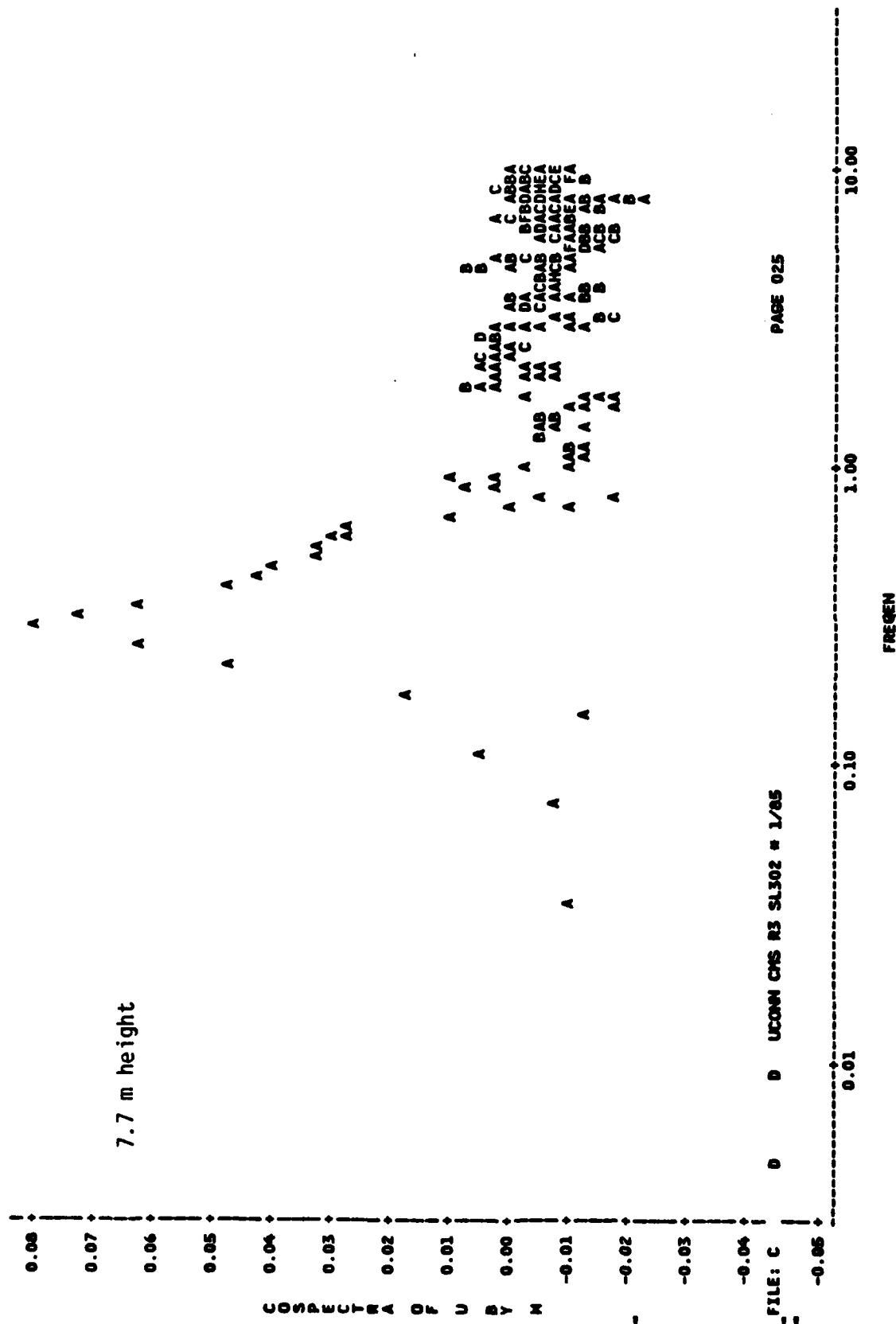


Figure 5.6d. uw cospectrum at the bottom of the canopy.

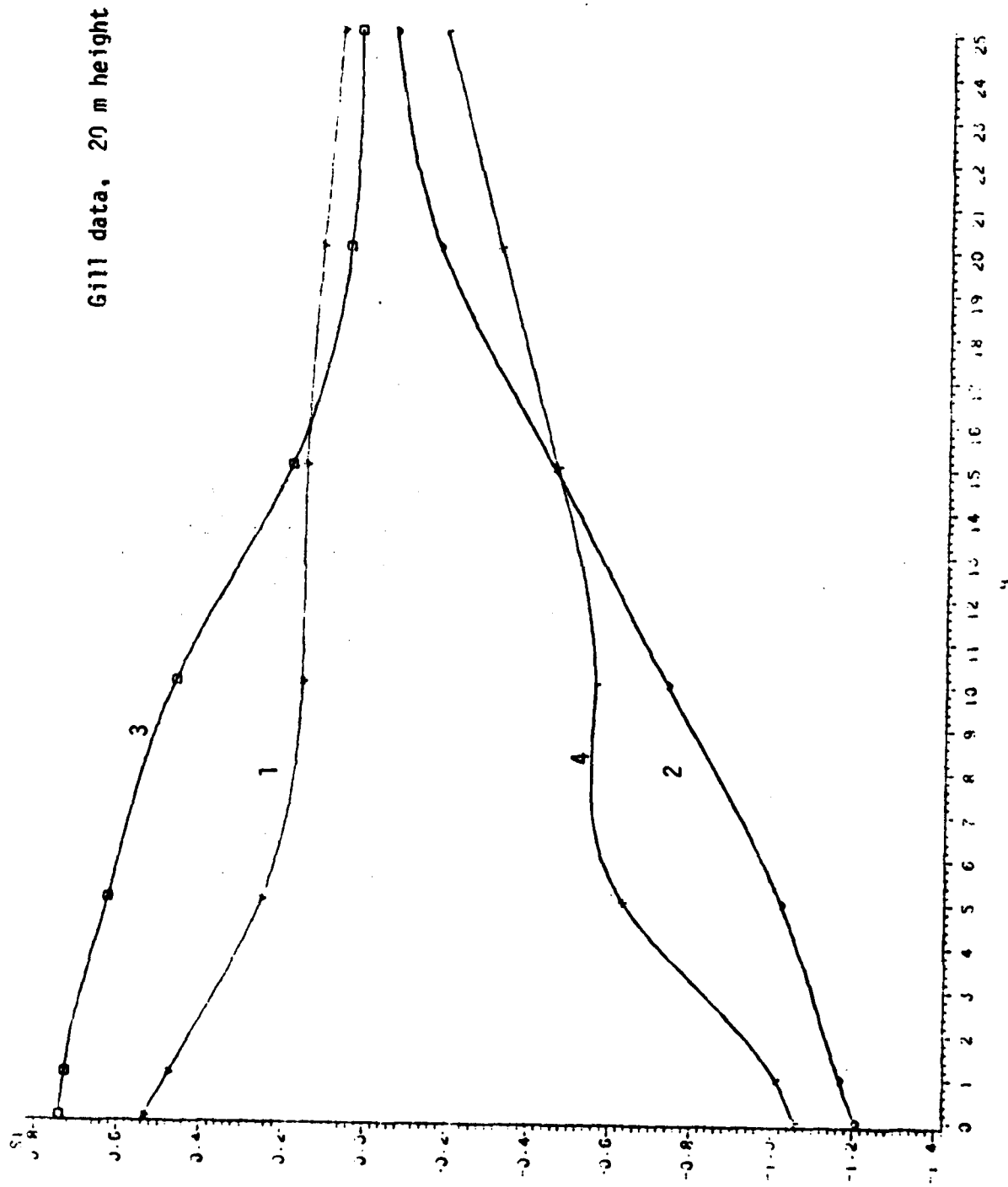


Figure 5.7a. Conditional analysis of u and w with a forest fetch. Calculated from the same data as figure 5.3.

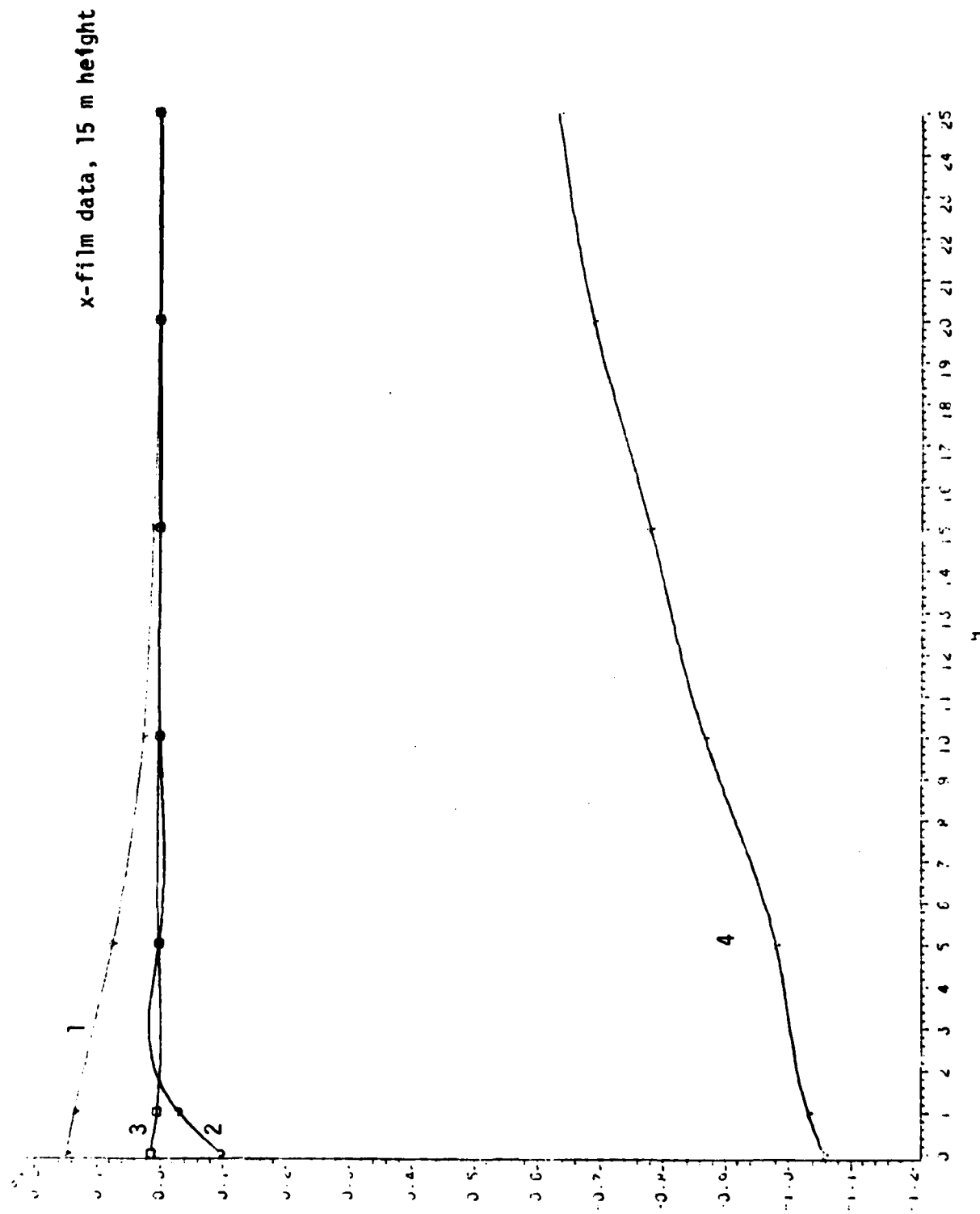


Figure 5.7b.

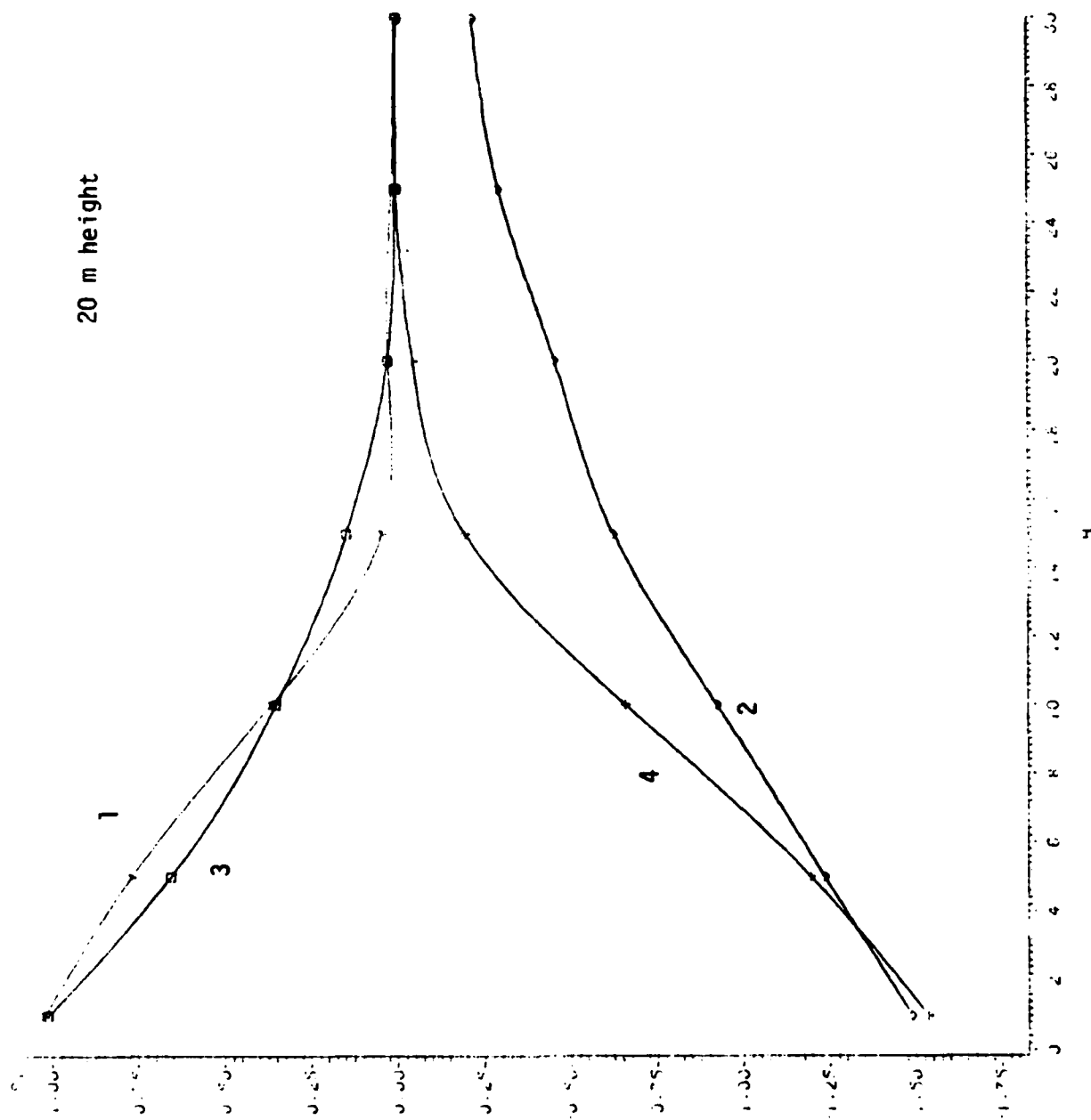


Figure 5.8a. Conditional analysis of u and w with the wind from the edge. Data is from figure 5.4. Quadrant numbers are shown.

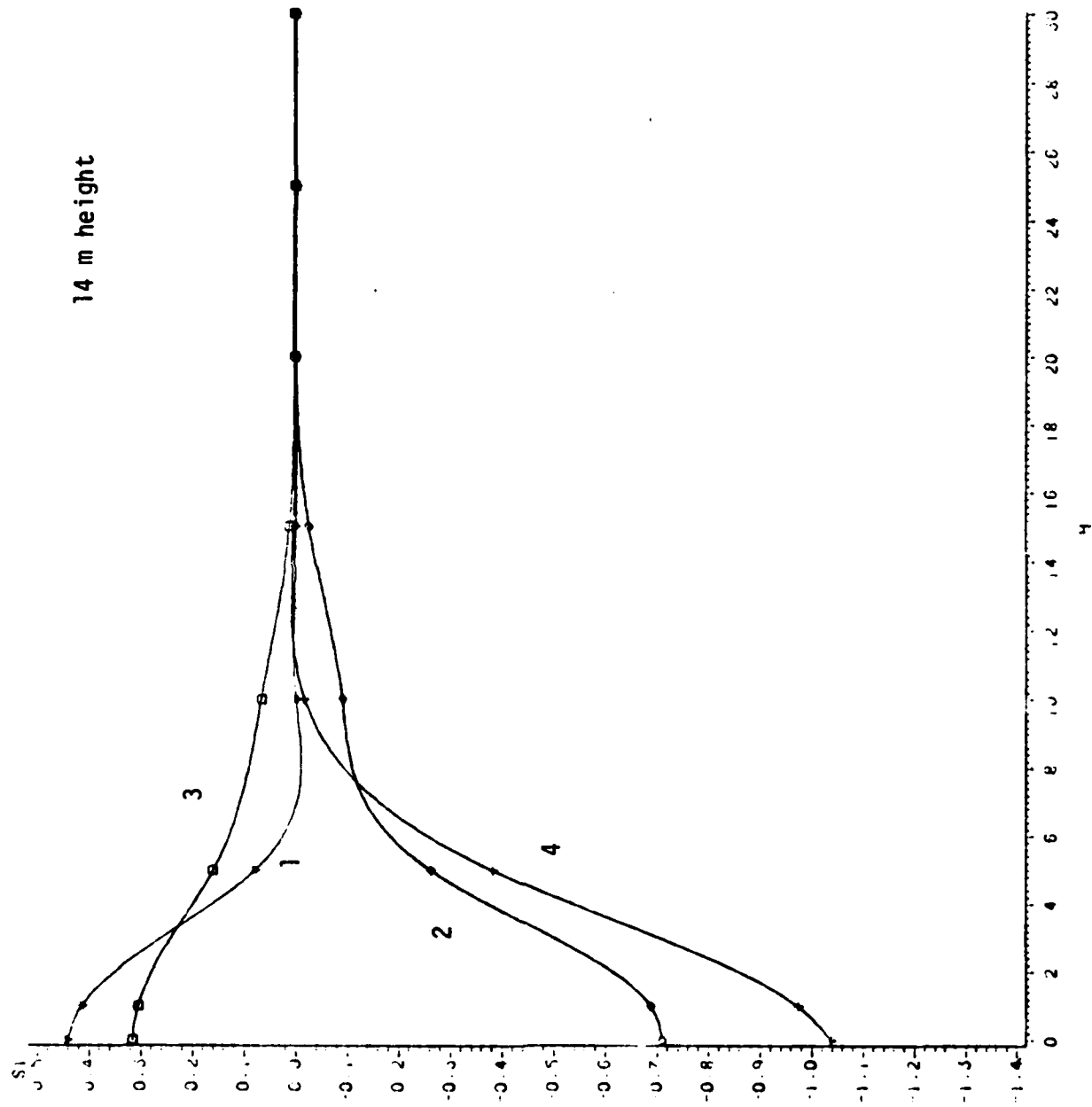


Figure 5.8b. As figure 5.8a.

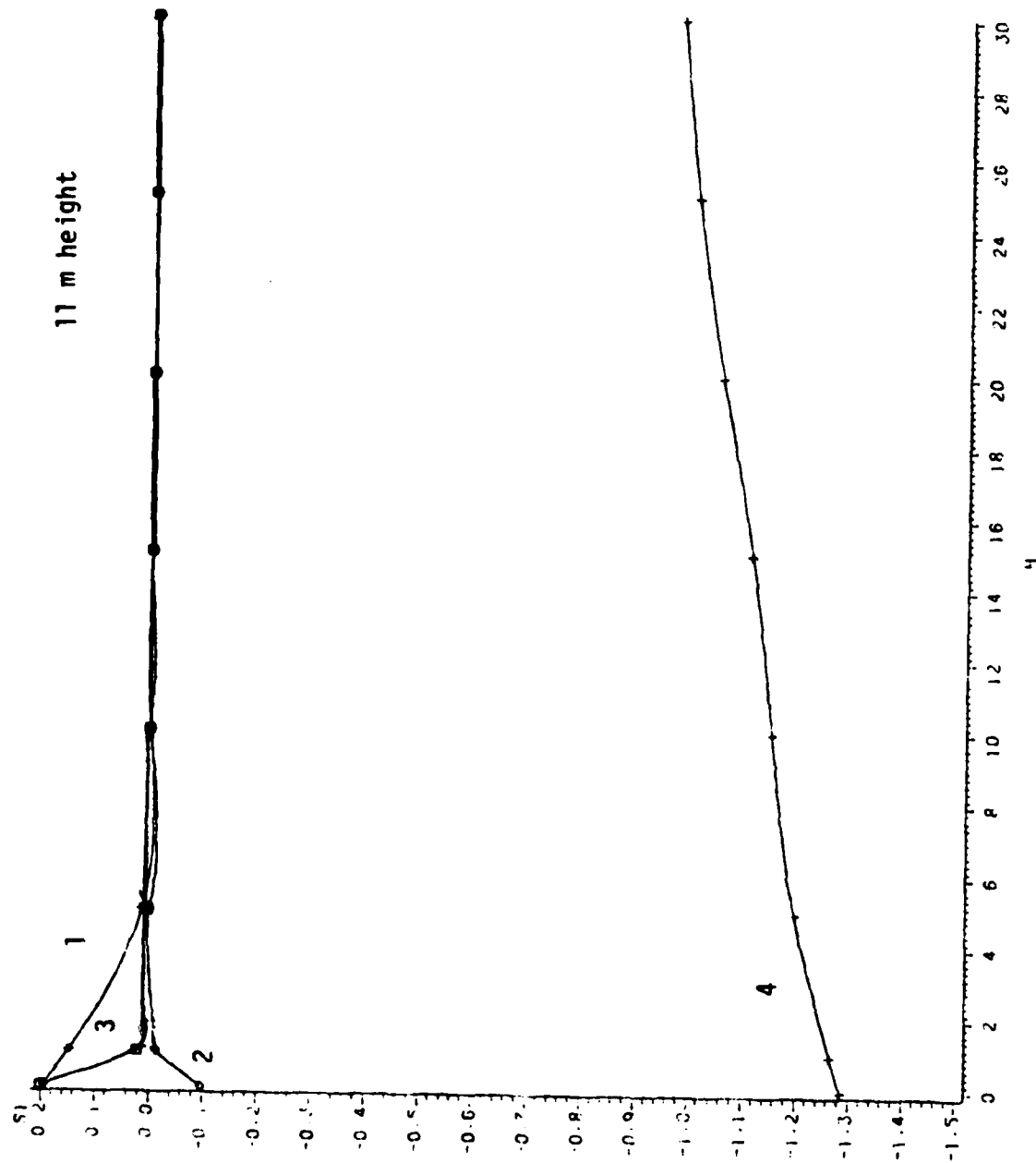


Figure 5.8c. As figure 5.8a.

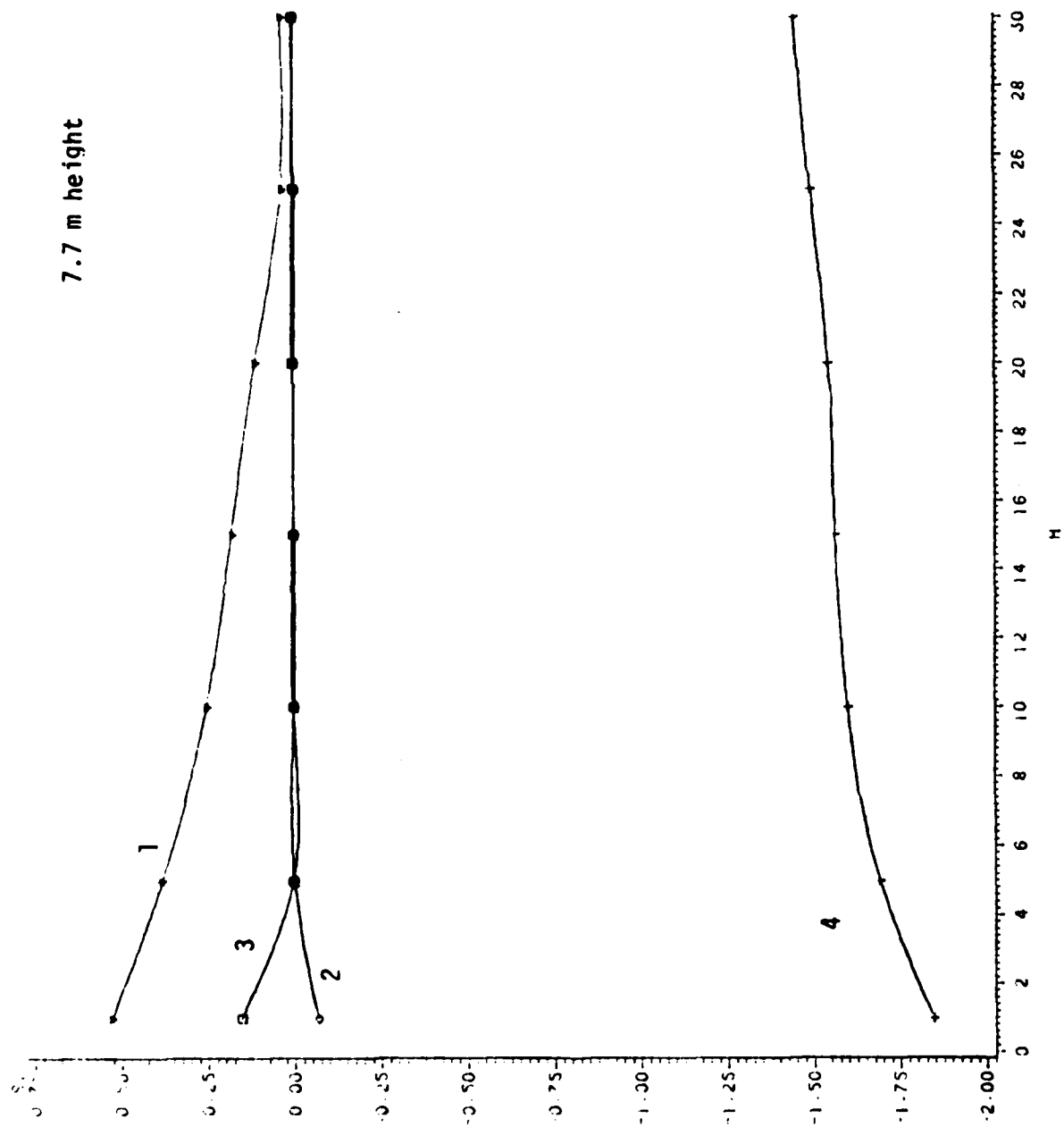


Figure 5.8d. As figure 5.8a.

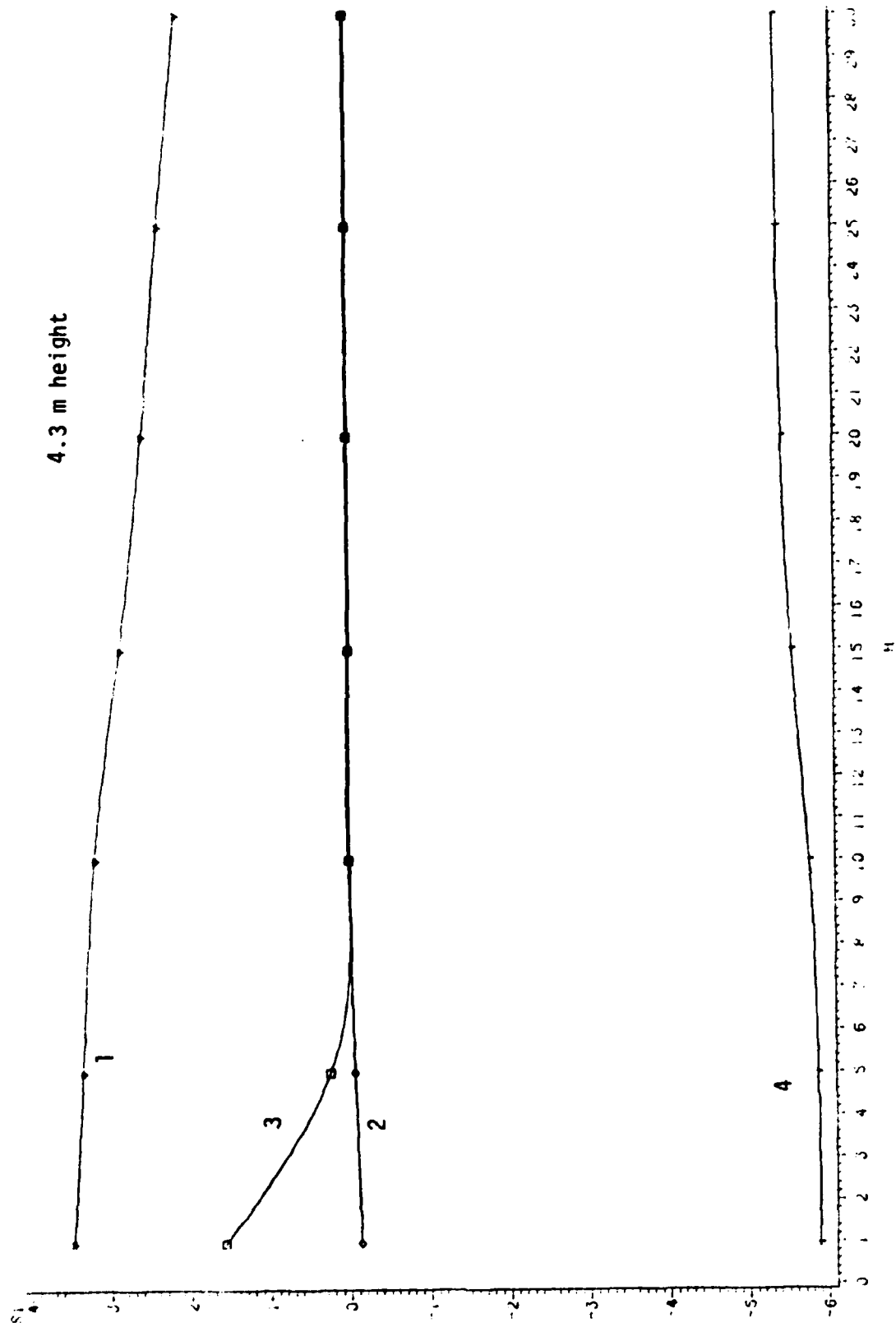


Figure 5.8e. As figure 5.8a.

END

FILMED

10-85

DTIC